





Applied Computational
Electromagnetics Society



Newsletter
Volume 21 – No. 3
ISSN 1056-9170



November 2006



**APPLIED COMPUTATIONAL ELECTROMAGNETICS SOCIETY
(ACES)**

NEWSLETTER

Vol. 21 No. 3

November 2006

TABLE OF CONTENTS

PERSPECTIVES IN CEM	
“Keep it Simple?” Alistair Duffy	6
THE PRATICAL CEMist	
“Proximity Loss Considerations for Compact Multiturn Transmitting Loop Antennas at HF” W. Perry Wheless Jr, Swati Maheshwari, and Michael A. McNees	8
FEATURE TECHNICAL ARTICLE	
“Quantifying experimental repeatability and simulation validation” Alistair Duffy and Kenneth Hodge	18
TUTORIAL	
“Numerical Analysis of IEEE Project 1597.1 Validation Problems” G. Antonini, M. Italiani, and A. Orlandi	32
TECHNICAL ARTICLES	
“CEMPAK: A Benchmarking System for Hardware and Software-Based Computational Electromagnetic Solvers” James Durbano, Ferando Ortiz, Ahmed Sharkawy, and Michael Bodnar	63
“Reduced Order Modeling for Metamaterial Transmission Lines” Giulio Antonini	78
ANNOUNCEMENTS:	
ADVERTISING Rates	104
DEADLINE for Submission of Articles.....	104
Last Word	104

PERMANENT STANDING COMMITTEES OF ACES, INC.
--

COMMITTEE	CHAIRMAN	ADDRESS
NOMINATION	Rene Allard	Penn State University PO Box 30 State College, PA 16804-0030 rja5@psu.edu
ELECTIONS	Rene Allard	Penn State University PO Box 30 State College, PA 16804-0030 rja5@psu.edu
FINANCE	Andrew Peterson	Georgia Institute of Technology School of ECE Atlanta, GA 30332-0250 peterson@ece.gatech.edu
PUBLICATIONS	Atef Elsherbeni	EE Department, Anderson Hall University of Mississippi University, MS 38677 atef@olemiss.edu
CONFERENCE	Osama Mohammed	Florida International University ECE Department Miami, FL 33174 mohammed@fiu.edu
AWARDS	Ray Perez	Martin Marietta Astronautics MS 58700, PO Box 179 Denver, CO 80201 ray.j.perez@lmco.com

MEMBERSHIP ACTIVITY COMMITTEES OF ACES, INC.

COMMITTEE	CHAIRMAN	ADDRESS
SOFTWARE VALIDATION	Bruce Archambeault	IBM 3039 Cornwallis Road, PO Box 12195 Dept. 18DA B306 Research Triangle Park NC 27709
HISTORICAL	(Vacant)	
CONSTITUTION & BYLAWS	Leo Kempel	2120 Engineering Building Michigan State University East Lansing, MI 48824 kempel@egr.msu.edu
MEMBERSHIP & COMMUNICATIONS	Vicente Rodriguez	ETS-LINDGREN L.P. 1301 Arrow Point Drive Cedar Park, TX 78613 rodriguez@ieee.org
INDUSTRIAL RELATIONS	Andy Drozd	ANDRO Consulting Services PO Box 543 Rome, NY 13442-0543 Andro1@aol.com

ACES NEWSLETTER STAFF

EDITOR-IN-CHIEF, NEWSLETTER

Bruce Archambeault
IBM
3039 Cornwallis Road, PO Box 12195
Dept. 18DA B306
Research Triangle Park, NC 27709
Phone: 919-486-0120
email: barch@us.ibm.com

EDITOR-IN-CHIEF, PUBLICATIONS

Atef Elsherbeni
EE Department, Anderson Hall
University of Mississippi
University, MS 38677
Email: atef@olemiss.edu

ASSOCIATE EDITOR-IN-CHIEF

Ray Perez
Martin Marietta Astronautics
MS 58700, PO Box 179
Denver, CO 80201
Phone: 303-977-5845
Fax: 303-971-4306
email: ray.j.perez@lmco.com

MANAGING EDITOR

Richard W. Adler
Naval Postgraduate School/ECE Dept.
Code ECAB, 833 Dyer Road,
Monterey, CA 93943-5121
Fax: 831-649-0300
Phone: 831-646-1111
email: rwa@att.biz

EDITORS

CEM NEWS FROM EUROPE

Tony Brown
University of Manchester
PO Box 88 Sackville Street
Manchester M60 1QD United Kingdom
Phone: +44 (0) 161-200-4779
Fax: +44 (0) 161-200-8712
email: Anthony.brown@manchester.ac.uk

TECHNICAL FEATURE ARTICLE

Andy Drozd
ANDRO Consulting Services
PO Box 543
Rome, NY 13442-0543
Phone: 315-337-4396
Fax: 314-337-4396
email: androl@aol.com

THE PRACTICAL CEMIST

W. Perry Wheless, Jr.
University of Alabama
PO Box 11134
Tuscaloosa, AL 35486-3008
Phone: 205-348-1757
Fax: 205-348-6959
email: wwheless@coe.eng.ua.edu

MODELER'S NOTES

Gerald Burke
Lawrence Livermore National Labs.
Box 5504/L-156
Livermore, CA 94550
Phone: 510-422-8414
Fax: 510-422-3013
email: burke2@llnl.gov

PERSPECTIVES IN CEM

Alistair Duffy
School of Engineering and Technology
De Montfort University
The Gateway
Leicester, UK LE1 9BH
+44(0)116 257 7056
apd@dmu.ac.uk

TUTORIAL

Giulio Antonini
UAq EMC Laboratory
Department of Electrical Engineering
University of L'Aquila
Poggio di Roio, 67040 Italy
Phone: +39-0862-43446
email: antonini@ing.univaq.it

ACES JOURNAL

EDITOR IN CHIEF

Atef Elsherbeni
Associate Editor-in-Chief Journal, Alexander Yakovlev
EE Department, Anderson Hall
University of Mississippi
University, MS 38677
Phone: 662-915-5382
email: atef@olemiss.edu

NEWSLETTER ARTICLES AND VOLUNTEERS WELCOME

The ACES Newsletter is always looking for articles, letters and short communications of interest to ACES members. All individuals are encouraged to write, suggest or solicit articles either on a one-time or continuing basis. Please contact a Newsletter Editor.

AUTHORSHIP AND BERNE COPYRIGHT CONVENTION

The opinions, statements and facts contained in this Newsletter are solely the opinions of the authors and/or sources identified with each article. Articles with no author can be attributed to the editors or to the committee head in the case of committee reports. The United States recently became part of the Berne Copyright Convention. Under the Berne Convention, the copyright for an article in this newsletter is legally held by the author(s) of the article since no explicit copyright notice appears in the newsletter.

BOARD OF DIRECTORS

EXECUTIVE COMMITTEE

Osama Mohammed, President
Atef Elsherbini, Vice President
Natalia Nikolova, Secretary

Allen W. Glisson, Treasurer
Richard W. Adler, Executive Officer

DIRECTORS-AT-LARGE

Randy Haupt	2007	Atef Elsherbeni	2008	C. J. Reddy	2009
Juan Mosig	2007	Michiko Kuroda	2008	Osama Mohammed	2009
Allen Glisson	2007	Andrew Drozd	2008	Natalia Nikolova	2009

ACES ELECTRONIC PUBLISHING GROUP

Atef Elsherbeni	Electronic Publishing Managing Editor
Matthew J. Inman	Site Administrator
Orin H. Council	Contributing Staff
Imran Kader	Past Site Administrator
Brad Baker	Past Staff
Jessica Drewrey	Past Staff
Chris Riley	Past Staff

Visit us on line at:
<http://aces.ee.olemiss.edu>

Keep it simple?

Alistair Duffy
apd@dmu.ac.uk

The last ‘Perspectives’ discussed satisficing and set out an implementation framework to support this. Satisficing was effectively presented as a ‘good enough’ strategy, not adding unnecessary complexity to the model nor excessive burdens on the computing aspects. Someone raised the question “is this KISS (Keep It Simple, Stupid) by another name?”

I am going to answer ‘yes’ to that, but with a caveat that simplest may not necessarily be best.

What is Keep It Simple, Stupid (KISS)? I thought I would take a straw poll to see what people think, so, asking colleagues, the general answer was that the simplest possible solution is best.

However, KISS is often described as a more modern, informal (and perhaps marginally insulting) interpretation of Occam’s Razor. Occam’s razor has a number of other connotations than just KISS.

The 14th Century English Franciscan Friar, William of Occam is credited with this parsimonious principle, which is stated in a couple of ways, depending on where you look:

“Entities should not be multiplied beyond necessity”

or

“Plurality should not be posited without necessity”

In other words “do not use more detail than you need to”

In science it has mostly been applied to explaining observations or selecting theories. Two of the main interpretations are:

- When deciding between models that give the same results, choose the simplest one.
- Choose the simplest of a set of classification rules that classify existing data equally well, because this is most likely to better classify future data.

As numerical modellers, this suggests that if we get adequate agreement between two or more simulations, the simpler implementation is the one we would want to use. This is where the link to satisficing comes in: the models should be as simple as possible but not over-simplified.

Naturally, any theory that can be applied to the natural world will have its opposition. There are a number of anti-razors that have been postulated over the years. One of the most famous was stated by a contemporary of William of Occam, Walter of Chatton, who said “If three things are not enough to verify an affirmative proposition about things, a fourth must be added, so if you need to add more detail to explain phenomena you must add more detail. It never really caught on in the way that Occam’s razor did (the ‘razor’ coming from the idea of shaving back to the bare essentials) and the core message was probably captured (along with Occam’s razor) by Einstein who said “The supreme goal of all theory is to make the irreducible basic elements as simple and as few as possible without having to surrender the adequate representation of a single datum of experience”, i.e. simple without being too simple.

So how does this relate to satisficing and to KISS?

Occam's razor is most often used as a philosophical threshold for classification, grouping and selection, i.e. making sense of observations and theories. In the previous issue, we discussed satisficing in a more proactive way, looking at creating models and undertaking simulations that were simple enough but not too simple, with a structured approach to achieving a satisfied outcome. KISS suggests that the goal is in achieving the simplest possible result or implementation.

So, answering the question. "Keep It Simple, Stupid" and satisficing are very similar views. While KISS has been claimed to be a modern and informal interpretation of Occam's razor, it does imply an aim of over-simplification, whereas the satisficing approach discussed in the last issue tends to favour the view of keeping things as simple as possible, but not too simple.

Bibliography

Discussions of Occam's razor can be found in most books dealing with the philosophy of science. Quality encyclopaedias (such as the Encyclopaedia Britannica) have articles on Occam and Occam's razor.

However a couple of accessible URLs that can help in finding out a little more about Occam's razor are:

Wikipedia: http://en.wikipedia.org/wiki/Occam%27s_razor

McGill University: <http://cgm.cs.mcgill.ca/~sooss/cs644/projects/jacob/>

Proximity Loss Considerations for Compact Multiturn Transmitting Loop Antennas at HF

W. Perry Wheless, Jr., Swati Maheshwari, and Michael A. McNees
Department of Electrical and Computer Engineering
The University of Alabama
Tuscaloosa, AL 35487
Contact Email: wwheless@eng.ua.edu

Abstract—Progress in a continuing research project is reported here. The objective of the research is to quantify the feasibility of using physically compact RF inductors as effective transmitting antennas for HF (3-30 MHz) communications. Proximity losses for the closely spaced turns of helically wound, air core RF inductors fabricated with either wire or tubing are substantial, and must be accounted for in any predictive model. A capability for estimation of total loss (proximity loss plus high-frequency ac ohmic loss) has been developed which, when combined with radiation pattern and gain calculations from a numerical method such as the Method of Moments (MoM), gives a more accurate and reliable prediction of performance for a coil antenna than is available from MoM or proximity loss values, taken individually.

I. INTRODUCTION

There is considerable interest in small antennas for HF radio communication applications, especially in the context of portable and mobile operations. The geometry under consideration here is helically wound, air core RF inductors, fabricated with wire or tubing. A specific example is the coil (RF inductor) whose photograph appears in Figure 1. This 57 μH inductor is made with 1.27 cm (0.5 inch) diameter silver-plated copper tubing. There are 22 turns, total, in a length of 44 cm (slightly more than 17 inches), so the center-to-center turn spacing is 2 cm. The coil diameter is approximately 30 cm (12 inches). This particular RF inductor was originally part of an antenna tuning unit (ATU) circuit at a 50 kW AM broadcast station.

The coil axis in Figure 1 is vertically aligned, with a section of 10 cm (4 inch) diameter PVC pipe supporting the frame of the coil and providing a nominal elevation of approximately 0.6m above the large plywood dolly base which is partially visible in the lower part of the photograph. Two of three bars for securing the coil turns in place are clearly visible in Figure 1, and these support structures are made of micalex. To create a feed point, a gap of approximately 1.25 cm was created by cutting that length out of the coil tubing and soldering two heavy brass tabs with 0.25-inch brass hardware to secure the center conductor and braid, respectively, of RG-8 50 Ω coaxial cable. A short section of coax is shown attached to the coil in Figure 1; note the black heatshrink (toward the lower left in the picture) which secures six cylindrical ferrite chokes to the cable.



Figure 1. A compact coil (multi-turn loop) antenna.

II. BACKGROUND

An early source of interest in loop antenna configurations for HF communications was the quad antenna, generally credited to Clarence Moore as his solution to corona discharge problems with yagis at high altitude while he was at the shortwave missionary radio station HCJB in Quito, Ecuador, in the early 1940s. A basic two-element quad array is depicted in Figure 2. The driven elements are electrically 1λ in circumference (i.e., $\frac{\lambda}{4}$ on each side), and the reflectors are slightly longer.

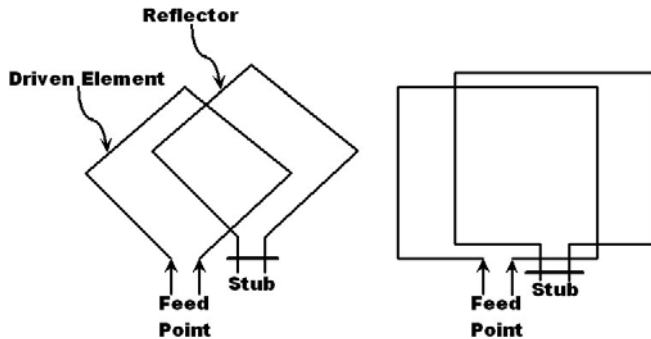


Figure 2. Basic two-element quad array.

Quad-yagi comparisons suggests that the quad excels with respect to gain, is similar in SWR characteristics, and lags with respect to front-to-back ratio. Favorable experience in applications solidified the quad as a popular directional wire antenna for both the HF and VHF spectrum. The principal drawback of the full-sized quad is that it is physically cumbersome to construct and deploy. Physical size of the quad may fairly be described as large at frequencies below 14 MHz, becoming preclusive below 7 MHz.

As a compromise, the amateur radio community led the quick adaptation to using the driven element from a quad array alone as a single loop. Experiments with the loop mounted horizontally soon followed and this work, in turn, inspired efforts toward emulating 1λ loop performance with versions of reduced size. One of the more complete collection of practical guidelines to HF compact loop construction is in [1], which contains specific designs [2] as well.

The next logical step in compact loop antenna development was multiturn loops, and this class of physically small antennas has received some attention over the past thirty years (see, for example, [3]). Clever variations on the simple circular or square loop geometries have been devised, such as the incorporation of fractals [4], [5]. Nonetheless, more success has been achieved with small multiturn loop receiving antennas [6] than with transmitting antennas.

III. TERMINOLOGY

Loops are generally divided into two classes: those loops for which the total conductor length and maximum linear dimension of a turn are very small relative to the operating wavelength, and those for which the total conductor length and loop dimensions become comparable to the wavelength.

A more precise definition of an electrically small loop is one in which the current has the same magnitude and phase everywhere in the loop. To reasonably comply with this condition, the working compromise is that the loop's total conductor length should not exceed (approximately) 0.1λ . A "large" loop, then, is one in which the current amplitude and phase are not required to be constant everywhere in the loop. In practice, a conductor length of 0.5λ is generally taken to be the minimum for a loop to be described as large.

Especially for portable and/or mobile operation, physical size is the more important parameter. Therefore, the descriptor "compact" has been adopted here to identify the class of (potential) multiturn loop antennas of interest, and is hereafter the shorthand notation for "physically compact." In some cases, a physically compact multiturn loop (that is, a coil) may qualify as electrically small at certain proposed frequencies of operation, and simultaneously qualify as electrically large at other higher operating frequencies.

IV. EFFICIENCY AND PROXIMITY LOSS

A straightforward measure of antenna radiation efficiency is given by

$$\eta = \frac{R_{Rad}}{R_{Rad} + R_{Loss}}, \quad (1)$$

usually expressed as a percentage.

For a single-turn transmitting loop, R_{Loss} is essentially the conductor's ac resistance (but also includes connection resistances and embedded tuning reactance losses which are generally negligible when $R_{Rad} > 0.25\Omega$), approximated by

$$R_{ac} = \frac{0.996 \times 10^{-6} \sqrt{f}}{d} \quad (2)$$

with frequency f in Hz, conductor diameter d expressed in inches, and R_{ac} in Ohms per foot. Skin effect is responsible for increasing the effective resistance as frequency is increased, corresponding to the increased energy loss experienced by fluids forced to maintain a constant flow rate when directed into a pipe of smaller diameter. Anecdotal accounts of practical experience suggests that the loop conductor should be at least 0.75 inch diameter, if made of copper, to achieve reasonable transmit efficiency.

For multiturn loops with turns closely spaced, there is an additional loss arising from what is known as *proximity effect*. The source of the observed effect is the fact that the circumferential current distribution changes as the current-carrying coil turns are brought close together, changing the surface current (per square meter) flowing at surfaces adjacent to other conductors. Higher loss than suggested by a skin effect analysis results because the current flow is compressed and flows through a smaller cross-sectional area than if the neighboring turns were absent.

The order of magnitude of the effect is indicated in the following excerpt from page 5-12 of reference [1]:

As the efficiency of a loop antenna approaches 90%, the proximity effect is less serious. But unfortunately, the less efficient the loop, the worse the effect. For example, an 8-turn transmitting loop with an efficiency of 10% (calculated by the skin-effect method) actually only has an efficiency of 3% because of the additional losses introduced by the proximity effect.

When the coil conductor is segmented for Moment Method analysis by a code such as EZNEC, the numerical procedure returns a complex (magnitude/phase) current value for each

segment. However, it appears that closely spaced parallel conductors pose a challenge for the numerical technique, and that it does not account for the significant current compression loss associated with the proximity effect. The plausibility of this conclusion has been investigated by means of the following specific case study.

V. A SPECIFIC CASE STUDY: GATES ATU COIL

The RF inductor shown in the photograph of Figure 1 was selected for a detailed engineering study. This $57 \mu H$ coil was originally manufactured by Gates Radio Company for use in high-power AM broadcast service. Its relatively large diameter silver-plated tubing and turn-to-turn spacing that was originally selected for MF applications suggested that this coil might hold significant promise for use as a transmitting antenna at HF.

To begin, the coil geometry was segmented (using an octagonal approximation to its circular cross section), similar to the illustration in Figure 3, and preliminary numerical analysis conducted with the Method of Moments code EZNEC [16]. For purposes of this study, the following specific frequencies were selected: 1.9, 3.8, 7.3, 10.1, 14.25, 18.1, and 21.3 MHz. These frequencies are all in, or at the edge of, amateur radio bands so that transmit as well as receive experiments could be conducted. Figures 4 and 5 illustrate the elevation pattern results obtained.

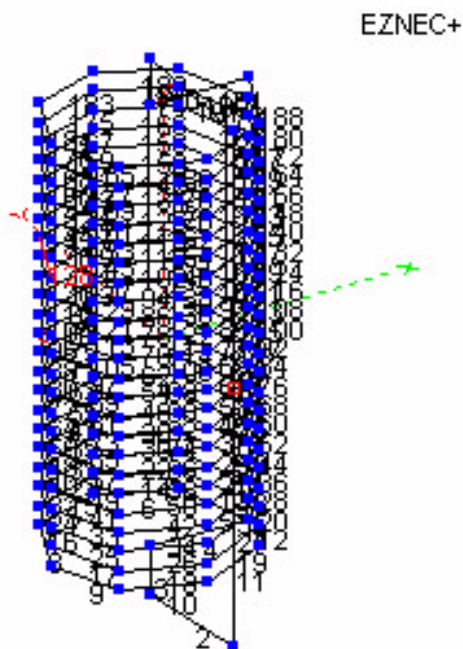


Figure 3. MoM segmentation, octagonal approximation.

Because the total conductor length of the coil tubing is about 22 m, approaching half-wavelength natural resonance length near the 7 MHz (40 meter) band, and armed with the -4.51 dBi gain prediction for 7.3 MHz from the computer analysis, it

was decided to initiate experimental observations in the 40m band. The coil center-feed terminals were connected to the output of a MFJ HF antenna tuning unit, as shown in the photograph of Figure 6 through a section of 50Ω that was less than 1 meter in length. From there, another 15-meter long 50Ω coaxial cable was used to connect the MFJ tuner input to a 100W HF transceiver inside.

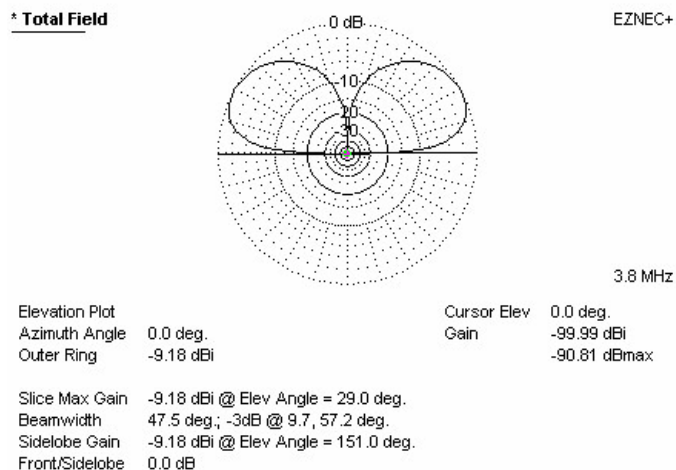


Figure 4. Elevation plot for 3.8 MHz.

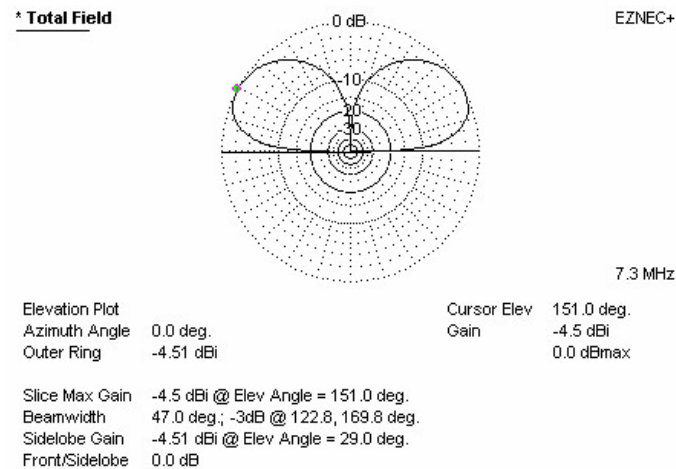


Figure 5. Elevation plot for 7.3 MHz.

Numerous radio contacts were made in the 40m amateur bands with the coil deployed on its plywood dolly inside the bed of a pickup truck (see photograph in Figure 6, which shows the coil antenna being connected to the ATU), and the immediate results were exhilarating. Both transmit and receive signals were fully comparable to a full sized horizontal center-fed dipole mounted at approximately 40 feet (12.2 m). In some instances, the coil exhibited superior

performance! Since the 21 MHz (15m) amateur band is at an odd multiple of 40m, so the coil conductor length again approaches a natural resonance, contacts on the 15m band followed - with similarly astonishing results. From Alabama, first-day contacts included stations from Africa to Asia.



Figure 6. Coil on platform in truck bed.

Unfortunately, when cylindrical coax-diameter ferrite “beads” were placed on the cable section between the coil feed point and the ATU, the performance on both 40m and 15m plummeted. All those bodacious signals and superlative long-distance signal reports were mostly attributable to currents flowing on the outside of the coax braid and blind chance selection of a day with outstanding propagation conditions for the initial testing!

Six ferrite chokes were added to the short coil feed pigtail, secured by enclosure with heatshrink tubing, and the “choked” pigtail connector was used in all subsequent experimentation.

Seeking an explanation for the large discrepancy subsequently observed between NEC2 performance prediction and actual practice, the compact coil HF antenna project proceeded to obtain quantitative results for potentially significant additional proximity effect losses.

VI. PROXIMITY LOSS PROGRAM INTRODUCTION

A literature search revealed that Glenn Smith, now a professor of electrical engineering at Georgia Tech, conducted the most thorough scientific study available of proximity loss. Dr. Smith’s work dates from the early 1970s, while he was still working with R.W.P. King at Harvard University. It was deemed a necessity to be able to reproduce the results reported in his papers, principally [7], and to develop a modernized computer code (in MATLAB [8]) which would allow contemporary users to make proximity loss predictions about coils of geometries (and operating frequencies) different from those of high priority to Dr. Smith in his original work.

VII. MATHEMATICAL PRELIMINARIES

In [7], the solutions for two cases of proximity loss calculation are treated. First, in the case when two parallel, closely-spaced cylindrical conductors are present, the Jacobi elliptic integrals and functions are used to determine the normalized current distribution in each conductor and, also, the normalized additional ohmic resistance per unit length due to the proximity effect. In the second case, that of an even number of conductors (greater than two), a least squares methodology is used. The second case will be addressed later; some review remarks about the elliptic integrals and functions relevant to the first case are made here.

Jacob Bernoulli encountered a form of elliptic integral in 1679 and, in 1694, he made an important step in the theory of elliptic integrals. See [9] for a brief tutorial on the elliptic integral, from which the following excerpt is taken:

Elliptic integrals can be viewed as generalizations of the inverse trigonometric functions and provide solutions to a wider class of problems. For instance, while the arc length of a circle is given as a simple function of the parameter, computing the arc length of an ellipse requires an elliptic integral. Similarly, the position of a pendulum is given by a trigonometric function as a function of time for small angle oscillations, but the full solution for arbitrarily large displacements requires the use of elliptic integrals. Many other problems in electromagnetism and gravitation are solved by elliptic integrals.

A very useful class of functions known as elliptic functions is obtained by inverting elliptic integrals to obtain generalizations of the trigonometric functions. Elliptic functions (among which the Jacobi elliptic functions and Weierstrass elliptic function are the two most common forms) provide a powerful tool for analyzing many deep problems in number theory, as well as other areas of mathematics.

Theorem 1: If $R(x, y)$ is a rational function in x and $y = \sqrt{P(x)}$, namely

$$R(x, y) = \int \frac{A(x)dx}{B(x)} \stackrel{\text{OR}}{=} \int \frac{A(x) + B(x)\sqrt{P(x)}}{C(x) + D(x)\sqrt{P(x)}} dx \quad (3)$$

where $P(x)$ is a polynomial of degree three or four with no repeated factors, then the integral

$$\int R(x, \sqrt{P(x)}) dx \equiv \int R(x, y) dx \quad (4)$$

can always be expressed in terms of elliptic integrals [13]. For a proof, see [14].

It is necessary to apply the above theorem to achieve an analytical solution for the proximity loss associated with a pair of conductors, and there are three classifications of elliptic integrals:

$$\underline{1^{st} \text{ Kind:}} F(k, \phi) = \int_0^\phi \frac{d\theta}{\sqrt{1 - k^2 \sin^2 \theta}}, \quad 0 < k < 1 \quad (5)$$

$$\underline{2^{nd}}: E(k, \phi) = \int_0^\phi \sqrt{1 - k^2 \sin^2 \theta} d\theta, \quad 0 < k < 1 \quad (6)$$

$$\underline{3^{rd}}: \Pi(k, \phi, a) = \int_0^\phi \frac{d\theta}{\sqrt{1 - k^2 \sin^2 \theta} (1 + a^2 \sin^2 \theta)}, \quad (7)$$

$$\text{for } \begin{cases} 0 < k < 1 \\ a \neq k, 0 \\ n = -a^2 \end{cases}.$$

Parameter ϕ is called the *amplitude* and k the *modulus*. Number n is called the characteristic and can take any value $(-\infty, \infty)$ regardless of other variables. When $\phi = \frac{\pi}{2}$, these become known as the *complete elliptic integrals*, with the special designations

$$\underline{1^{st} \text{ Kind}}: F(k, \frac{\pi}{2}) \implies K(k) = K$$

$$\underline{2^{nd} \text{ Kind}}: E(k, \frac{\pi}{2}) \implies E(k) = E \quad (8)$$

$$\underline{3^{rd} \text{ Kind}}: \Pi(k, \frac{\pi}{2}, a) \implies \Pi(k, a) = \Pi.$$

Useful infinite series representations for K and E , and results for limiting cases $m \rightarrow 0$ and $m \rightarrow 1$ are well known and readily available in references such as [13], [15]. Inversion of elliptic integrals leads to elliptic functions which fall into two categories - the Weierstrass and Jacobi elliptic functions, with the Jacobi elliptic functions considered the standard form. The three basic Jacobi functions are

$$\begin{aligned} sn(u) &= sn u = \sin \phi = x \\ cn(u) &= cn u = \cos \phi \\ dn(u) &= dn u = \sqrt{1 - m \sin^2 \phi} \end{aligned} \quad (9)$$

with the third relation giving $\phi = \arcsin(sn u) = am u$, the amplitude. The Jacobian elliptic functions are doubly periodic. K and iK' are the ‘‘real’’ and ‘‘imaginary’’ quarter-periods of these functions, defined by

$$K(m) = K = \int_0^{\frac{\pi}{2}} \frac{d\theta}{\sqrt{1 - m \sin^2 \theta}} \quad (10)$$

and

$$iK'(m) = iK' = i \int_0^{\frac{\pi}{2}} \frac{d\theta}{\sqrt{1 - m' \sin^2 \theta}} \quad (11)$$

with $0 < m < 1$ and $m + m' = 1$. Both K and K' are real numbers. Finally, if one wishes to use the modulus k instead

of the parameter m , equations 10 and 11 become

$$K(k) = K = \int_0^{\frac{\pi}{2}} \frac{d\theta}{\sqrt{1 - k^2 \sin^2 \theta}} \quad (12)$$

and

$$iK'(k) = iK' = i \int_0^{\frac{\pi}{2}} \frac{d\theta}{\sqrt{1 - (k')^2 \sin^2 \theta}} \quad (13)$$

where $(k')^2 = 1 - k^2$.

TABLE I	
Elliptic Integral Reference Table of Variables	
Variable	Description
k	Modulus
k'	Complementary Modulus
$m = k^2 = \sin^2 \alpha$	Parameter
$m' = 1 - m$	Complementary Parameter
$\alpha = \sin^{-1} k$	Modular Angle
$\phi = am u$	Amplitude
$q = e^{-\frac{iK'}{K}}$	Nome
$K = K(k)$	Quarter Period
$K' = K(k')$	Imaginary Quarter Period

VIII. SOLUTION FOR TWO WIRES

For the two cylindrical wires case, assuming constant (i.e., equal) current flowing in both conductors, the analytical solution in [7] uses Jacobi elliptic integrals and functions to calculate the normalized current distribution on each conductor and, from that, the normalized additional ohmic resistance per unit length arising from the proximity effect. Smith [7] adapted the conformal mapping electrostatic solution reported by Whipple [10] to the context of the problem of present interest, and arrived at the following as the solution for the normalized current distribution (Eq. 30 in [7]):

$$g(\theta) = \frac{2(1+k)K(k)}{\pi} \operatorname{csch} \alpha (\cosh \alpha - \cos u) \quad (14)$$

$$\times dn \left(\frac{(1+k)K(k)}{\pi} u, \frac{2\sqrt{k}}{1+k} \right)$$

with

$$u = \sin^{-1} \left(\frac{\sin \theta \sinh \alpha}{c/a + \cos \theta} \right)$$

$$\alpha = \ln \left[\frac{a}{c - (c^2 - a^2)^{\frac{1}{2}}} \right]$$

$$\frac{K'(k)}{K(k)} = \frac{2\alpha}{\pi} \quad (15)$$

$$0 \leq u \leq \frac{\pi}{2} \text{ for } 0 \leq \theta \leq \cos^{-1} \left(\frac{a}{c} \right)$$

$$\frac{\pi}{2} \leq u \leq \pi \text{ for } \cos^{-1} \left(\frac{a}{c} \right) \leq \theta \leq \pi.$$

in addition to the entries of Table I. Calculation of the modulus k requires the so-called theta functions, summarized in Table II below.

Table II	
Theta Functions	
$\Theta_1(z, q) = \Theta_1(z) = 2q^{\frac{1}{4}} \sum_{n=0}^{\infty} (-1)^n q^{n(n+1)} \sin(2n+1)z$	
$\Theta_2(z, q) = \Theta_2(z) = 2q^{\frac{1}{4}} \sum_{n=0}^{\infty} q^{n(n+1)} \cos(2n+1)z$	
$\Theta_3(z, q) = \Theta_3(z) = 1 + 2 \sum_{n=1}^{\infty} q^{n^2} \cos(2nz)$	
$\Theta_4(z, q) = \Theta_4(z) = 1 + 2 \sum_{n=1}^{\infty} (-1)^n q^{n^2} \cos(2nz)$	

The normalized additional ohmic resistance per unit length attributable to proximity effect is then

$$\frac{R_p}{R_0} = \left(\frac{2K}{\pi} \right)^2 \left[2 \operatorname{ctnh} \alpha \left\{ \frac{E(K, k)}{k} - \frac{(k')^2}{2} \right\} \right] - (1 + 2 \operatorname{csch}^2 \alpha) \quad (16)$$

(Eq. 31 in [7]) where $E(K, k)$ is the complete elliptic integral of the second kind and $(k')^2 = 1 - k^2$.

Noting that $2c$ is the center-to-center conductor spacing and a is the conductor radius, the normalized surface current distributions as a function of angle θ (see Figure 7) for two conductors at various ratios $\frac{c}{a}$ are shown in Figure 8. The results, computed with MATLAB, closely emulate those in Fig. 3 of reference [7]. MATLAB does not have built-in support for all the elliptic functions, so custom code was written to calculate the elliptic function values for substitution into 16. The *half-period ratio* τ is related to the real and imaginary quarter periods by

$$\tau = \frac{iK'}{K} = \frac{2\alpha}{\pi}. \quad (17)$$

Subsequently, the value of *nome* is obtained from

$$q = e^{-\frac{\pi K'}{K}} = e^{i\pi\tau}. \quad (18)$$

Table II contains the theta function formulas used to calculate the elliptic modulus

$$k = \left(\frac{\Theta_2}{\Theta_3} \right)^2. \quad (19)$$

The value of z in the Table II relations is zero here. Parameter m is obtained from k , and is used as the argument in the MATLAB function “ellipj” to evaluate the elliptic integrals of the first and second kinds.

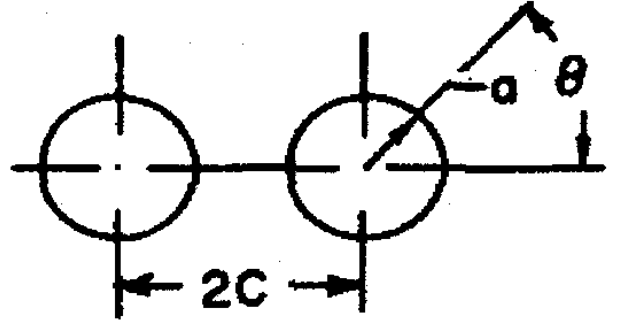


Figure 7. Two-conductor geometry.

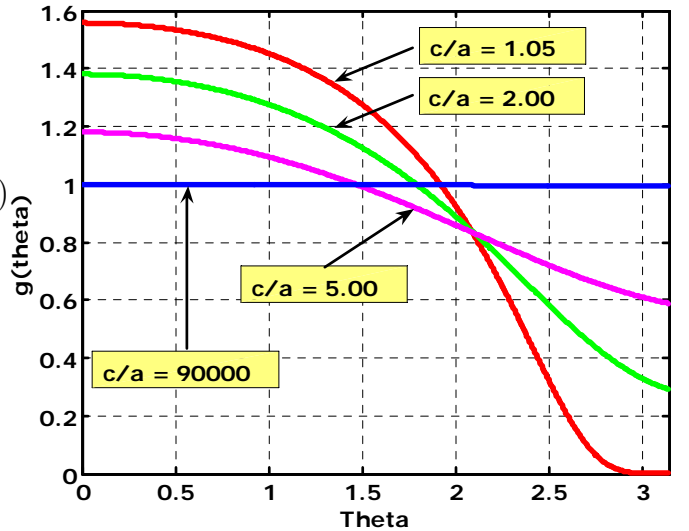


Figure 8. Normalized surface current distribution for different wire spacings.

IX. SOLUTION FOR MORE THAN TWO CONDUCTORS

For more than two circular conductors, a closed form solution (in contrast to the two-wire case) cannot be found, and [7] proceeds to apply an approximation method - namely,

undetermined coefficients - to obtain current distributions and total ohmic resistance per unit length. Again, constant current is assumed. A trigonometric series is the expansion representation for the normalized surface current density:

$$g_m(\theta) = 1 + \sum_{p=1}^q a_{mp} \cos(p\theta) \quad (20)$$

where m is the wire number, q now represents the number of harmonics (and is not the nome, as before), and the a_{mp} factors represent Fourier coefficients. The simplification of an even number of wires in the system is taken. The Fourier coefficients are calculated via a matrix generated by the method of least squares, with an "Indicator function" involved in the process.

$$I(\theta, m - \ell, p) = \begin{cases} \frac{1}{(1-s^2)(-s)^{p+1}}(As^2 + Bs + C), & p = 1, 2, \dots, q \\ \frac{-1}{s(1-s^2)}(Bs + 2C), & p = 0 \end{cases} \quad (21)$$

where

$$s = \left[4(m-\ell)^2 \left(\frac{c}{a}\right)^2 + 1 + 4(m-\ell) \left(\frac{c}{a}\right) \cos\theta \right]^{\frac{1}{2}}$$

$$A = \cos[\theta - (p-1)\Psi]$$

$$B = 2 \left[1 + 2(m-\ell) \left(\frac{c}{a}\right) \cos\theta \right] \cos(p\Psi)$$

$$C = \cos[\theta + (p+1)\Psi]$$

$$\Psi = \pi - \tan^{-1} \left(\frac{\sin\theta}{2(m-\ell) \left(\frac{c}{a}\right) + \cos\theta} \right), \quad m - \ell = 1, 2, \dots$$

$$\Psi = \tan^{-1} \left(\frac{-\sin\theta}{2(m-\ell) \left(\frac{c}{a}\right) + \cos\theta} \right), \quad m - \ell = -1, -2, \dots$$

The equation key to determination of the coefficients a_{mp} can be written simplistically as

$$\sum_{p=1}^q a_{mp} t_{kp}^m + \sum_{\substack{\ell=1 \\ \ell \neq m}}^{\frac{n}{2}} \sum_{p=1}^q a_{mp} t_{kp}^{m\ell} = s_{mk}, \quad \begin{cases} m = 1, 2, \dots, \frac{n}{2} \\ k = 1, 2, \dots, q \end{cases} \quad (22)$$

which is equivalent to the matrix equation

$$\begin{bmatrix} T_{11} & T_{12} & \dots & T_{1, \frac{n}{2}} \\ T_{21} & T_{22} & \dots & T_{2, \frac{n}{2}} \\ \vdots & \vdots & \ddots & \vdots \\ T_{\frac{n}{2}, 1} & T_{\frac{n}{2}, 2} & \dots & T_{\frac{n}{2}, \frac{n}{2}} \end{bmatrix} \begin{bmatrix} A_1 \\ A_2 \\ \vdots \\ A_{\frac{n}{2}} \end{bmatrix} = \begin{bmatrix} S_1 \\ S_2 \\ \vdots \\ S_{\frac{n}{2}} \end{bmatrix} \quad (23)$$

where the submatrices within the partitioned T matrix are

$$T_{ii} = \begin{bmatrix} t_{11}^i & t_{12}^i & \dots & t_{1,q}^i \\ t_{21}^i & t_{22}^i & \dots & t_{2,q}^i \\ \vdots & \vdots & \ddots & \vdots \\ t_{q,1}^i & t_{q,2}^i & \dots & t_{q,q}^i \end{bmatrix}, \quad T_{ij} = \begin{bmatrix} t_{11}^{ij} & t_{12}^{ij} & \dots & t_{1,q}^{ij} \\ t_{21}^{ij} & t_{22}^{ij} & \dots & t_{2,q}^{ij} \\ \vdots & \vdots & \ddots & \vdots \\ t_{q,1}^{ij} & t_{q,2}^{ij} & \dots & t_{q,q}^{ij} \end{bmatrix},$$

$$A_i = \begin{bmatrix} a_{i,1} \\ a_{i,2} \\ \vdots \\ a_{i,q} \end{bmatrix} \quad \text{and} \quad S_i = \begin{bmatrix} s_{i,1} \\ s_{i,2} \\ \vdots \\ s_{i,q} \end{bmatrix}.$$

Expansion series coefficients a_{mp} , obtained by solving the matrix equation in standard fashion by multiplication with A^{-1} , are substituted into Eqn. (20) to give normalized surface current distribution graphs such as those in Figures 9 through 11 for the illustrative (half) spacing to radius ratio $\frac{c}{a} = 2$ in a 6-wire system. The results for conductors 4 (left middle) to 6 (left end) are known by symmetry. The interested reader should also see the original family of plots in Fig. 4 of reference [7], which are confirmed by the calculations done in this study.

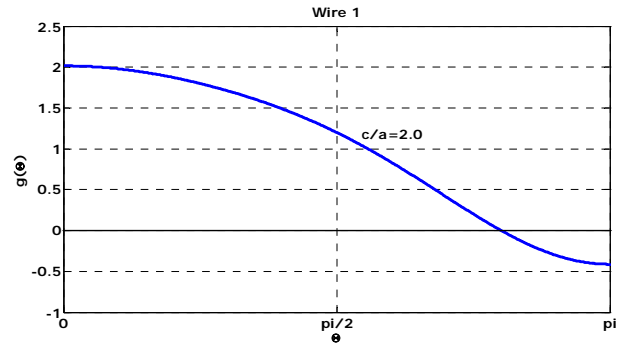


Figure 9. Surface current distribution, wire #1 (right end).

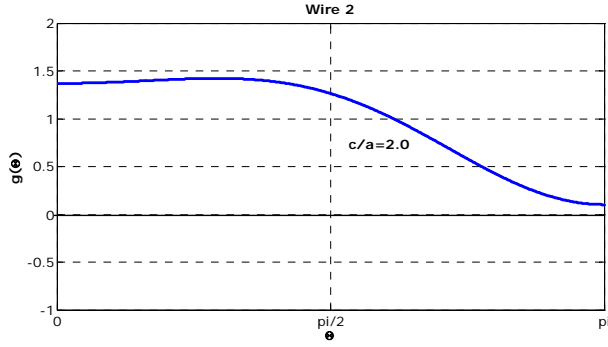


Figure 10. Surface current distribution, wire #2 (next to end).

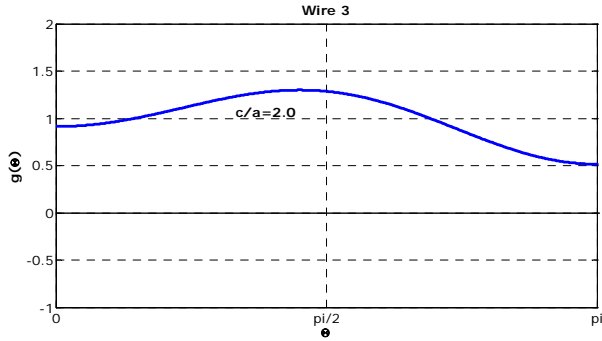


Figure 11. Surface current distribution, wire #3 (right middle).

The same a_{mp} coefficients are used to get the additional ohmic resistance per unit length due to proximity effect from

$$\frac{R_p}{R_0} = \frac{R - nR_R}{nR_R} = \frac{1}{2n} \sum_{m=1}^n \sum_{p=1}^q |a_{mp}|^2 \quad \Omega/m \quad (24)$$

where R_R is the Rayleigh formula for high-frequency resistance per unit length of a circular conductor, according to

$$R_R = \frac{2P}{|I|^2} = \frac{R^S}{2\pi a} = \frac{1}{2\pi a} \left(\frac{\omega\mu_0}{2\sigma} \right)^{\frac{1}{2}} \quad \Omega/m \quad (25)$$

$$\Rightarrow R^S = \left(\frac{\omega\mu_0}{2\sigma} \right)^{\frac{1}{2}} \quad (26)$$

and R is the ohmic resistance for n parallel wires, with all conductors carrying the same current, given by

$$R = \frac{R^S}{2\pi a} \sum_{m=1}^n \left(1 + \frac{1}{2} \sum_{p=1}^q |a_{mp}|^2 \right). \quad \Omega/m \quad (27)$$

The right hand expression in Eqn. (24), with the double summation of $|a_{mp}|^2$, is the form used for practical calculations.

X. SPECIFIC CASE STUDY

The subject specific case study is the multiturn loop (coil) transmitting antenna shown in Figure 1 and described in the ‘‘Introduction’’ section of this paper. For this 22-turn coil with $\frac{c}{a} = 1.667$ (center-to-center spacing of turns = 2 cm), after first calculating the \underline{T} and \underline{S} matrices discussed above, the matrix equation is solved for the coefficients (\underline{A} matrix) using MATLAB. Then the normalized additional resistance from the proximity effect follows from Eqn. (24):

$$\frac{R_p}{R_0} = \frac{1}{2n} \sum_{m=1}^n \sum_{p=1}^q |a_{mp}|^2 = 0.8979 \quad \Omega/m \quad (28)$$

Since the total conductor length for the coil is about 22 m,

$$\left(\frac{R_p}{R_0} \right)_{total \ prox} = 22 \times 0.8979 = 19.75 \quad \Omega \quad (29)$$

and the total resistance per unit length (from 27) may be calculated from

$$R = \frac{\sqrt{\frac{2\pi f \mu_0}{2\sigma}}}{2\pi \times (0.6 \times 10^{-2})} [2 \times 22.16] = 0.30263 \sqrt{f} \quad \frac{\Omega}{m}, \quad (30)$$

noting that symmetry in the $|a_{mp}|^2$ numbers allows summation of half the index values to be computed (= 22.16) and that result doubled ($\times 2$).

For the subject coil antenna, selected numerical results are tabulated in Table III, where ‘‘Total R’’ is R in $\frac{\Omega}{m}$ multiplied by the conductor length 22.16 m, and loss in dB is from $10 \log \left(\frac{Total \ R}{73} \right)$. The reference normalization value of $R_0 = 73 \quad \Omega$ was chosen because we wish to consider loss relative to the 73 Ω purely resistive input impedance associated with a naturally resonant half-wave dipole.

TABLE III			
Case Study Resistance Results, $c/a = 1.667$			
Freq. (MHz)	R (Ω/m)	Total R (Ω)	Loss in dB
1.9	417.1	9177.2	20.99
3.8	589.9	12978.5	22.50
7.3	817.7	17988.5	23.92
10.1	961.8	21158.8	24.62
14.25	1142.4	25132.8	25.37
18.1	1287.5	28325.11	25.89
21.3	1396.7	30727.2	26.24

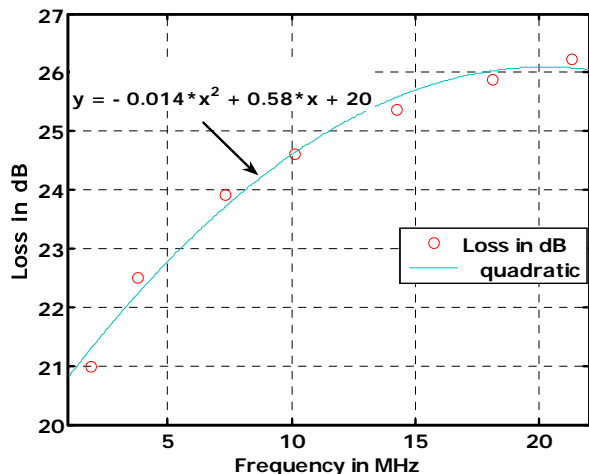


Figure 12. Proximity loss for Gates ATU coil.

As a brief but informative digression, Table IV hypothesizes about the results if the coil tubing radius a is held constant, but the turn-to-turn spacing is varied. The takeaway from Table IV is that, as expected, the proximity loss decreases as the turn spacing $2c$ is increased.

Spacing $2c$ in cm	$\frac{c}{a}$	$\frac{R_p}{R_0}$ in $\frac{\Omega}{m}$
1.5	1.25	2.507
1.8	1.5	1.238
1.92	1.6	1.005
2.0	1.667	0.886
2.04	1.7	0.834
2.4	2.0	0.526
3.0	2.5	0.295
3.6	3.0	0.190
4.0	3.333	0.150
4.2	3.5	0.134
4.8	4.0	0.099

The plausibility of the “loss in dB” figures from Table III was tested experimentally, as discussed in the following section.

XI. COMPARISON TO MEASUREMENTS AND CONCLUSIONS

The hypothesis is that NEC gain prediction by EZNEC and similar codes, even when real conductor loss is selected in the analysis program, is inadequate in the case of closely spaced parallel conductors such as in the case of the subject Gates ATU coil antenna. Further, it is asserted that the MoM numerical analysis fails to account for proximity loss, so that the addition of predicted proximity loss should give predicted gain values considerably closer to real-world signal observations.

A full measurements program has been only partially completed as of this writing. The results reported here, therefore, should be taken as significant but incomplete and reflective

of conditions that do not allow the association of meaningful error bars. However, a preliminary interpretation may be made here with reasonable reliability.

The subject coil antenna was set up in an unobstructed area, with a 130-foot long horizontal dipole (at height approximately 13 m) in the near vicinity. Received signals at selected HF bands were observed by switching the two antennas, routed through MFJ tuners for impedance matching, into a Ten-Tec Corsair II receiver. Signal strength readings were taken from the analog front-panel S-meter of the Corsair II, which was determined to be calibrated to acceptable commercial radio standards. Incoming signals were from various (often unknown) compass bearings, distances (angles of arrival), and no attempt was made to correct for pattern effects of the large dipole at higher frequencies. Small data samples were collected on some seven different days. Propagation conditions made it difficult to acquire data at 18.1 MHz, and 21 MHz was essentially dead (any signals heard on the dipole were too weak to quantify accurately on the coil) on all days available for experimentation. The available data is presented in Table V below.

Table V

Predicted versus Measured Received Signal Strengths

(A) 3.8 MHz nominal	
Number of signal measurements:	27
Average measured coil vs dipole (dB):	-38.3
Proximity loss prediction:	-22.5
EZNEC gain (dBd) prediction:	-11.4
Sum of PL and EZNEC predictions:	-33.9
Discrepancy (measured-predicted) dB:	-4.4

(B) 7.2 MHz nominal	
Number of signal measurements:	31
Average measured coil vs dipole (dB):	-20.6
Proximity loss prediction:	-23.9
EZNEC gain (dBd) prediction:	-6.7
Sum of PL and EZNEC predictions:	-30.6
Discrepancy (measured-predicted) dB:	+10.0

(C) 10.1 MHz nominal	
Number of signal measurements:	25
Average measured coil vs dipole (dB):	-20.5
Proximity loss prediction:	-24.6
EZNEC gain (dBd) prediction:	-5.25
Sum of PL and EZNEC predictions:	-29.85
Discrepancy (measured-predicted) dB:	+9.35

(D) 14 MHz nominal	
Number of signal measurements:	32
Average measured coil vs dipole (dB):	-28.3
Proximity loss prediction:	-25.4
EZNEC gain (dBd) prediction:	-4.3
Sum of PL and EZNEC predictions:	-29.7
Discrepancy (measured-predicted) dB:	+1.4

(E) 18.1 MHz nominal	
Number of signal measurements:	10
Average measured coil vs dipole (dB):	-29.4
Proximity loss prediction:	-25.9
EZNEC gain (dBd) prediction:	-3.9
Sum of PL and EZNEC predictions:	-29.8
Discrepancy (measured-predicted) dB:	+0.4

The total conductor length for the subject coil gave a natural resonance close to the 7.0 - 7.3 MHz 40-meter band. This fact likely accounts for at least part of the unexpectedly good coil performance as an antenna in this nominal frequency range. It is also noteworthy that the 10.1 MHz (nominal) measurements included several instances, at different points in time, of measurements on the time standard station WWV in Fort Collins, Colorado. Similarly, the 7.2 MHz (nominal) measurements included several measurements, at different times, of the Canadian time standard CHU on 7.335 MHz.

Overall, the results presented in Table V clearly support the merit of the hypothesis that a correction for proximity loss should be added to pattern gain predictions from NEC in order to obtain electrical performance predictions more consistent with that generally observed in actual practice.

XII. FUTURE WORK AND FINAL REMARKS

It is apparent that more measured data is required to improve confidence in the preliminary conclusion reached here, especially in the vicinity of the 7.2 and 10.1 MHz bands. Additional measurements comparing coil and dipole received signal strengths will be made in the near future.

The calculation of proximity loss assumes constant current in all the coil turns. For the specific case study here, at 3.8 MHz a free space wavelength is close to 79 m, so the 22 m of tubing used to make this coil is approximately 0.28λ . At 7.2 MHz, the coil conductor becomes approximately 0.53λ . Provision for current that is not constant could improve the results to a significant degree, and this refinement represents a second activity reserved for future work.

The collection of MATLAB code(s) required to make new individualized proximity loss calculations is not yet in a user-friendly form. Work toward having a final software product that can be made available in the public domain is continuing.

A practical finding of this work is that compact multiturn loop antennas similar to one studied in detail here may, indeed, be effective as portable/mobile antennas for HF communications if fed with coaxial line of appreciable length (at least 15 meters) without the ferrite choke assembly employed in this study to suppress currents on the coax braid. In such unbalanced operation, it has been observed that the coil plus coax system becomes competitive with a half-wave dipole.

REFERENCES

[1] *The ARRL Antenna Handbook, 19th Edition*, Newington, CT: The American Radio Relay League, 2000, Chapter 5 (especially pages 5-12 through 5-19).
 [2] Hart, T., "Small, high-efficiency loop antennas," *QST*, June 1986, pp. 33-36.

[3] Smith, G.S., "Radiation efficiency of electrically small multiturn loop antennas," *IEEE Trans. Ant. and Prop.*, Sept 1972, pp 656-657.
 [4] Best, Stephen, Advances in Electrically Small Antennas, a short course at the 2004 IEEE International Symposium on Antennas and Propagation, Monterey, CA, June 2004.
 [5] Best, S.R. and Morrow, J.D., "The effectiveness of space-filling fractal geometry in lowering resonant frequency," *Antennas and Wireless Propagation Letters*, Volume: 1, Issue: 5, 2002, p 112 - 115.
 [6] Kraus, J.D. and Marhefka, R.J., *Antennas for All Applications, 3rd Edition*, New York: McGraw-Hill, 2002, pp. 217-220.
 [7] Smith, G., "Proximity effect in systems of parallel conductors," *J. Appl. Phys.*, vol. 43, no. 5, pp 2196-2203, May 1972.
 [8] MATLAB is a registered trademark of The Mathworks, Natick, MA, web URL <http://www.mathworks.com/>.
 [9] Web URL <http://mathworld.wolfram.com/EllipticIntegral.html>.
 [10] Whipple, F.J.W., "Equal parallel cylindrical conductors in electrical problems," *Proc. Roy. Soc. (London) A* 96, 465 (1920).
 [11] Wheeler, H.A., "Fundamental limitations of small antennas," *Proc. IRE*, vol. 35, pp 1479-1484, Dec. 1947.
 [12] Whittaker, E.T. and Watson, G.N., *A Course on Modern Analysis*, 4th Edition, Cambridge, England: Cambridge University Press, 1952, Ch. 22.
 [13] Abramowitz, M. and Stegun, I.A., *Handbook of Mathematical Functions*, New York: Dover Publications, 1 June 1965, Chapters 16 and 17.
 [14] Bowman, F., *Introduction to Elliptic Functions with Applications*, New York: Dover Publications, 1981.
 [15] Andrews, L.C., *Special Functions for Engineers and Applied Mathematicians*, New York: Macmillan Publishing, 1985, p. 110.
 [16] EZNEC is a software product of Roy Lewallen, as described at <http://www.eznec.com/>.
 [17] Vinoy, K.J., Jose, K.A., Varadan, V.K., and Varadan, V.V., "Resonant frequency of Hilbert curve fractal antennas," *Antennas and Propagation Society International Symposium*, 2001. IEEE, Volume: 3, 8-13 July 2001, p 648 - 651.
 [18] Xuan Chen, Safieddin Safavi Naeini, and Yaxin Liu, "A down-sized printed Hilbert antenna for UHF band," *Antennas and Propagation Society International Symposium*, 2003. IEEE, Volume: 2, 22-27 June 2003, p 581 - 584.
 [19] Best, S.R. and Morrow, J.D., "On the significance of current vector alignment in establishing the resonant frequency of small space-filling wire antennas," *Antennas and Wireless Propagation Letters*, vol. 2, no. 13, 2003, p 201 - 204.
 [20] Vinoy, K.J., Abraham, J.K., and Varadan, V.K., "Fractal dimension and frequency response of fractal shaped antennas," *Antennas and Propagation Society International Symposium*, 2003. IEEE, Volume: 4, 22-27 June 2003, p 222 - 225.

A note from the Technical Feature Article Editor

The following paper was originally presented at the International Wire and Cable Symposium in November 2005 (www.iwcs.org). While the focus of the paper was on the cabling industry, it has been included here as a technical feature article because of its relevance to CEM. In particular, if we are comparing data visually, it does not matter whether the origin is simulation, measurements or a combination, the same cognitive processes are in play. We still want to know if one comparison is better than another one and by how much. Those cognitive processes combine tacit and explicit, academic and experiential knowledge; all of which color the decisions we make. This means that a group of experts will probably not all agree on the overall quality of any comparison. But that is not necessarily a bad thing: the more disagreement we have, the more we need to look at the comparison to understand why such a spread of agreement has resulted; the more agreement we have, the more confident we can be of the decision about whether our model has been improved, for example. In terms of trying to understand whether there has been an improvement, there is a clear need to quantify what we see, in a way that we can relate to. This means capturing opinion and looking to put a numerical value to a subjective judgment. “Quantifying experimental repeatability and simulation validation” presents some thoughts on knowledge and how the different types of knowledge contribute to a group’s decision making, how to capture and quantify the groups view of the results and how to automatically compare the results using the Feature Selective Validation (FSV) method and the Integrated Error Against Log Frequency (IELF) method. The implications for CEM validation are clear and the work presented in the paper captures a number of the underlying ideas for the IEEE’s Standard in development on validating computational electromagnetics (IEEE Project P1597).

Quantifying Experimental Repeatability and Simulation Validation

Alistair Duffy
De Montfort University
Leicester, UK

+44 (0)116 257 7056 apd@dmu.ac.uk

Kenneth Hodge
Brand-Rex Ltd
Glenrothes, Fife, UK

+44 (0)1592 778 555 khodge@brand-rex.com

Abstract

Data bandwidth requirements are continually increasing, stretching the limits of the physical channel. There is no respite in the need to continually reduce design cycles and improve product performance. The result of these two factors is that the volume of information generated during design and conformity assessment is increasing as the requirements and the complexity of the results being compared are increasing but the time available to obtain these results and process them is decreasing. There is clearly a need for tools that can be used to support the decision making of a range of professionals from design engineers to those making technical recommendations on purchasing decisions. That is, a tool that provides some quantification and objectivity for those aspects of the decision making that have, hitherto, relied on subjective judgment. This paper discusses some support tools that may find application in the cabling community.

Introduction

Until recently, cabling design was dominated by incremental changes directed by the increasing knowledge base of a handful of engineers and technicians in a number of individual companies. This picture is changing for a number of reasons:

1. Leaner companies have fewer design office staff to develop a 'group' explicit and tacit knowledge.
2. Consolidation in the industry has opened up the need for distributed design teams.
3. The push for greater bandwidth means that the designs themselves need to be able to operate much closer to much tighter limits.
4. Design cycle times are much reduced compared with a few years ago, with the resulting need to invest in, and rely on, virtual prototyping tools.
5. The higher frequencies in which cabling systems, particularly structured cabling, operate result in the graphical representation of parameters like return loss, cross-talk and attenuation being visually more complex.
6. The increase in general complexity of systems results in less clear-cut technical requirements for purchasing decisions.
7. While all measurements will be subject to errors and measurement artifacts, the fact

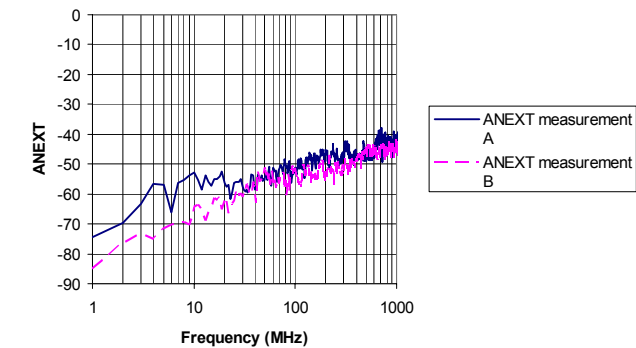
that distributed teams may be measuring the same product in several sites and comparing their results with third party measurements, the question remains: just how similar are these results?

These factors suggest a clear need for technologies that can help to compare visually complex data, allowing a quantification of what is ostensibly a subjective judgment, providing some intelligence into the physics behind the perceived artifacts and allowing a rational basis for discussion and debate. This paper addresses these issues by providing a brief overview of knowledge, how teams make use of different forms of knowledge and then reports on current work to support this interplay of knowledge in terms of visual rating of graphical data and then computer assessment of the data.

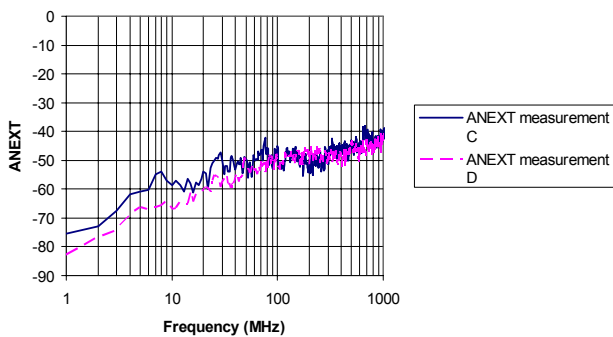
These tools are likely to have particular use for engineers who want to go beyond simple pass/fail metrics. For example, getting the right (or at least best) decision can be a little like playing hide-and-seek: it is always more helpful to be told "warmer" or "colder" rather than simply "no". A further example is in the selection of a product for installation or the selection of a modeling tool for analysis: being able to find a way of quantifying the quality of the solution compared to other vendors or the quality in terms of consistency is potentially profitable. A final

area where these tools may be applied is in quantifying the difference between a number of (virtual) incremental prototypes and a ‘golden’ product.

An illustration of this discussion can be seen by reference to Figure 1, which shows two pairs of ANEXT measurements.



(a)



(b)

Figure 1. Two pairs of ANEXT measurements (a) comparison of measurements ‘A’ and ‘B’ (b) comparison of measurements ‘C’ and ‘D’

A valid question is which of these two sets of results is better and how can we justify this decision? This may originate from a desire to determine whether two measurement protocols are more repeatable, whether either of two facilities has better repeatability, whether either of two vendors can supply more consistent cabling. In trying to generate a rule-based comparison for this data, one may be tempted to ask the following questions:

1. Is the number of maxima / minima the same?

2. If not, how many differences are there and at what frequencies?
3. What is the amplitude difference between the two data sets for each feature in the traces?
4. How close do the amplitude trends agree across the graphs

As for comparing another iteration of the design with this (or comparing measurements taken by someone else), one may be asking whether the differences have increased or decreased. For the data in Figure 1, that could mean upwards of 20 – 30 individual pieces of information, all of which would need to be weighted differently. The next question then becomes how to identify these individual metrics and their weighting, which would probably be answered by suggesting a detailed survey of a large number of engineers given a substantial set of original data to compare. This brings us on to the next point about the tools used to support the decision making: they must bear some relation to the way in which a group of engineers would approach the comparison.

In comparing the individual traces of Figure 1, anyone so doing would be unlikely to overtly create a personal rule base. The measure of the quality of the comparison will be based on an overall ‘feel’ for the data based on experience and knowledge of the system. It is likely that two general aspects of the curves will be considered. Firstly, the overall envelope of the data would be considered, so the overall level would be considered to be somewhere between ‘good’ and ‘excellent’ but the differences below 10MHz would have an impact on the final decision. Secondly, the location, depth and quantity of the ‘high – Q’ features would be considered and because there is a fairly close mapping (but some differences around the nulls) it is likely that the assessment would be ‘good’ or even ‘very good’, giving a probable overall assessment of ‘very good’. Note that the terms ‘excellent’, ‘very good’ and ‘good’ cannot be precisely defined *a priori* but only *a posteriori*, that is through usage

and application by a knowledgeable body of analysts.

This concept of definition through usage rather than through declaration can seem confusing or even confused. However, section 2, dealing with knowledge, will show how this concept is regularly used.

Knowledge [1]

Knowledge is the basis on which all decisions are made, whether they are corporate strategy or tactical technical issues. In all cases, not all the important information will be known and it is the ability to make decisions based on imperfect or conflicting information, which almost defines a good engineer.

Knowledge is often considered to be either tacit or explicit, that is, knowledge which is known but cannot be codified and knowledge which can be codified. For example, the experimental procedures are readily committed to paper but the skills of the person who can say, by visual inspection, how good a set of results is are much more difficult to access. Hermeneutic knowledge, as proposed by Heidegger, is the tacit knowledge that underpins individual and collective understanding, it shapes what we do and how and why we do it, but we may not be able to explain to others why this is the case. Hence, it is not only the tacit knowledge that has been learned as part of a job, which needs to be considered, it is also the wider background of the individuals involved. This will also be discussed briefly later in this section when discussing Sensemaking.

One model that is useful to explain how the tacit knowledge of one person can be converted to explicit knowledge and/or used to develop tacit knowledge of another is the SECI model of Nonaka and Takeuchi[2]. This model operates as:

S Socialization. Tacit to tacit knowledge sharing. The way in which tacit knowledge in one person develops as a result of the tacit

knowledge of another. A craft apprenticeship is one example of this.

- E Externalization. Tacit to explicit knowledge sharing. This is the key to knowledge creation and can be undertaken by metaphor and analogy.
- C Combination. Explicit to explicit knowledge sharing. This takes that which exists in written or other explicit form to generate new information.
- I Internalization. Explicit to tacit knowledge sharing. This is done by practicing what exists in written form by, for example, verbalization or creation of diagrams.

Taking, for an example, the comparison of measurements to assess repeatability, tacit knowledge sharing could come through an experienced engineer showing ‘good’ and ‘bad’ results to a less experienced engineer. This ‘socialization’ allows the experience of the one to pass to the other without being expressly stated. An element of externalization will occur when the less experienced engineer seeks to identify why one comparison is ‘good’ or ‘bad’ and, by query and enquiry, some rules emerge. Combination would then occur when these rules are shared with a wider audience or are built into procedures. Internalization would happen when the less experienced engineer took this set of rules and, through experience integrated them with the tacit knowledge developed from the experienced engineer. In the case of Figure 1 and the associated discussion, the development of the rule-base would be an example of “Combination”, but the more common occurrence of one engineer showing this to a less experienced one and saying simply “this is a good comparison”, with only a few observations, would be “Socialization”

Other writers [3] on the subject suggest that there can be no direct translation between tacit and explicit knowledge. They further suggest that groups as well as individuals may possess tacit knowledge and what an individual does is shaped by their own tacit knowledge, the explicit

knowledge to which they have access, the tacit knowledge of the group to which they belong in this instant and the explicit knowledge to which the group has access. The combination of these factors results in “knowing as action”; essentially what is done by the individual and/or the group reflects the combined knowledge, both tacit and explicit, of the individual and the group. The model does help to explain how the outcome of analyzing the measurements by a group of engineers can differ to that when the results are compared by each engineer individually: the group possesses a different level of tacit knowledge to that of the individual. Figure 2 presents this illustratively. In addition to the knowledge of the individual, “Genres” refers to common understandings or behavior by the group, such as ignoring deep nulls in a graph but concentrating on the amplitude of the peaks, this action may not be overtly recognized, but everyone does it. Explicit group knowledge is represented by the standards to which everyone is working or stories emanating from the tacit group behavior.

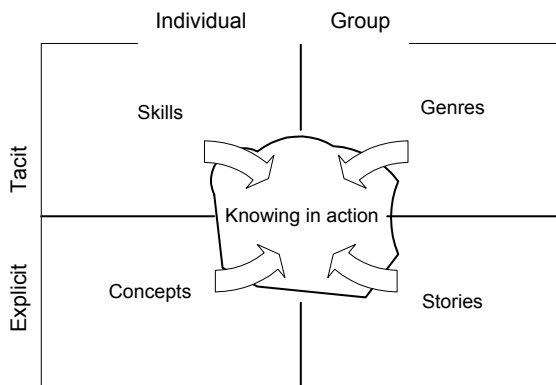


Figure 2 Knowing in action (adapted from [3])

The management of knowledge is the “explicit and systematic management of a vital resource and the process of creation, organization, diffusion, use and exploitation”. Put another way, knowledge is a corporate asset, linked to organizational objectives and priorities, which is too important to leave to chance. Knowledge

management can be thought of as dividing into three categories:

- Creating and discovering,
- Sharing and Learning,
- Organizing and managing.

The process of data comparison largely falls into the category of sharing and learning as the engineers involved are predominantly discussing their interpretation of the data, trying to identify how others deal with the data and agreeing on the decisions that are made as part of the data comparison. One particularly important ‘structure’ which can enhance the knowledge sharing is the *Community of Practice*. These are self-organizing, largely informal, networks with a shared purpose; its members may not even formally know its existence. The encouragement of these within an organization and, where possible, across organizations working in the same area, could be one significant means of developing an understanding of how the data is compared, why decisions are made from these comparisons in the way that they are, and how technologies and techniques can be developed to assist in the rigor of the decision making process. As they are informal social networks with shared purpose, it is important that there is a high level of mutual trust which goes beyond the formal structures. In fact, Communities of Practice usually exist in a way which can span organizations and the layers within an organization in a way that would be difficult to create formally. A factor which is particularly important as cabling organizations become more geographically dispersed. The management of the communities involves providing conditions to encourage social links and provide or encourage leadership in learning and enquiry, thus let informal links thrive. Some initiatives to promote these structures [4] include formal and informal events at which possible members can network, the introduction of learning project (providing new knowledge such as new comparison techniques) or managing the artifacts produced by a community (such as software,

reports or papers). It is important that this sharing is undertaken at the right time; when engaged in a task *it is better to meet to do it rather than to meet to talk about it*. One technique that does help in the sharing of tacit knowledge is the exchange of ‘war stories’, the events organized as part of the support of a community of practice would be well placed to encourage this.

Some other approaches to sharing and developing knowledge are:

- Learning Networks. Rather more formal than the communities of practice, these are set up with the express intention of learning from each other and from outside the field of endeavour.
- Sharing Best Practice. It may be appropriate to instigate ‘master-classes’ to encourage those who are regarded as expert to share their knowledge with others.
- After Action Reviews. These started in the US military as a way of understanding the way in which decisions were made and actions taken. They are non-threatening and non-judgmental and are a positive way of learning from past actions and identifying both best and worst practice. The emphasis is on doing better next time rather than trying to identify how it could have gone better last time.
- Structured Dialogue and Interviews.
- Share-fares. Application of these in this setting may involve bringing examples of good practice to a general meeting and allowing ‘delegates’ to investigate other approaches to a problem in a more formally organized setting (although the actual interaction could be quite informal). One aim of these could be to encourage access to the many sources of knowledge held within an organization. Such knowledge could be held in the more formal structures such as libraries,

within the culture of the organization (culture being “the way we do things round here”), transformations of information or of physical artefacts (referring to processes and procedures), structures within the organisation (roles and responsibilities), ecology (setting that shapes behaviour, such as the way the R&D department is physically laid out).

- Cross-functional Teams. One way to identify how and why someone has done what they did is to ask the naïve questions and challenge the basis on which this was done. One way of doing this is to build cross-functional teams, which, in this case, would not just include high frequency or electromagnetic engineers but may also include those involved in a marketing function. One rule which must be adhered to is that all members of a cross-functional team bring as much as they take; although it should be noted that the form of give and take may be different.
- Decision Diaries. Engineers are generally good at learning by doing and learning from experience. The effect of this is that the background to, and the reasons for, certain decisions being taken may not be initially obvious. This has the disadvantage that it is more difficult for less experienced engineers to learn from them and the development of knowledge technologies can be hampered by limited, or assumed, information. Decision diaries, or a critical analysis in a log book of how decisions were taken, where a personal post mortem is undertaken can help to alleviate this minimal information. It also has the effect of improving self examination, possibly minimizing the effects of progressively developed ‘bad habits’.

Having considered a number of related concepts in the management of engineers’ knowledge, one

of the most important aspects of knowledge in practice is Sensemaking, i.e. turning data into action. One of the difficult aspects of this is to access the tacit knowledge of the members of a group. Some aspects, which may have relevance to the problem being considered, namely communities of practice and the SECI model, have already been outlined. The problem with trying to access tacit knowledge was summed up by Polyani as "We can know more than we can tell". Those doing data comparisons 'do it' but may not be able to describe how, what or why to others – this is a clear example of their tacit knowledge. There is a clear need to access this in order to codify the processes or ensure everyone does the same thing. (We must, however, be aware that “we know more than we are willing to tell.”)

In the previous discussions, knowledge and information have been used in a loosely interchangeable manner. One concept, which helps to clarify any differences, and also clearly reviews the relationship of knowledge with, for example, data is the knowledge hierarchy. It also helps, perhaps, to identify at what level the sharing of abilities is required.

Data are the observations made as part of an experiment: the cross-talk readings for example. Information can be thought of as data with context. Not only do we possess the cross-talk readings, but those readings are referred to the product under test, the test method and the standard's limit lines.

Knowledge is the information with meaning. Knowledge is the interpretation of that information e.g. trying to identify the causes of good / poor performance.

Wisdom is knowledge with insight. Perhaps the interpretation of the data with the details of the measurements known can lead to conclusions about the test method or the expectation of the

behavior of, for example, the installation being tested.

If the requirement is only to share data or information, then this need only be supported by information technology, which simply helps in the representation of this data. If, however, knowledge or wisdom is required to be shared, knowledge technologies need to be investigated. The difference between the two is that while information technologies simply support the representation of the data, knowledge technologies support the interpretation of the data. An example of this could be that Excel[®] can provide an easily customized data representation, the visual rating chart to be discussed next in this paper provides a framework to access the individual's tacit and explicit knowledge without constraining their opinions and the Feature Selective Validation (FSV) method discussed later in this paper supports the interpretation of the differences between two sets of data.

If groups of people from different backgrounds and companies are involved in the comparison, it is essential that differences between the individuals be accounted for. These differences may include background, experience, expectation and expertise. This is important because it is likely that this difference may mean that the 'sender' and 'receiver' of the message will interpret the message in different ways. This is a further example of the importance of accessing the tacit knowledge of the individuals and the groups to which they belong in order to turn received 'data' into useable information.

So far, this paper has discussed some pertinent knowledge management models and has looked at the way in which the original data can be made sense of. The next section addresses some of the key management issues involved in knowledge management.

Visual rating [5]

As discussed in the previous section, quantifying comparisons of data for measurement repeatability or for validation requires the capturing of knowledge, both tacit and explicit. Some aspects of a good or poor comparison can be specifically stated but in many other aspects, it is a case of 'I know a good comparison when I see it'. It is important that any approach used to support quantifying data comparisons is compatible with this concept. That is, the group response and the individual response should both be accessible. To do this, a visual benchmark was developed [6]. The individuals will categorize a comparison according to the binary decisions, resulting in six quantified and qualified categories. The resulting rating scale is shown in Figure 3.

The group response can then be determined by taking the mean (or median as desired) of the collection of individual responses. It is important to appreciate that the various experiences and backgrounds of the individuals will produce a variety of responses and, as there is no 'universal truth' because, for an educated and informed group, all responses are equally valid. The breadth of responses can say as much about the data being compared as the mean response itself. A group response that is highly focused on one category would suggest a high confidence in ascribing that category to the comparison. A group response that is equally spread over several categories gives a low confidence that a single category is sufficient to summarise the comparison. Or put another way, a wide spread of opinion suggests that there is a lot of scope for debate and argument, whereas a smaller spread of opinion is clear-cut. One important aspect of a visual rating tool is that it should not force users into giving an accepted answer. As a consequence, it should maintain the group mean rating (comparing results with and without using the scale). A further consequence of such a rating scale is that because it provides some

guidance, outlier opinion can be reduced without altering the overall average response for the group.

The choice of a six point scale is important because it results in a simple structure without excessive detail (as would result with a 10 point scale). Anything other than a binary decision tends to result in the middle option(s) being favored compared with those at the extremes, which introduces an extra (pseudo-)Gaussian confounding factor

A cursory review of the data in Figures 1(a) and 1(b) may suggest that comparison C-D is better than A-B. However, the visual rating scale encourages a more probing review. Using the Visual Rating Scale of Figure 3 on the data of Figure 1, both graphs would probably be regarded as 'Fair'. First, consider graph 1(a), while there is quite a difference in amplitude below about 20 MHz, the region between 20 MHz and 100MHz agrees well, there is a slight offset between 100 MHz and 400 MHz but above this, it is difficult to separate the curves. In general, above approximately 30 MHz, it is difficult to separate individual features. Secondly, consider graph 1(b), despite the offset, the general shape between the two measurements agrees quite well up to approximately 50 MHz, there is a clear difference between about 60 MHz and nearly 100 MHz but some differences in the trends above this as the 'envelopes' oscillate around each other. Thus, it would not be unexpected for each graph to be considered as having 'Reasonable agreement over many portions of the data'. A good case could probably also have been made to say that there is 'generally good agreement across the data' Depending on the background and interests of the engineers involved in assessing the data, some may regard the comparisons as having 'minor variations' and other 'minor agreement'. Hence, on that basis, it is difficult to separate the overall comparisons.

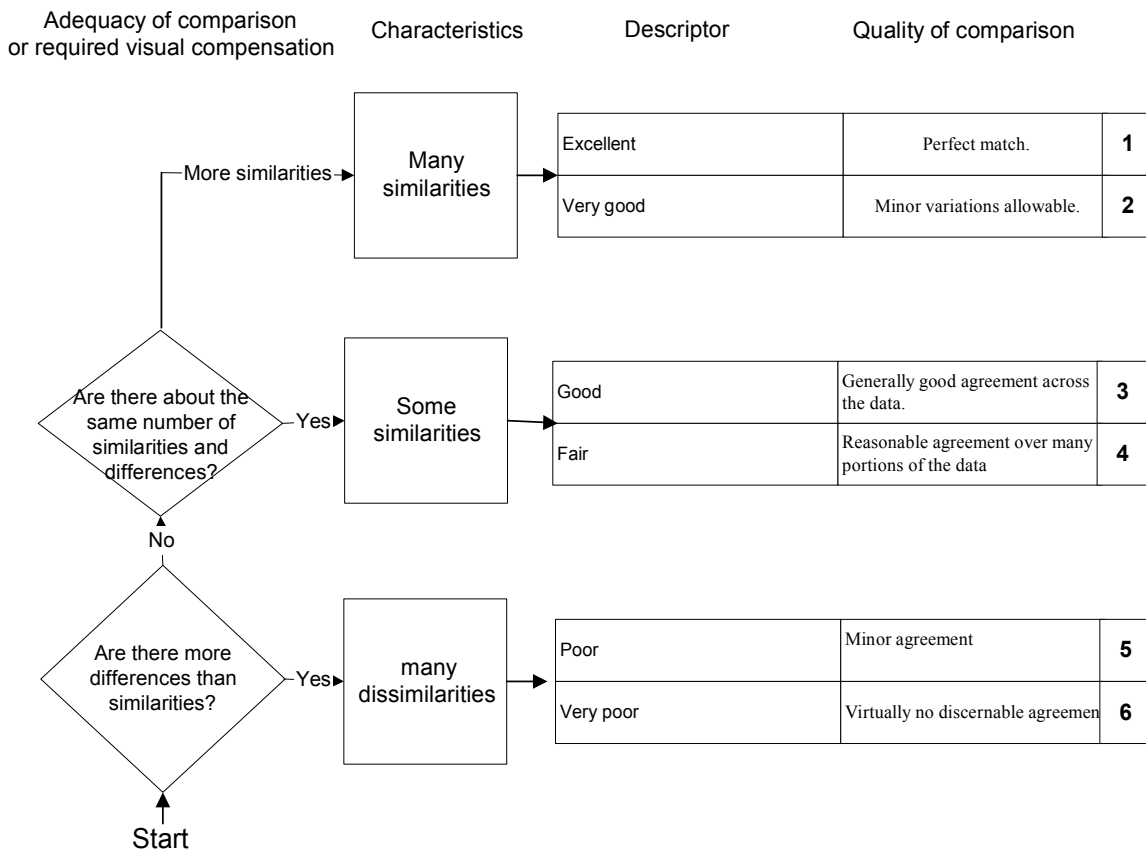


Figure 3 Visual rating scale (from [6])

Computer based assessment [7]

Having seen how individual and group knowledge can be accessed by using a simple rating chart, the next issue is can the data be processed automatically to achieve a similar level of information. Given the large quantities of data to be compared and the option to use optimization techniques in design which requires an objective measure of similarity (or fitness) [8], a computer based approach is very attractive. One such technique which is currently being considered as part of a forthcoming IEEE standard [9] is the Feature Selective Validation (FSV) method [10].

Initial development of the FSV technique was prompted by the need for error determination in the validation of numerical models against

experimental data, the desire to assess the effects of incremental design changes on numerical models and the benefits coming from being able to quantify experimental repeatability. The main prompting factor was that there existed no other acceptable way of comparing the data. The common thread that ran through visual inspections was that two aspects of any visual data were considered and combined into an overall judgment. These were the envelope / trend of the data and any resonance like structure (these are referred to here as ‘amplitude’ and ‘feature’). The FSV decomposes the original comparison, by initially Fourier transforming the data sets, into components that contain the amplitude and trend information and components that contain the feature information. These are the Amplitude Difference Measure (ADM) and the Feature Difference Measure (FDM).

These are taken as independent functions and combined into an overall goodness of fit measure, the global difference measure (GDM).

All of the ADM, FDM and GDM are usable as point-by-point analysis tools or as a single, overall, measurement. The point by point analysis allows clear identification of the aspects of the initial data which are primarily responsible for the degradation of the comparison in a way which is objective and can be readily communicated. The overall comparison value gives a similarly objective interpretation of the overall agreement. The ADM and FDM are obtained using the following equations.

$$ADM(f) = \frac{|(Lo_1(f)) - (Lo_2(f))|}{\frac{1}{N} \sum_{i=1}^N (|(Lo_1(i))| + |(Lo_2(i))|)} \quad (1)$$

$$FDM_1(f) = \frac{|Lo_1'(f)| - |Lo_2'(f)|}{\frac{2}{N} \sum_{i=1}^N (|(Lo_1'(i))| + |(Lo_2'(i))|)} \quad (3)$$

$$FDM_2(f) = \frac{|Hi_1'(f)| - |Hi_2'(f)|}{\frac{6}{N} \sum_{i=1}^N (|(Hi_1'(i))| + |(Hi_2'(i))|)} \quad (4)$$

$$FDM_3(f) = \frac{|Hi_1''(f)| - |Hi_2''(f)|}{\frac{7.2}{N} \sum_{i=1}^N (|(Hi_1''(i))| + |(Hi_2''(i))|)} \quad (5)$$

$$FDM(f) = 2(|FDM_1(f) + FDM_2(f) + FDM_3(f)|) \quad (6)$$

where Lo_1 and Lo_2 are the intensities of the low frequency components of the data sets 1 and 2 at data point f . This is obtained by Fourier transforming the data and inverse transforming the lowest 40% of the data.

Hi_1 and Hi_2 are the high pass component of the data sets, obtained by Fourier Transforming the data sets and inverse transforming the highest 60%. The single primes (') indicate the first derivative of the inverse Fourier transformed data sets with respect to the x-axis and the double primes (") indicate the second derivative of the inverse Fourier transformed data. A simple central-difference-based scheme has been used to determine the first and second derivatives.

It should be noted that summing for the ADM and the FDM point-by-point values overall quantitative values of these components can be obtained. The single values allow ready overall assessment and the point-by-point values allow easy identification of regions of poor comparison, which dominate the overall similarity rating. While this is not terribly important for simple structured results, it is very useful for busy data. The main benefit of the point-by-point results is that these can help to identify regions where attention needs to be focused during validation of the model or in the post-mortem phase.

The Global Difference Measure (GDM) is then obtained as either a single figure of merit

$$GDM = \sum_{f_{min}}^{f_{max}} \sqrt{(ADM(f))^2 + (FDM(f))^2}$$

or as a point-by-point result:
or

$$GDM(f) = \sqrt{(ADM(f))^2 + (FDM(f))^2} \quad (7)$$

Natural language descriptors have been assigned to the output from this technique and are useful in communicating the results in a meaningful way. It should be noted that there is not theoretical maximum value for the FSV technique, although most comparisons fall into the range 0 (there is no difference between the data sets) and about 2 (excursions much beyond this are possible, but rarely for an overall comparison). The relationship between the numerical values (for ADM, FDM and GDM) and the natural language descriptors is given in Table I.

Table 1 FSV interpretation scale

FSV value (quantitative)	FSV interpretation (qualitative)
difference ≤ 0.1	Excellent
$0.1 < \text{difference} \leq 0.2$	Very good
$0.2 < \text{difference} \leq 0.4$	Good
$0.4 < \text{difference} \leq 0.8$	Fair
$0.8 < \text{difference} \leq 1.6$	Poor
difference > 1.6	Very poor

It will be noted that the natural language descriptors used here correspond to the categories used in the visual rating scale. Probability density functions for the ADM, FDM and GDM, essentially the proportion of the point-by-point analyses within a particular qualitative category, which appear to mimic the spread that would be obtained by a group of engineers. Initial results for the FSV are very encouraging [5].

The FSV is particularly useful where the results to be compared are visually complex (that is, they could not be described to a third party with a single paragraph of text) but where individual features can be clearly discerned. Where individual features cannot be clearly discerned, but the envelope can, the Integrated Error against Logarithmic Frequency (IELF) method may be more suitable.

The (IELF) method [11] is based on the premise that in comparing data with a very high feature density, the overriding factor to be assessed is a function of the difference between the two traces. A single figure is obtained for comparison purposes by integrating (summing) the difference over the frequency range taken on a logarithmic axis. The same technique can also be applied to frequency bands (sub-frequencies), where there is a particular physical or system-dependent driver for doing this. The basic IELF equation is given in equation 8.

$$IELF = \frac{\sum_{i=1}^{n-1} |error_i| \cdot \{\ln(f_{i+1}) - \ln(f_{i-1})\} / 2}{\ln(f_n) - \ln(f_0)}$$

(8)

Where f are the frequency points being compared (from point 0 to point n , resulting in $n+1$ discrete frequencies), $|error_n|$ is the difference between the two data sets at the n^{th} data point.

A small modification to the IELF involves summing the elements halfway between the data points in order to improve the approximation to the difference in the measured data. This modification is given in equation 9.

$$IELF \text{ mod} = \frac{\sum_{i=1}^{n-1} |error_i| \cdot \{\ln(\frac{f_{i+1} + f_i}{2}) - \ln(\frac{f_i + f_{i-1}}{2})\}}{\ln(f_n) - \ln(f_0)}$$

(9)

As with FSV, in the IELF method, a value of zero indicates a perfect comparison. There is no upper limit on the quality factor produced, which enhances its ability to discriminate differences in overall quality for poor comparisons as well as for close comparisons.

With reference to the data of Figure 1, the IELF method, using equation 8 gives a value for Figure 1(a) of 7.8 and for 1(b) of 5.5. Clearly suggesting that 1(b) is better – although the lack of scaling does not allow a more absolute level to be gauged nor a conclusion drawn as to how much it is better. Figure 4 compares the differences on which the IELF values are based.

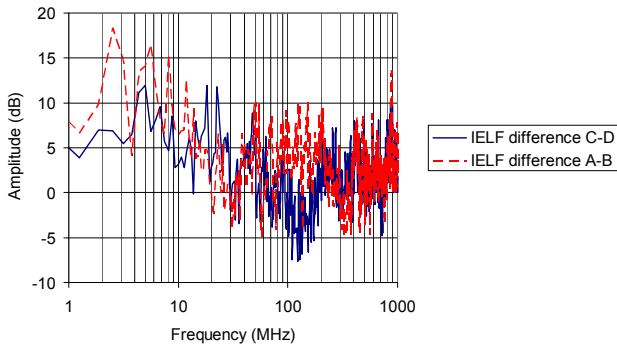


Figure 4 IELF differences

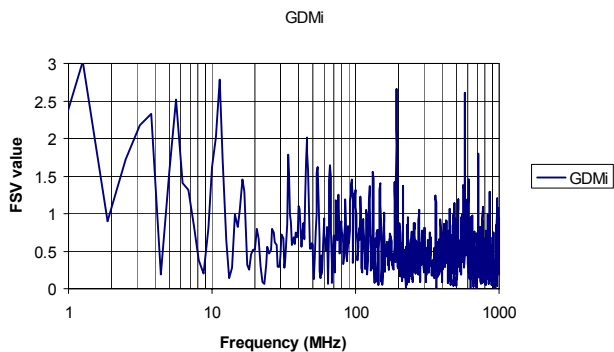
One observation from the differences is that the comparison C-D has less error below approximately 20 MHz and between 50 MHz to 200 MHz than comparison A-B.

Applying the FSV routine to these comparisons gives the values for the ADM, FDM and GDM as in Table 2

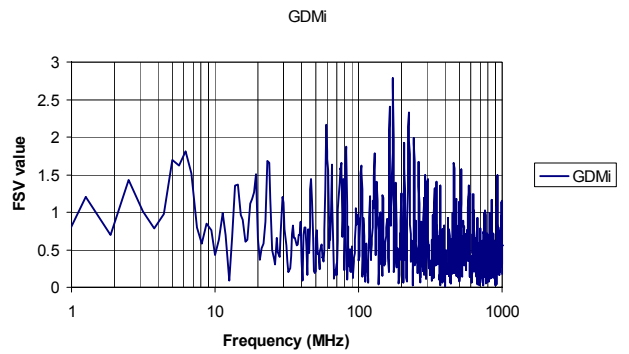
Table 1 FSV values for the data of Figure 1

	Comparison A-B	Comparison C-D
ADM	0.24 (Good)	0.26 (Good)
FDM	0.42 (Fair)	0.43 (Fair)
GDM	0.52 (Fair)	0.55 (Fair)

So the FSV routine suggests that there is not much difference in the original comparisons overall, but A-B has a slight advantage. The reasons can be seen with reference to Figure 5, the point by point analysis of the Global Difference Measure.



(a)

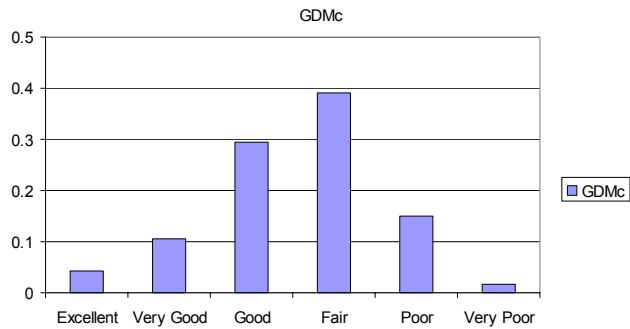


(b)

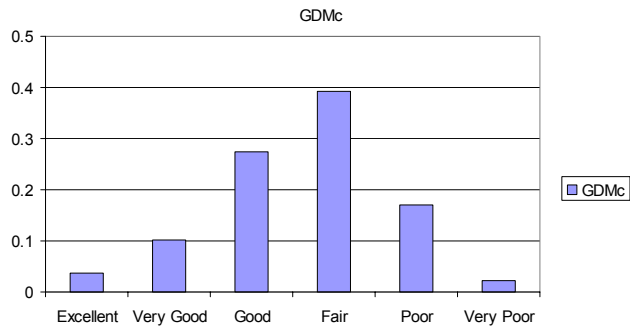
Figure 5 FSV Global Difference Measures (a) for Figure 1(a) and (b) for Figure 1(b).

This is particularly important in that it shows that above approximately 70 MHz comparison A-B (figure 5(a)) is more consistently between 0.5 and 1 – 1.5 but the comparison C-D alternates between regions of very low GDM to regions actually higher than for comparison A-B. An important factor is that comparison C-D is better below approximately 20 MHz than comparison A-B. A benefit of the point-by-point analyses is that they can help to direct efforts intended to improve the comparisons, measurements, or models and thereby marshal limited resources. Considering Figure 5(a), FSV is drawing attention to the lower frequency differences (<10 MHz) and to two features at ~ 200 MHz and 600 MHz: it would be helpful to investigate these first. For Figure 5(b), interest in the differences around 200 MHz should be considered.

Given the observation that the confidence histograms show broad agreement with the overall opinions of groups of engineers, it is instructive to review the FSV data and compare back to the initial observations of the visual rating scale. Figure 6 shows the confidence histograms for the data of Figure 5.



(a)



(b)

Figure 5 FSV Global Difference Measure Confidence Histograms (a) for Figure 5(a) and (b) for Figure 5(b).

The initial observation is that there is marginally more of Figure 5(a) that would be regarded as being ‘Good’ and slightly less ‘Poor’ and ‘Very Poor’. The important point here is that the broadness of the histograms suggest very little emphasis should be placed on the second decimal place.

Discussion

This paper has described a number of approaches to quantifying what may normally be a subjective assessment of data using a visual rating scale, the Integrated Error against Log Frequency (IELF) method and the Feature Selective Validation (FSV) method. The advantages of each have been introduced. Testing the approaches involved a difficult challenge of identifying which of two pairs of data has a better comparison. A brief visual review of the data would suggest Figure 1(b) to be better. However, a more detailed visual

review, supported by the visual rating scale, made the decision much more difficult, i.e. it would be difficult to decide between the two using the visual rating scale (although this would only be a proper test if it involved a statistically significant group size) but it helps to justify why the decision is difficult. The IELF method said that C-D was a better comparison but there is no absolute scale, so it is difficult to judge by how much. FSV suggested that A-B is a better comparison, but by very little.

It should be noted that FSV works on a linear rather than logarithmic scale in its current implementation but the results were plotted on a logarithmic scale for consistency; IELF is naturally based on a logarithmic scale.

What this paper has shown is that there are tools available that can help in quantification, and therefore in objective decision making. There is no single ‘right’ approach but a significant benefit of using any / all of these approaches is that it encourages an objective discussion about the data which fosters a combination of the individual’s tacit and explicit knowledge coming to play in the individual’s contribution to the overall opinion of a group.

Acknowledgements

The work reported in this paper is the subject of international interest, particularly within the EMC community. It gives the authors pleasure to acknowledge the ongoing support, contributions and critical dialogue of Professor Antonio Orlandi (University of L’Aquila, Italy), Dr Anthony Martin (MIRA Ltd, UK), Dr Dawn Coleby (University of Leicester, UK), Dr Bruce Archambeault (IBM, NC, USA), Dr Andrew Drozd (ANDRO Computational Solutions, Rome, NY, USA), Dr Christopher Jones (BAE Systems, Warton, UK) and Professor Robert Simpson (Simtronics Ltd, Preston, UK)

References

- [1] AP Duffy, “EMC Comparison: A technical problem or a knowledge

- management issue?", Zurich EMC Symposium, 2003
- [2] I. Nonaka and H. Takeuchi, "The knowledge-creating company: How Japanese companies create the dynamics of innovation", 1995, Oxford University Press.
- [3] SDN Cooke and JS Brown "Bridging epistemologies: the generative dance between organizational knowledge and organizational knowing", Organizational Science, 1995
- [4] E Wenger, "Communities of Practice", 2000, Cambridge University Press.
- [5] B Archambeault, S Connor, A Duffy, "Comparing FSV and human responses to data comparisons", IEEE International Symposium on EMC, Chicago, 2005.
- [6] DE Coleby and AP Duffy, "A visual interpretation rating scale for validation of numerical models", International Journal for Computing and Mathematics in Electrical and Electronic Engineering (COMPEL) in press.
- [7] A Duffy, A Martin, G Antonini, A Ciccomancini Scogna, A Orlandi, "Issues in validation of complex valued simulations for signal integrity analysis" IEEE International Symposium on EMC, Santa Clara, 2004
- [8] C Dole, H Sasse, A Duffy "Particle swarm optimization for broadband coaxial cabling", 2004 IWCS, Philadelphia.
- [9] http://grouper.ieee.org/groups/emc/emc/ieee_emcs_sdcom/p1597/ieee_emcs_sdcom/p1597/ieee_emcs_p1597_main.htm
- [10] AJM Martin, "Quantitative data validation (Automated visual evaluations), PhD Thesis, De Montfort University, UK, 1999.
- [11] RJ Simpson, CR Jones, I MacDiarmid, A Duffy, D Coleby, "The Integrated Error against Log Frequency (IELF) method for CEM validation", IEEE International Symposium on EMC, Chicago, 2005.

Author biographies

Alistair P. Duffy was educated at Conyers School, Yarm; University College, Cardiff, and Nottingham University. He is currently a Principal Lecturer in Communication Engineering at De Montfort University, Leicester. Particular research interests include experimental, numerical and analytical applications for electromagnetics. Particular emphasis for this in recent years has been in communication cable design and analysis. Other aspects of this interest include microwave and rf heating and novel antennas. A substantial interest is in the formal comparison of complex data sets.

Kenneth G. Hodge holds a BEng from Liverpool University and an MSc from Warwick University. He is currently a representative to BSI and CENELEC committees working on LAN cabling. Ken has been working in the cable industry since 1982, he was initially involved with the development of optical and copper data communication and telecommunication cables, then transferred to the R&D facility as Design Manager Optical Cables. He is now Technical Manager at Brand-Rex (Part of Honeywell).

Numerical Analysis of IEEE Project 1597.1 Validation Problems

G.Antonini, M. Italiani, A.Orlandi

UAq EMC Laboratory
Dept. of Electrical Engineering
University of L'Aquila
L'Aquila
Italy

1. INTRODUCTION

There is no doubt that the actual computational electromagnetic (CEM) scientific community is concerned about the validation and verification (V&V) [1] of the results generated by the numerical simulations. This attitude is justified by the need for reliable technologies and repeatable methods for assessing the electromagnetic performances of complex systems and/or devices. This is the reason of the IEEE Project 1597.1 aiming to develop standards for CEM computer modeling and technique validation [2,3]. Inside of this Project, a number of standard electromagnetic compatibility (EMC) and signal integrity (SI) problems have been identified and translated into models to be analyzed by means of different CEM techniques.

In this work, three of them have been selected and used to analyze the impact of the variation of some geometrical properties or simulation parameters' settings on final results. They can be, for example, size of aperture, number of aperture, component placement on PCBs, mesh size and density, etc. The three benchmarks investigated cover a range of applications from a standard shielding problem, to a typical PCB structure up to a meandered line very often encountered in SI analysis.

In the first benchmark, dealing with the shielding properties of a metallic enclosure, it has been investigated the sensitivity of the numerical outputs to the characteristic of the discretization grid used for the numerical analysis. The second benchmark considers the impact of the correct numerical modelling of the reference plane in a PCB structure when a slot is open in this plane. Finally, the third benchmark looks on how the modelling of the meander, of the reference plane and of the substrate can change the results obtained by numerical analysis.

The numerical simulations have been performed by using CST STUDIO SUITE 2006 [4], a software based on the Finite Integration Technique (FIT) [5].

The Feature Selective Validation (FSV) technique [6,7] is used as conceptual tool for the data comparison between different simulations. This technique is one of those mentioned in the IEEE Project 1597.1. In the next section, the FSV technique is briefly recalled and the main figure of merits used along this paper explained and commented.

2. THE FEATURE SELECTIVE VALIDATION (FSV)

The Feature Selective Validation (FSV) techniques aims to perform the comparison of different datasets by mimic the behaviour of a group of experienced engineers when they perform such a comparison by means of a visual approach. [5],[6].

The FSV method is based on the decomposition of the original data into two parts: amplitude (trend/envelope) data and feature data. The former component accounts for the slowly varying data across the data set and the latter accounts for the sharp peaks and troughs often found in CEM data. The numerical figures of merit obtained as output from the FSV procedure can be converted in a natural language descriptor (excellent, very good, good, fair, poor, very poor comparison). In the two references mentioned above it is described the rigorous theory behind this method. In the following it is only reported the essential meaning of the FSV figures of merit used along the text.

They are:

ADM (Amplitude Difference Measure) and FDM (Feature Difference Measure) which are two figures of goodness-of-fit between the two data set being compared. The former quantifies the comparison of the trends of the two datasets (the slowing varying shapes of the data), the latter quantifies the comparison of the rapidly changing shapes of the data (the features). Their point-by-point numerical values can be converted in a natural language descriptor scale. These single figure goodness-of-fit values combine to give the GDM.

GDM (Global Difference Measure) which is an overall single figure goodness-of-fit between the two data sets being compared. This allows a simple decision to be made about the quality of comparison. This may be numerical or converted to a natural language descriptor (excellent, very good, good, fair, poor, very poor). This is obtained from the overall figures for the two components, the amplitude difference measure and the feature difference measure.

GDMc, ADMc, FDMc which give a probability density function which shows the proportion of the point-by- point analyses of each of the components that falls into the six natural language descriptor categories. These figures of merits (the “c” stands for “confidence”) provides a measure of confidence in the single figure comparison, giving some information as to how much emphasis can be placed on the single figure of merit.

While the mean value of the ADM and FDM (and subsequently the GDM) provides a single figure goodness-of-fit measure, there are two aspects of the confidence histograms that help in the interpretation of the confidence histograms. These are:

1. How concentrated the histogram bars are at one extreme or the other.
2. How dispersed the histogram bars are around the mean value.

Both of these can help in deciding whether it is reasonable to give both the ADM and the FDM a similar level of importance or whether to concentrate more on one or the other.

It has been proposed in [Barcellona 06] that these two elements can be combined by using a Grade-Spread chart which gives a numerical value to the Grade by counting how many categories are required (starting from Excellent) for the cumulative total of the histogram to exceed a given value. A numerical value is given to the Spread by counting how many adjacent categories (starting from the largest) are required to cumulatively exceed a given value. A default value for both the grade and spread has been set at 85% in producing this paper, but this may be varied according to requirements. For example, consider the GDM values of Table I due to the comparison of a pair of data sets.

Table I – Numerical values for GDM

Category	Value
Excellent	0.1
Very Good	0.15
Good	0.3
Fair	0.21
Poor	0.24
Very Poor	0

To obtain the Grade, start with the Excellent category and cumulate a total as categories are added. For an 85% total, the Grade is Excellent – Poor, i.e. 5 categories and therefore a Grade of 5. To obtain the Spread, start with the highest category (in this case Good) and add the adjacent highest values categories to obtain 85%, in this case Good + Fair + Poor + Very Good > 85%, so therefore the Spread is 4. These values can be presented graphically on a Grade-Spread Chart. Where the Grade gives a visual indication of the quality of the comparison and the Spread gives a visual indication of the level of confidence that can be placed on this assessment. It emphasizes that a wide Spread gives a poorer overall quality of result than a wider Grade. This, implemented for the data in Table I gives the chart in Fig. 1a.

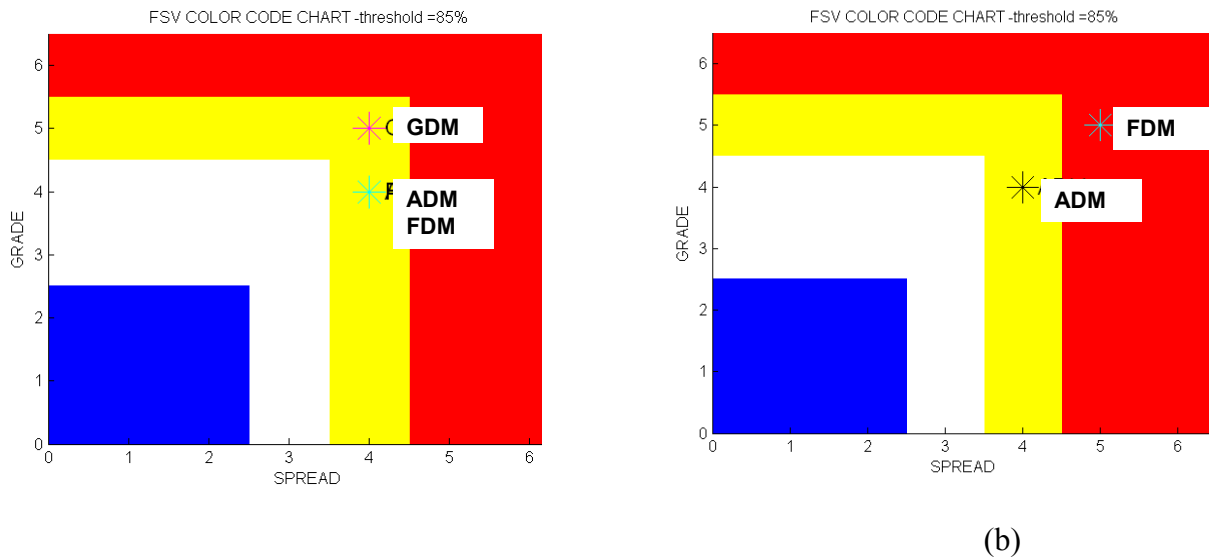


Fig. 1 – (a) Grade-Spread chart of ADM, FDM, GDM for the original data in Table I, (b) Grade-Spread chart of ADM, FDM.

In Fig. 1a ADM and FDM are identical (Yellow) which suggests that they should both be given equal weighting. Subsequently, if this was part of a validation process, movement from Yellow to White or Blue would suggest that there has been an overall improvement in the performance. Considering now the Grade-Spread Chart given in Figure 1b, the figure gives a visual indication of the relative quality of the FDM measure compared with the ADM measure suggesting that in analyzing the data, more emphasis should be given to the ADM. In a practical sense, this may mean that the FDM could be overtly de-rated in discussions about the quality of the comparison or that when looking to improve the simulation or the experiment on which this result is based, analysis of the point-by-point data of the ADM could be considered in preference to the GDM or ADM and

FDM together. In the next chapters, some IEEE Project 1597.1 models will be considered and analyzed.

3. A SHIELDING STANDARD PROBLEM

Shielding effectiveness of an enclosure is a complex matter, in which a lot of different phenomena are involved; for example, electrical and geometrical parameters of the material of the walls, apertures and grids, joints and contacts (connections) (including the use of gaskets, springs, overlaps,...), internal and external cabling and cable feed-through or connectors, and internal boards and backpanels. In most cases, the total shielding effectiveness is determined by the combination of all these effects, some with greater impact than others. As a consequence, determining the shielding effectiveness of a real enclosure is not a simple matter. In order to investigate the effects of simulation settings on numerical results, a complex metal enclosure has been defined, as is shown in Fig. 2. This enclosure includes an internal source, and apertures with different holes sizes.

They have been considered the enclosure in two different configurations: with small holes (see Fig. 2) and with a single large hole as in Fig. 3.

The aim is to compute and compare the magnitude of the electric field at a distance of 3 m by front side of the enclosures for different mesh settings. For both cases different mesh settings have been used and then the comparison of the results varying the mesh are shown. The detailed description of the whole system follows below.

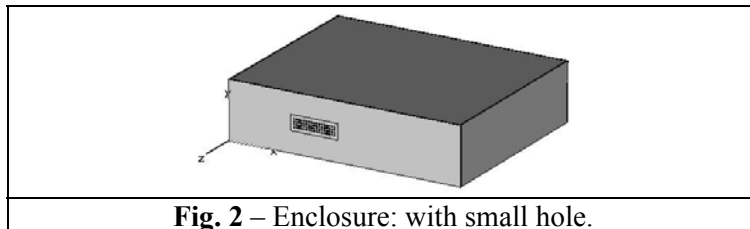


Fig. 2 – Enclosure: with small hole.

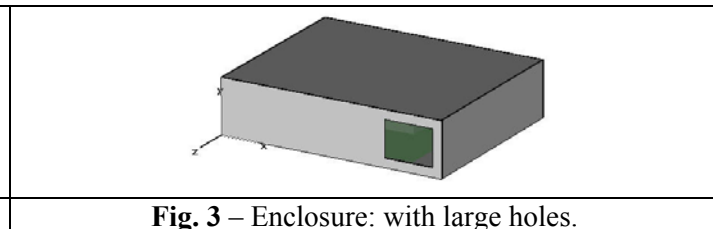


Fig. 3 – Enclosure: with large holes.

The geometrical dimensions of the entire structure are shown in Fig. 4. The analysis has been performed in the frequency range 0.1GHz - 2GHz.

Enclosure Dimensions and Materials (see Fig. 4):

The enclosure is 370 mm x 90 mm x 300 mm (x , y , z axis); walls' thickness is 2 mm; all enclosure walls are made up of Perfect Electric Conductors (PEC).

Aperture Dimensions (see Fig. 4):

The large hole have sizes 80 mm x 60 mm whose bottom left corner is placed at x = 275mm, y = 15mm. The small holes are organized as a matrix of 4 rows per 17 columns. Each small holes is 2 mm x 2 mm. The holes matrix bottom right corner is placed at x = 104.5 mm, y = 38 mm; the spacing between each small hole is 2 mm.

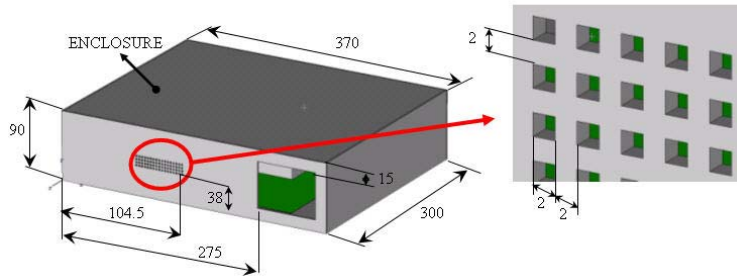


Fig. 4 - Geometrical dimensions of the enclosure; small holes and large hole. (All dimensions is in mm).

ElectroMagnetic (EM) Source Description: Dimensions, Materials and Location (see Fig. 5):

The EM source, i.e. a PCB, is simulated as follows: there is a metal plane in PEC material with dimensions 260 mm x 0.017 mm x 280 mm. Over the metal plane there is a dielectric substrate of FR4 whose dimensions are 260 mm x 0.25 mm x 280 mm; its dielectric permittivity is $\epsilon_r = 4.3$ and no dielectric losses are considered. A trace in PEC material is placed over the dielectric substrate (microstrip configuration); the trace has dimensions 0.4mm x 0.017mm x 280mm and is centered on the plane perpendicular to the slotted panel. A heatsink (solid metal rectangular object) in PEC material of 160 mm x 20 mm x 100 mm is centered 5 mm above the reference plane covering the trace.

The reference plane, with over the trace, is placed horizontally in the enclosure and is 10 mm away from the front panel and 10 mm above the bottom enclosure wall.

The trace is driven, with respect the reference plane, by a voltage signal whose waveform is depicted in Fig. 6. The voltage source and load terminations are of 50 ohm.

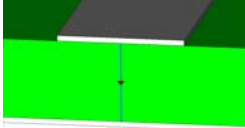
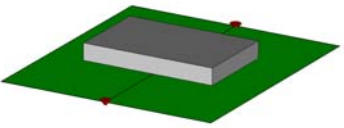
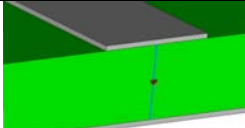
	DISCRETE PORT AS VOLTAGE SOURCE	
		
	DISCRETE PORT AS 50Ω LOAD	

Fig. 5 – Overview of the EM source; discrete port is used as a voltage source; discrete port is used as a 50Ω load.

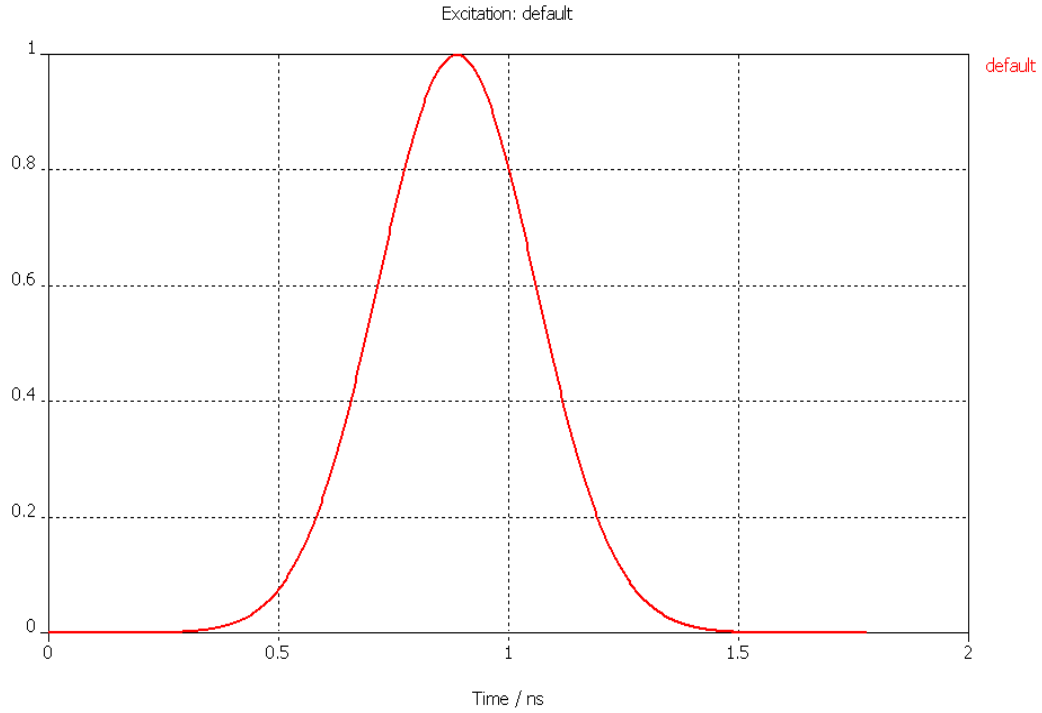


Fig. 6 – Excitation signal supplying the discrete port.

3.1 Enclosure with small holes

Considering the enclosure with small holes shown in Fig.2, it has been computed the magnitude of the electric field for two mesh settings: fine mesh and coarse mesh.

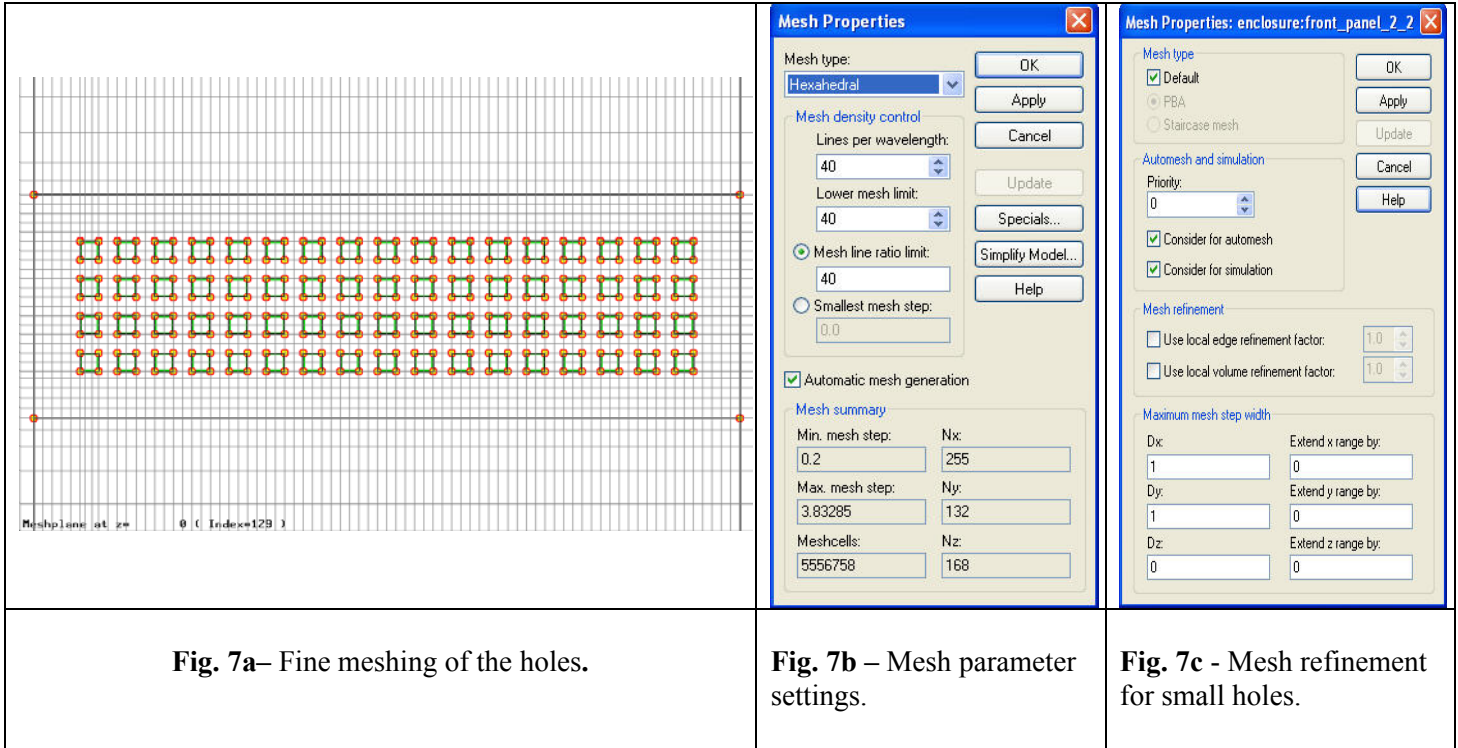
The magnitude of the electric field is computed as in (1):

$$E(f) = \sqrt{E_x^2(f) + E_y^2(f) + E_z^2(f)} \quad (1)$$

Where $E_x(f)$, $E_y(f)$ and $E_z(f)$ are the magnitude of the computed components of the electric field at distance of 3 m from the front side of the enclosure.

Fine mesh

The case with fine mesh is shown in Fig. 7a. The free space of the holes has been meshed with several lines in order to improve the reliability of the simulation. A summary of the basic settings is in Fig. 7b.



To add mesh line in holes', empty space a refined mesh is used whose settings are shown in Fig. 7c. For structure, elements of high importance for the simulation a maximum step width for every coordinate direction can be specified. The automatic mesh generator will not exceed this step width at the bounding box of this structure element.

Coarse mesh

The case with coarse mesh is shown in Fig. 8a and 8b. The mesh lines are placed in order to contour each holes without mesh lines in the free space of the holes. In Fig. 9 it is shown the comparison of the computed electric field magnitude for the case of fine and coarse mesh of the holes at a distance of 3 meter from the center of the front panel of the enclosure as depict in Fig. 10. Fig.11 shows the FSV comparison.

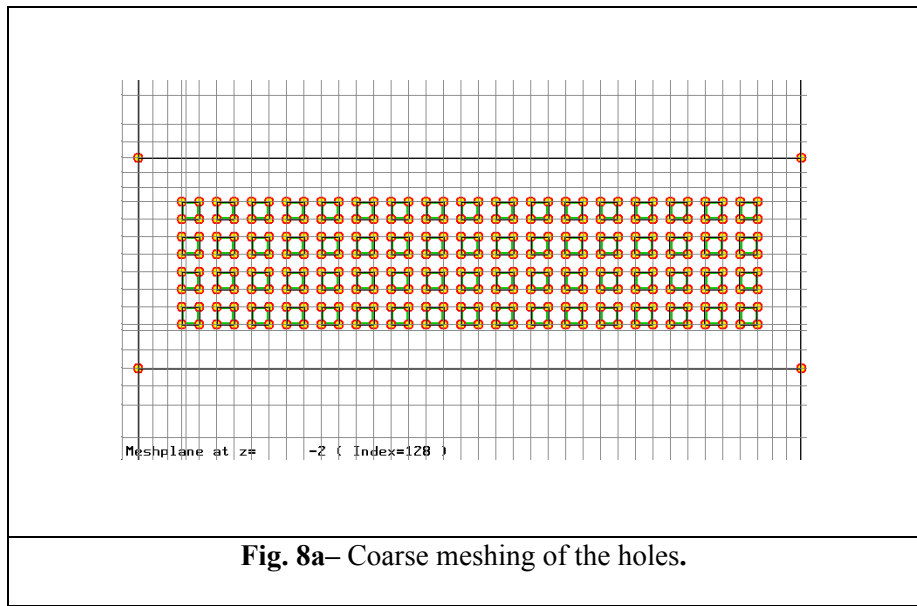


Fig. 8a– Coarse meshing of the holes.

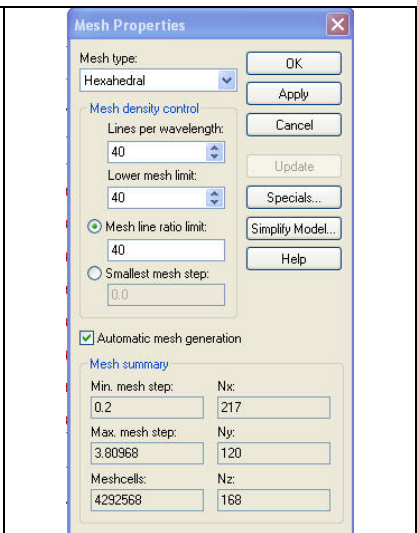


Fig. 8b – Mesh parameter settings.

Small holes: fine and coarse mesh results comparison

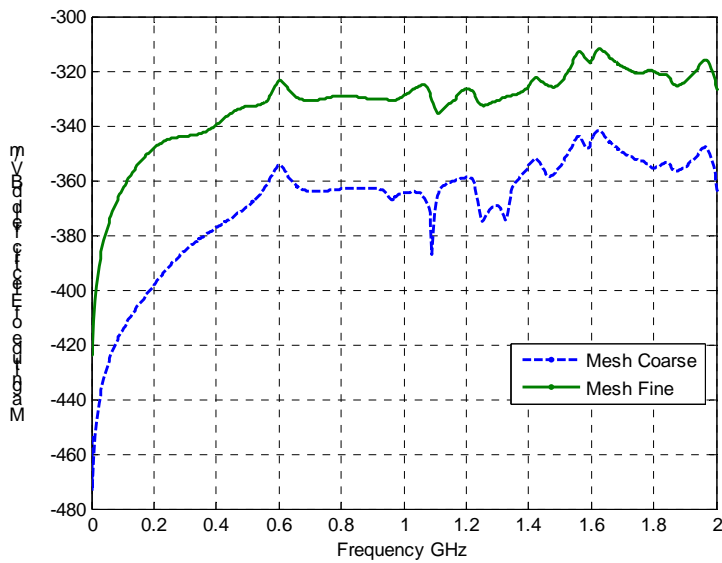


Fig. 9 – Small holes configuration: comparison the electric field magnitude at a distance of 3 m from the center of the front panel of the enclosure for coarse and fine mesh.



Fig. 10 – Electric field probe's distribution. Three probes are used each one of them for each component of the electric field.



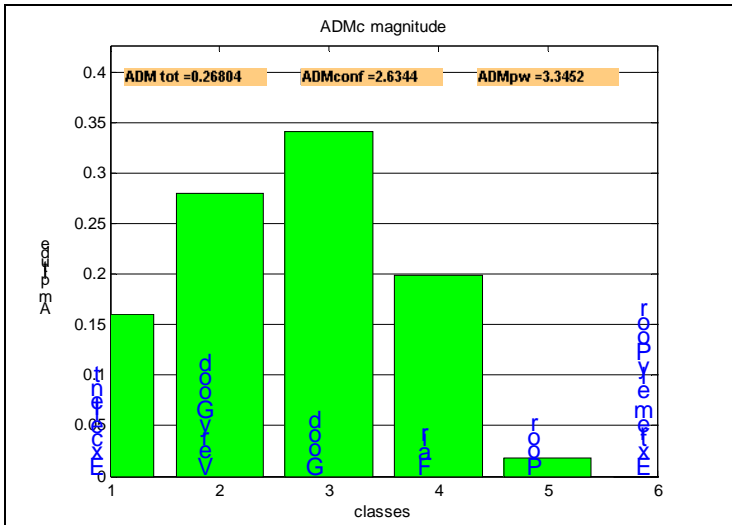


Fig. 11a – ADMc confidence histogram referred to Fig. 9.

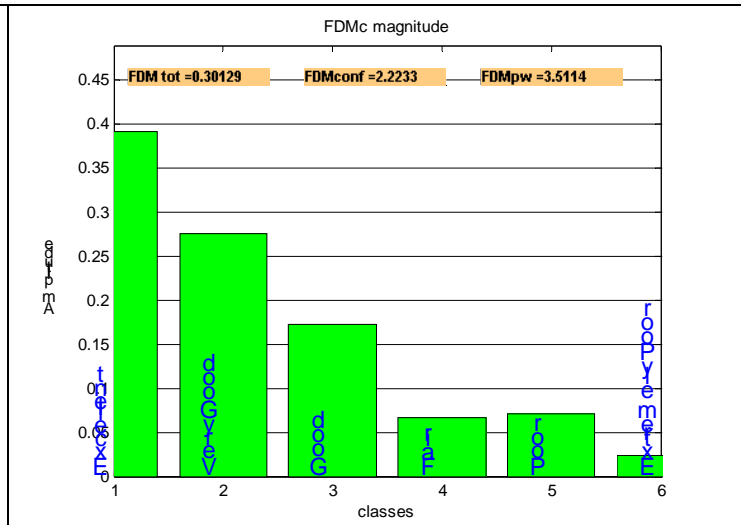


Fig. 11b - FDMc confidence histogram referred to Fig. 9.

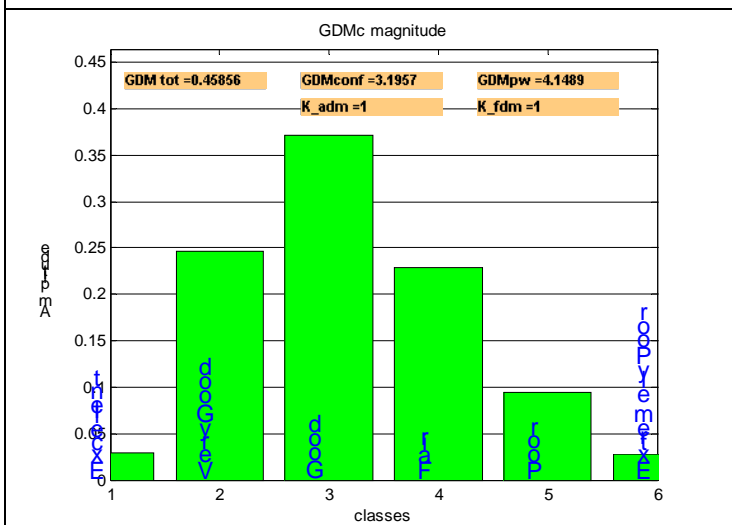


Fig.11c - GDMc confidence histogram referred to Fig. 9.

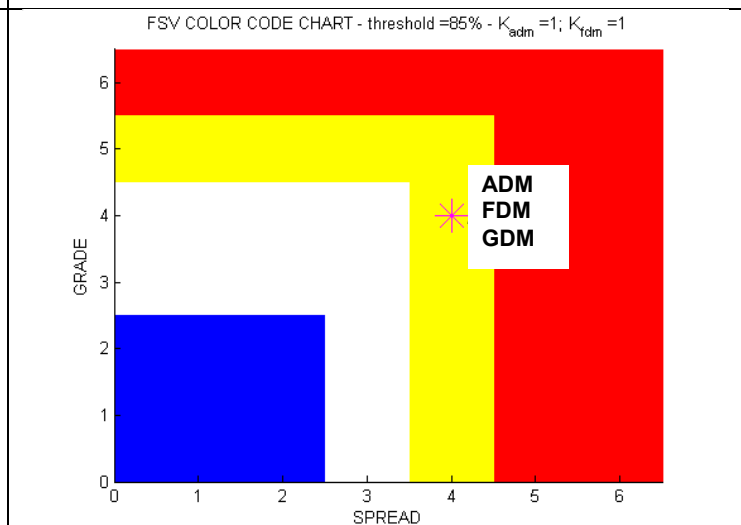


Fig. 11d – GRADE-SPREAD chart referred to Fig. 9.

3.2 Enclosure with large hole

Considering the enclosure with large hole as depict in Fig. 3, it has been computed the magnitude of the electric field for two mesh settings: fine mesh and coarse mesh.

The magnitude of the electric field is always computed, as in (1).

Fine mesh

The case with fine mesh is shown in Fig. 12. The free space of the large hole has been meshed with dense mesh lines. In Fig. 12b there is a summary of the mesh parameters.

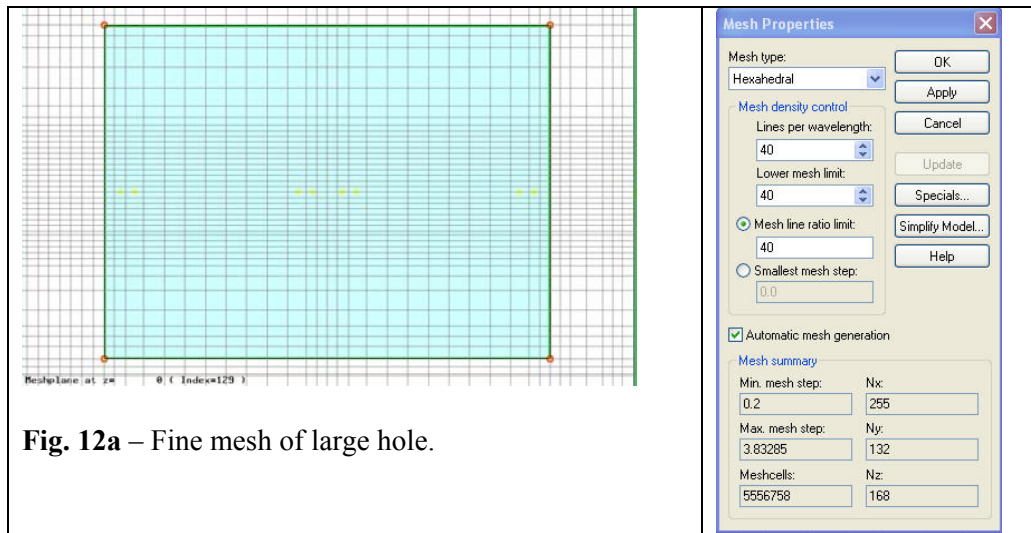


Fig. 12a – Fine mesh of large hole.

Fig. 12b – Mesh parameter settings.

Coarse mesh

The case with coarse mesh is shown in Fig. 13. The mesh lines are much less dense than those in Fig. 12a. Fig. 13b reports the corresponding settings.

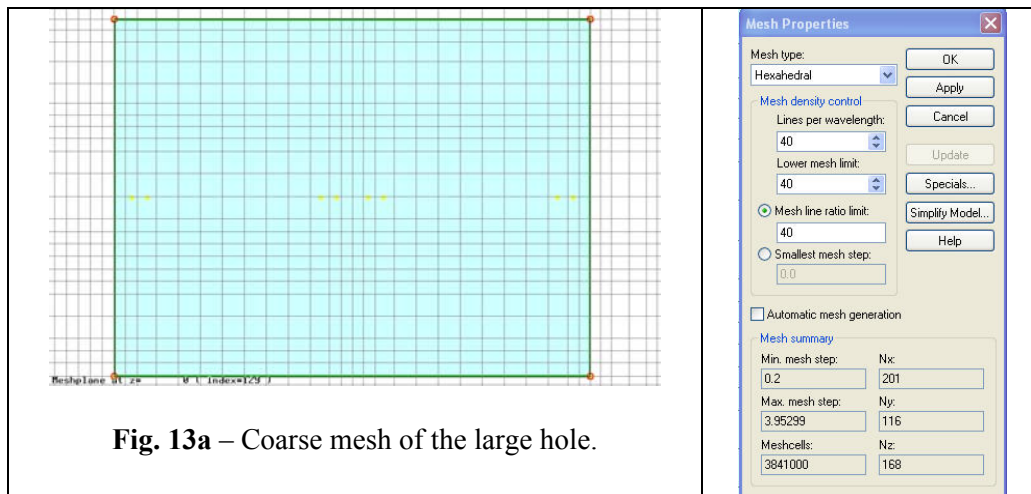


Fig. 13a – Coarse mesh of the large hole.

Fig. 13b – Mesh parameter settings.

Large hole: fine and coarse mesh results comparison

In Fig. 14, it is shown the comparison of the magnitude of the electric field computed for the case of fine and coarse mesh at a distance of 3 meters from the center of the front panel of the enclosure. In Fig. 14b, a zoom of the electric field magnitude from 1.4 GHz to 2 GHz is used to emphasize the difference between the compared curves. Fig. 15 shows the corresponding FSV comparison.

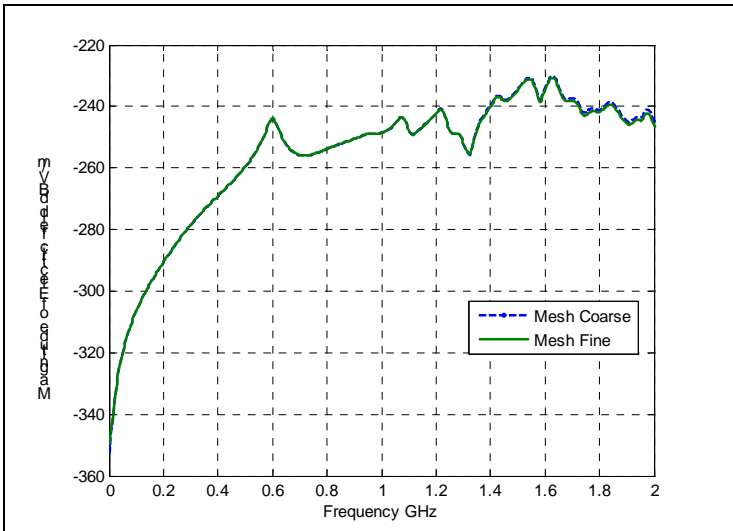


Fig.14a - Comparison the electric field magnitude at a distance of 3 m from the center of the front panel of the enclosure for coarse and fine mesh: large hole.

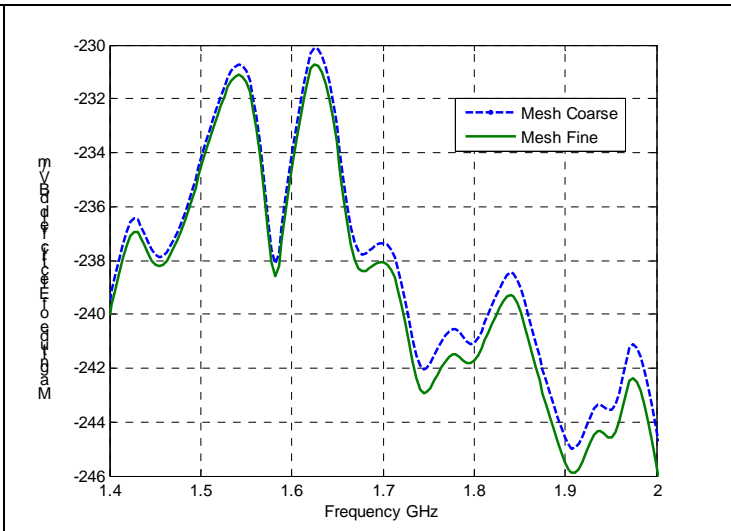


Fig. 14b – Comparison the electric field magnitude at a distance of 3 m from the center of the front panel of the enclosure for coarse and fine mesh; zoom in frequency range from 1.6 GHz to 2 GHz: large hole.

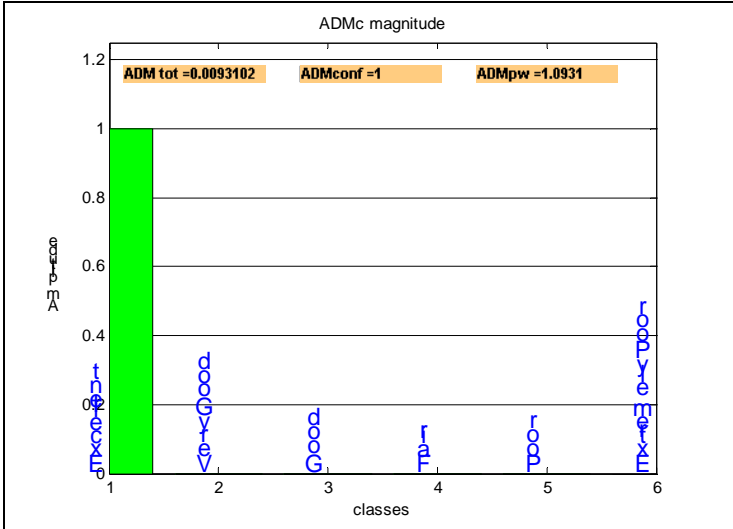


Fig. 15a - ADMc confidence histogram referred to Fig. 14a.

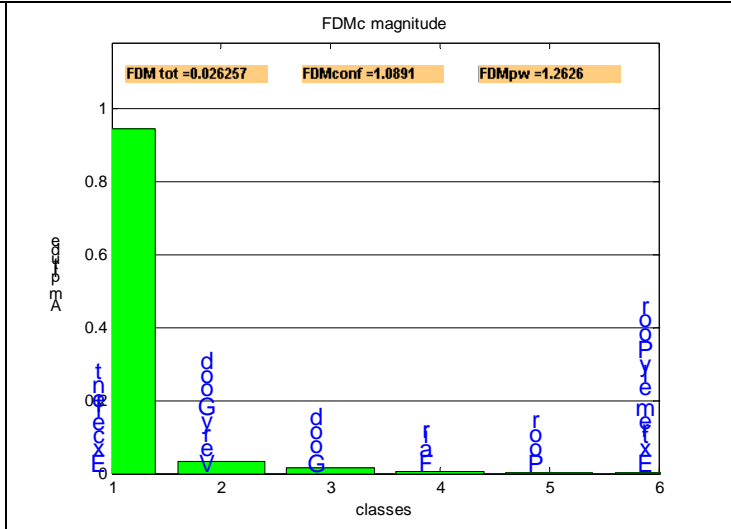


Fig. 15b - FDMc confidence histogram referred to Fig. 14a.

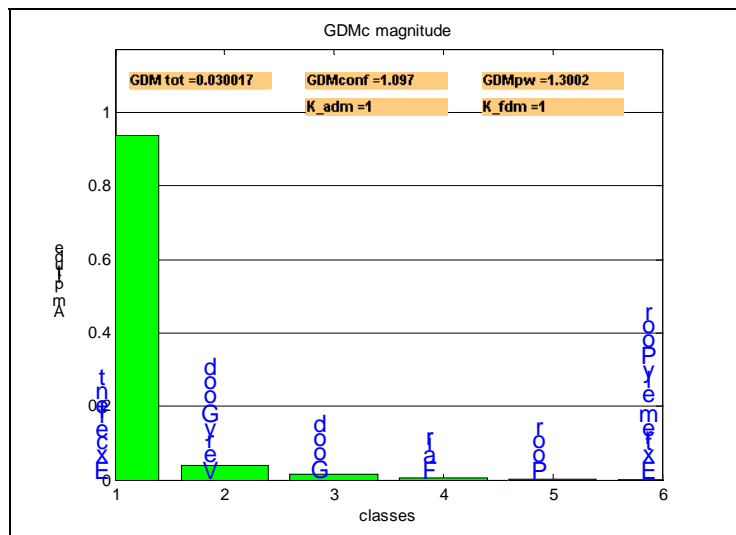


Fig. 15c - GDMc confidence histogram referred to Fig. 14a.

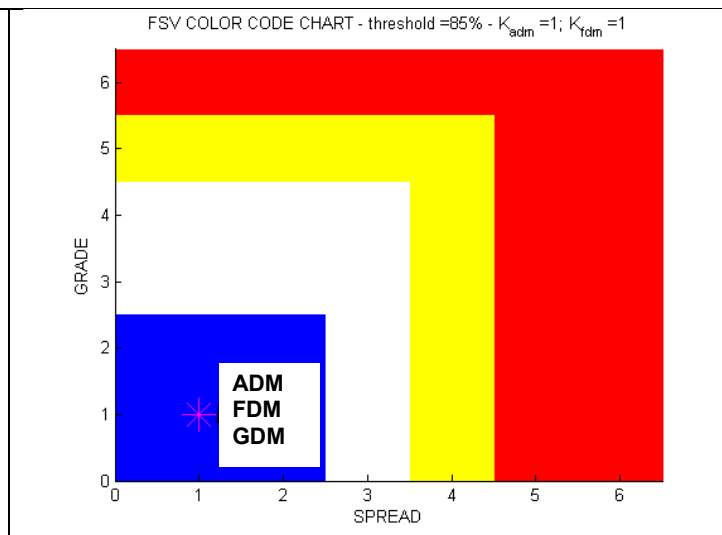


Fig. 15d - GRADE-SPREAD chart referred to Fig. 14a.

3.3 Remarks

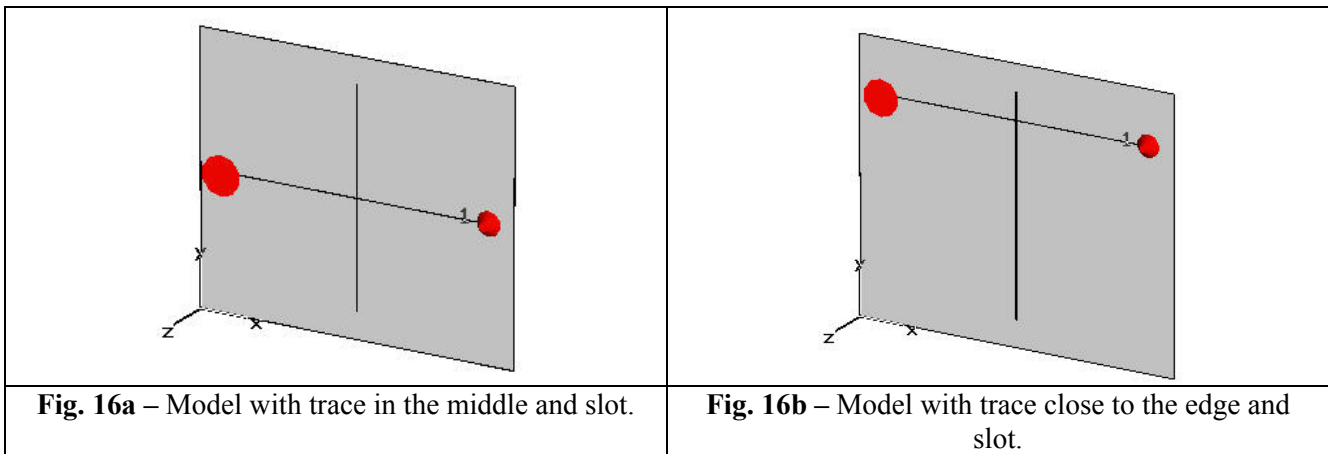
The results in terms of magnitude of the electric field computed 3 meters distant from the front side of the enclosure are different for the different mesh setting parameters used considering small holes or large hole.

In the case of small holes the comparison of the results due to different mesh setting shows the curves have the same shape but are different in the details. The difference is about 30 dB and is uniform along the considered frequency range.

4. A PCB STANDARD PROBLEM

The emissions from a PC board where a trace is run over a split in the ground-reference plan is due to a complex interaction of the return current ‘loop’ in the ground-reference plane, and the extra ‘bunching’ of return current near the edge of the ground-reference plane. These effects result in an increase of radiated emissions, and a negative EMI impact.

The aim of this section is to compute and compare the maximum of the electric field over a spherical surface 3 m away from the center of the PCB for different simulations mesh settings. The board with slot on reference plane and trace in the middle of the substrate and the board with slot in the reference plane and the trace over the substrate close to the board edge, as shown in Fig.16, have been investigated. For both cases, different mesh settings for the slot have been used and then the comparison of the results of varying the mesh are shown. The detailed description of the whole system follows in the next section.

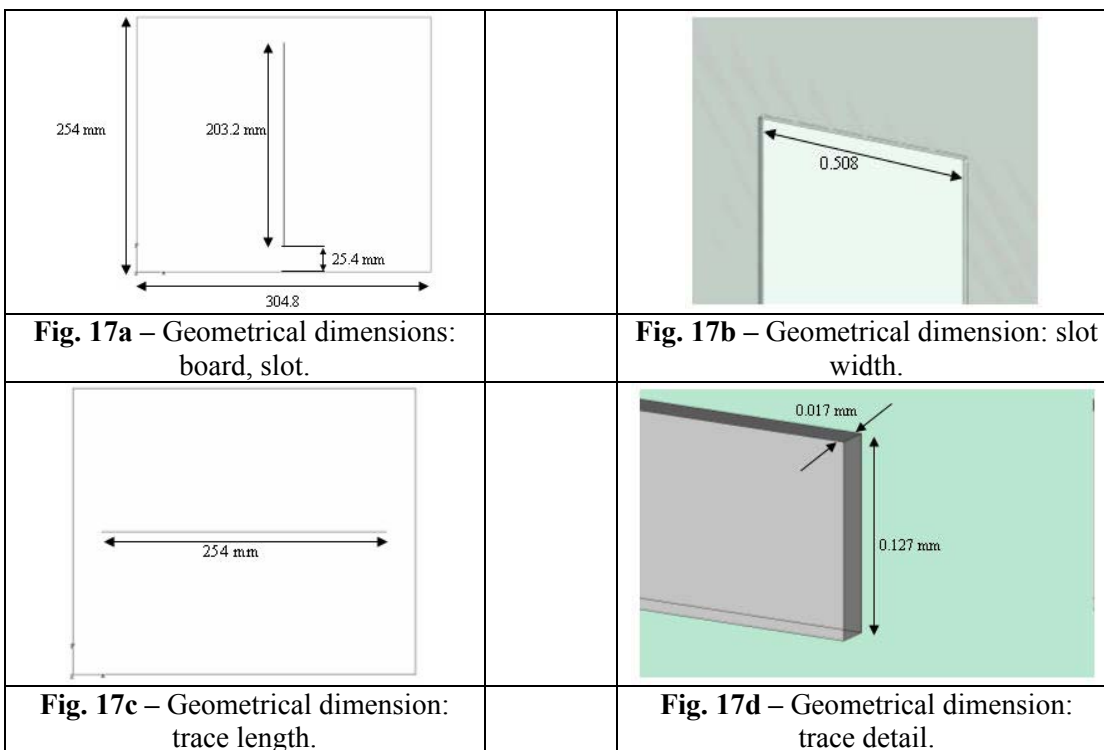


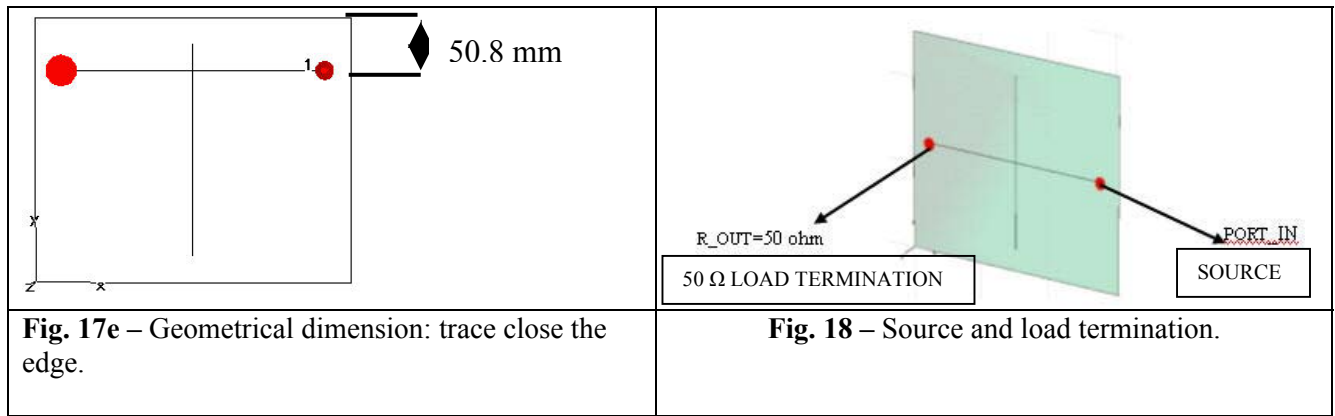
The geometrical dimensions of the entire structure are shown in Fig. 17. The analysis has been performed in the frequency range 0.1GHz - 2GHz.

PCB Dimensions and materials (see Fig. 17):

The PCB is simulated as follows: there is a metal plane (*Reference Plane*) in PEC material with dimensions 304.8 mm x 254 mm x 0.017 mm (x, y, z axis). Over the metal plane there is a dielectric substrate of FR4 whose dimensions are 304.8 mm x 254 mm x 0.127 mm; its dielectric permittivity is $\epsilon_r = 4.7$ and no dielectric losses are considered. The trace in PEC material is placed over the dielectric substrate (microstrip configuration); the trace has dimensions of 254 mm x 0.127 mm x 0.017 mm and is considered in two different positions: centered or close to the upper edge respectively (see Fig.16a and Fig. 16b).

The slot is centered in the reference plane and its dimensions are 0.508 mm x 203.2mm.





Source / load termination (see Fig. 18):

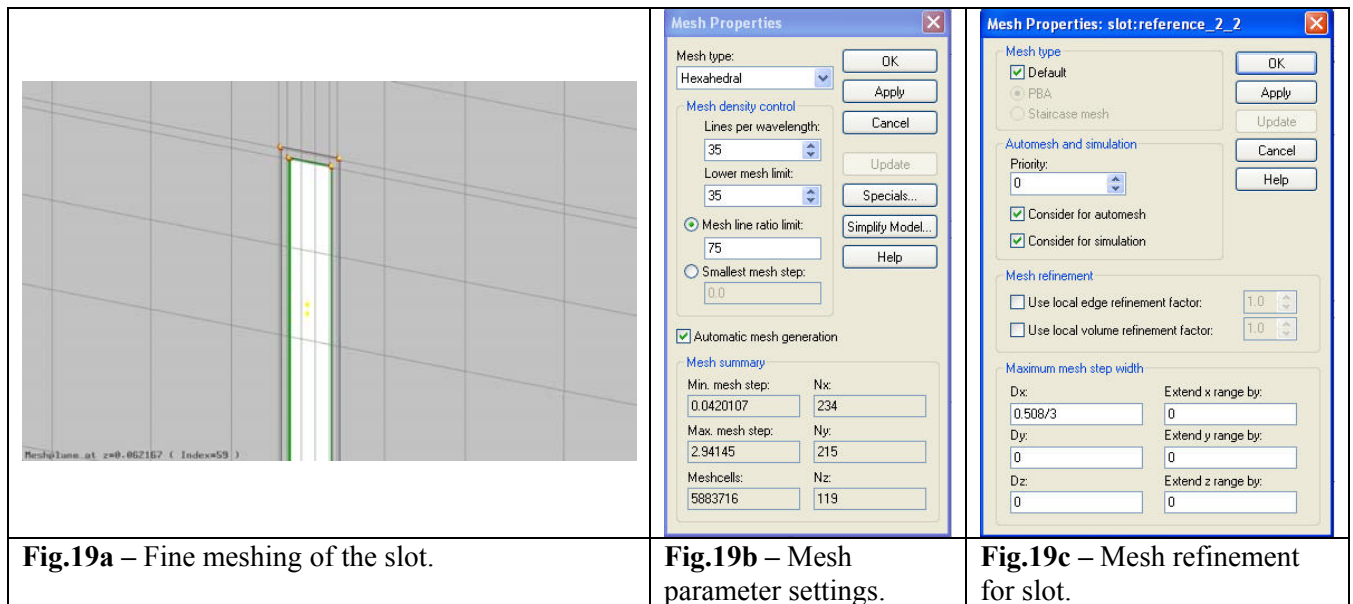
The metal plane (representing the PCB reference plane) and the trace over a dielectric are driven by a 3.3 V voltage source in the above mentioned frequency range. The source and load terminations are of 50 Ω as in Fig. 18.

4.1 Board with slot, trace in the middle

Considering the board with slot on reference plane and trace in the middle, it has been computed the maximum electric field over a spherical surface 3 m away from the center of the PCB for two mesh settings of the slot: fine mesh and coarse mesh.

Fine mesh

The case with fine mesh is shown in Fig. 19 in which are also reported the mesh properties. The free space of the slot has been meshed with several mesh lines.



Coarse mesh

The case with coarse mesh is shown in Fig 20. The mesh line is placed in order to contour the slot without any mesh lines in the free space of the slot.

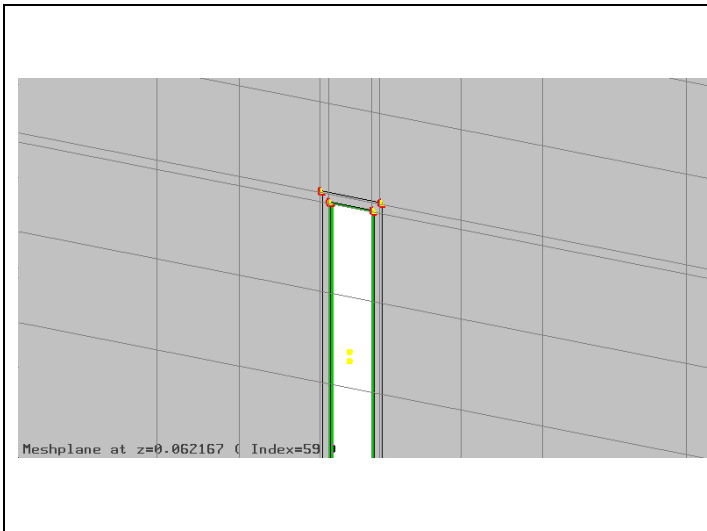


Fig. 20a – Coarse meshing of the slot.

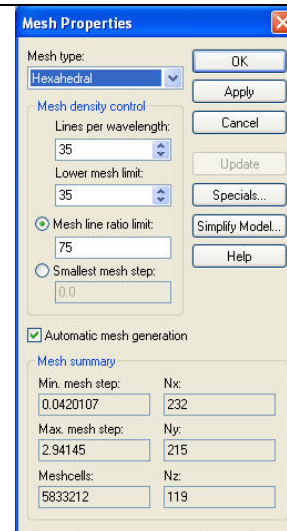


Fig. 20b – Mesh parameter settings.

Board with slot, trace in the middle: fine and coarse mesh results comparison

In Fig. 21 is shown the comparison, for slot's fine and coarse mesh, of the maximum electric field computed over a spherical surface at a distance of 3 meter from the center of the PCB for the case board with slot, trace in the middle. Fig. 22 shows the FSV comparison.

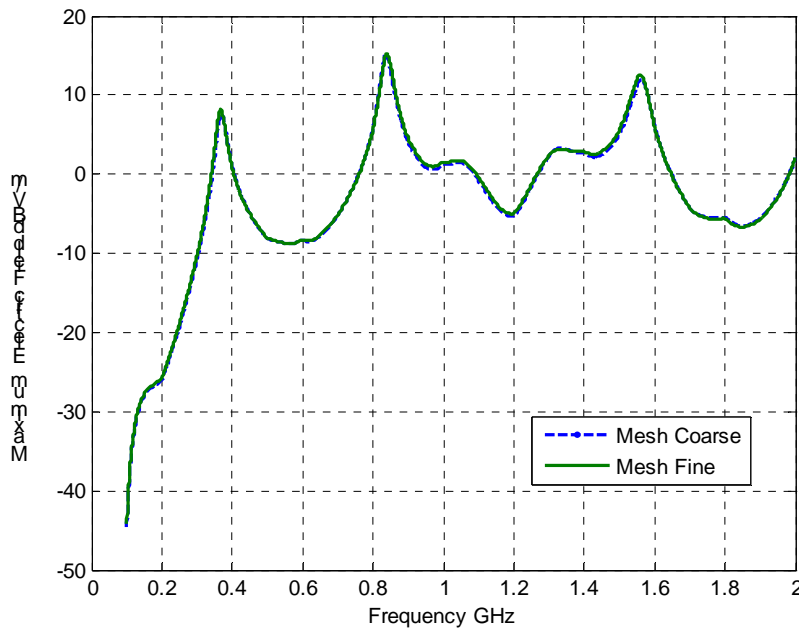


Fig. 21 – Comparison of the maximum electric field computed over a spherical surface at a distance of 3 meter from the center of the PCB: board with slot trace in the middle, fine and coarse mesh.

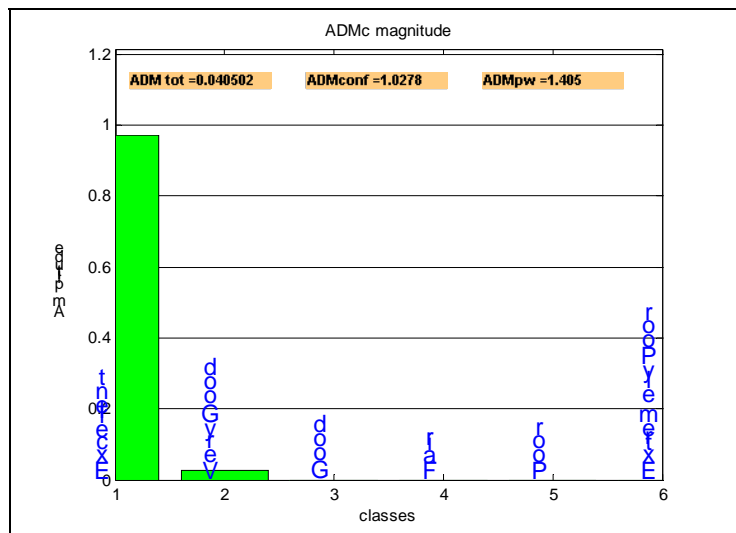


Fig. 22a - ADMc confidence histogram referred to Fig. 21.

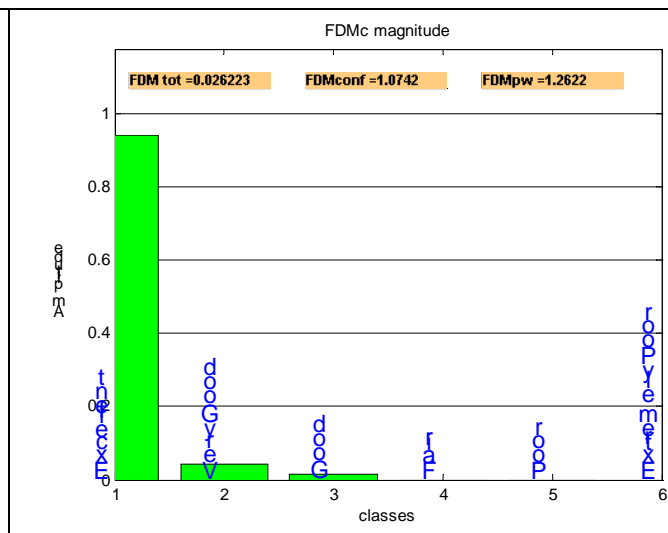


Fig. 22b - FDMc confidence histogram referred to Fig. 21.

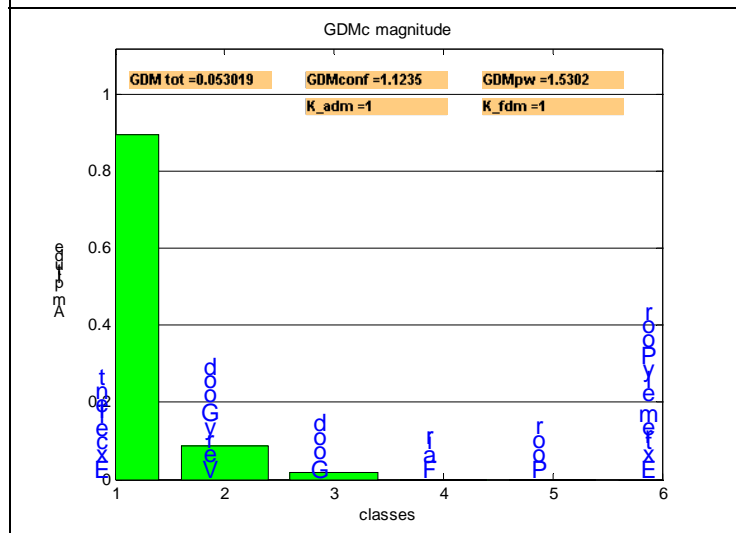


Fig. 22c - GDMc confidence histogram referred to Fig. 21.

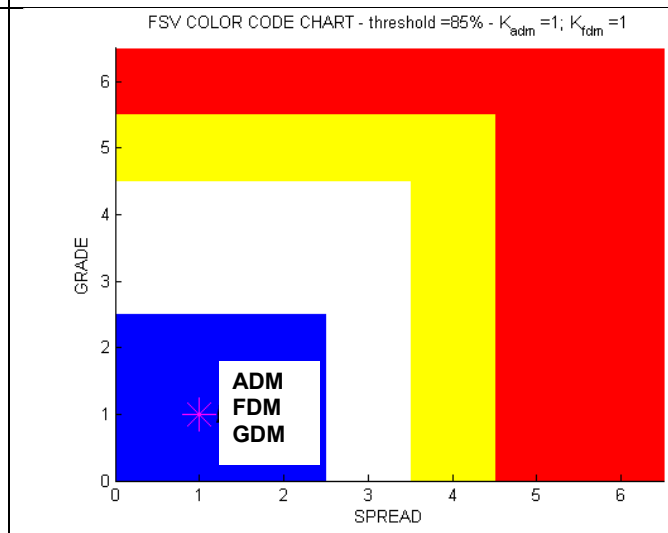


Fig. 22d - GRADE-SPREAD chart referred to Fig. 21.

4.2 Board with slot, trace close to the board edge

Considering the board with slot on reference plane and trace close to the board edge of the substrate, it has been computed the maximum electric field over a spherical surface 3 m away from the center of the PCB for two mesh settings of the slot: fine mesh and coarse mesh..

Fine mesh

For the case with fine mesh, (see Fig. 23a), the parameters of the mesh settings are as in Fig. 23b and 23c. The free space of the slot it has been filled with several mesh lines.

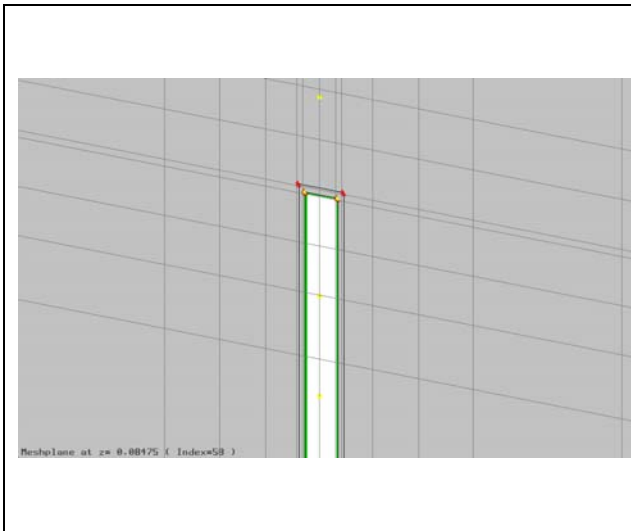


Fig. 23a – Fine mesh of the slot.

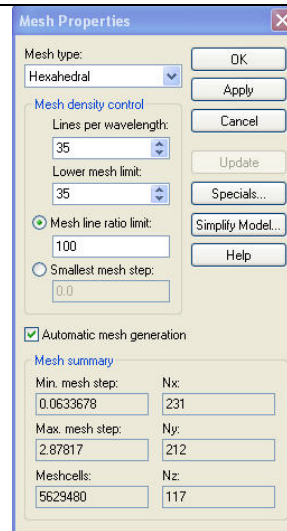


Fig. 23b – Mesh parameter settings.

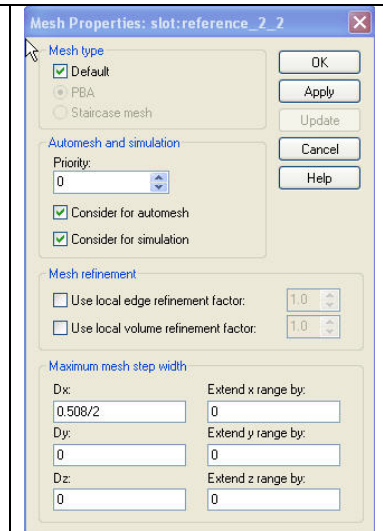


Fig. 23c – Mesh refinement for the slot.

Coarse mesh

The parameters settings for the case with coarse mesh are shown in Fig. 24 along with the meshed slot. The mesh lines are placed in order to contour the slot without any vertical line in the free space of the slot.

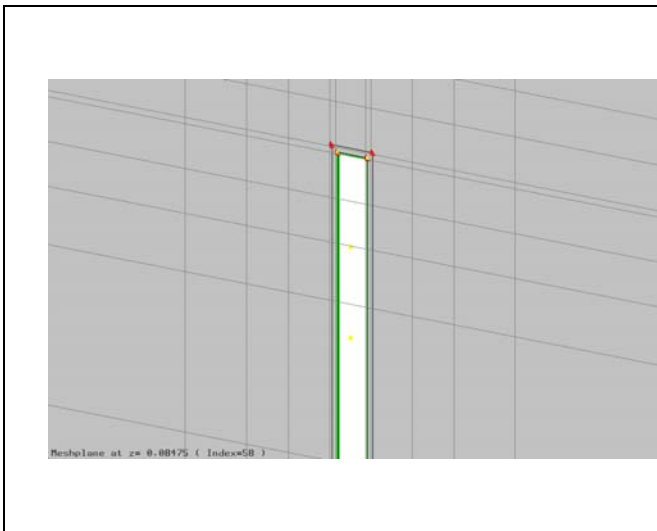


Fig. 24a – Coarse meshing of the slot.

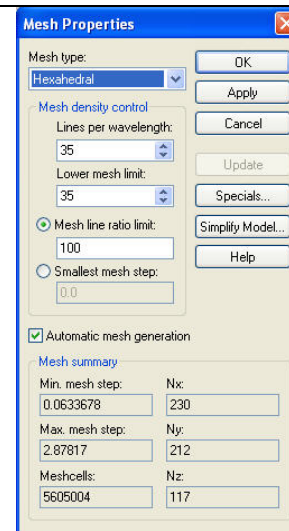


Fig. 24b – Mesh parameter settings.

Board with slot, trace close to the edge: fine and coarse mesh results comparison

In Fig. 25 is shown the comparison, for slot's fine and coarse mesh, of the maximum electric field computed over a spherical surface at a distance of 3 meter from the center of the PCB for the case board with slot, trace close to the board edge. Fig. 26 shows the FSV comparison.

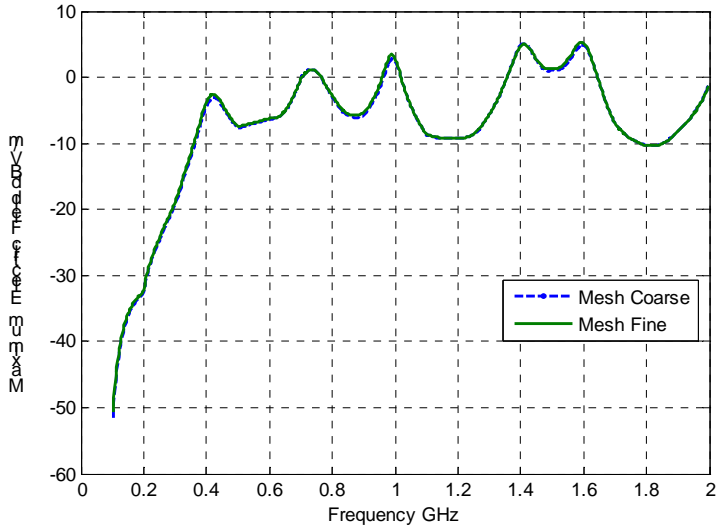


Fig. 25 – Comparison of the maximum electric field computed over a spherical surface at a distance of 3 meters from the center of the PCB: board with slot, trace close to the board edge.

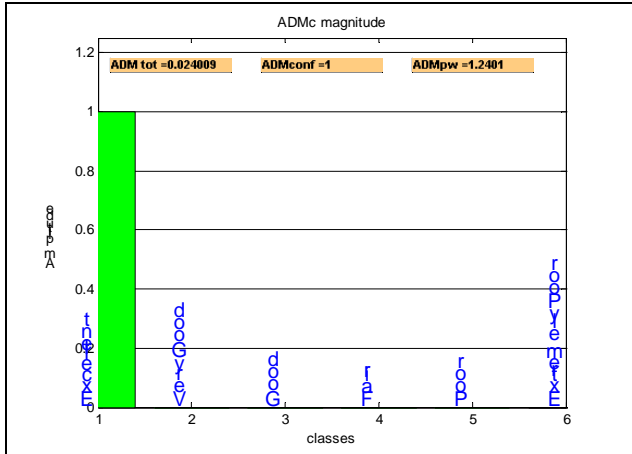


Fig. 26a – ADMc confidence diagram referred to Fig. 25.

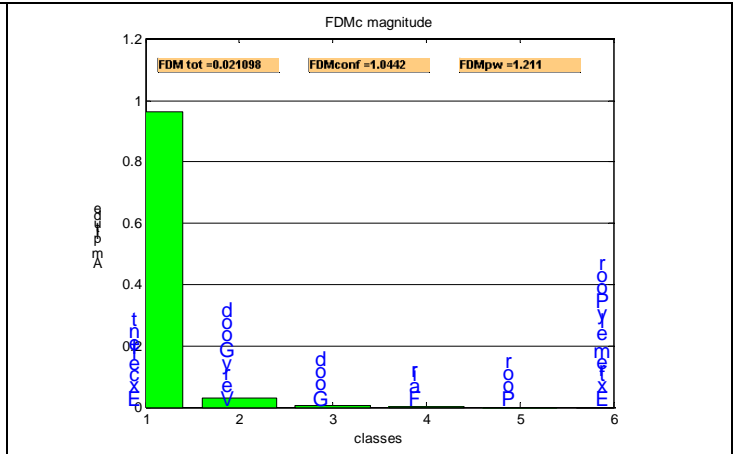


Fig. 26b - FDMc confidence diagram referred to Fig. 25.

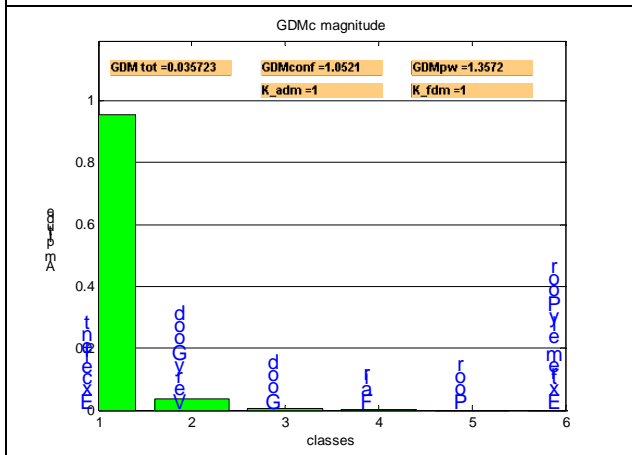


Fig. 26c - GDMc confidence diagram referred to Fig. 25.

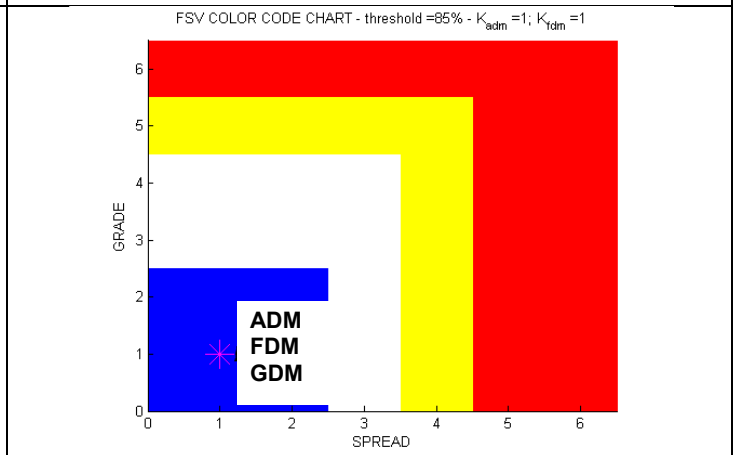


Fig. 26d – GRADE-SPREAD chart referred to Fig. 25.

4.3 Remarks

The comparison of the maximum electric field computed over a spherical surface at a distance of 3 meters from the center of the PCB between models with fine and coarse mesh either for the case with trace in the middle and trace close to the board edge is in good agreement. The slot meshing on reference plane has a little impact on the computed results.

5. A SIGNAL INTEGRITY STANDARD PROBLEM

This model concerns the performance of a delay line on a printed circuit board. Signal traces are often created in various serpentine shapes to lengthen the trace length and achieve a desired delay. The coupling between the legs of the serpentine delay line can create significant distortion in the pulse, which is not simulated in typical transmission line based simulation tools. The distortion can easily cause timing problems as well as create common mode currents, which can cause, in turn, EMC problems.

In this chapter, it has been investigated the electromagnetic behavior of a board on which a meander delay or an equivalent length straight line is printed. For the first case, the aim is to compute the transient voltage waveform across the load termination depending on the simulations mesh settings. It has been analyzed the impact of the meander meshing on the computed results. For the second case it has been analyzed the impact of the GND plane extension on the transient voltage waveform across the load termination and the impact of the dielectric meshing. A detailed description of the systems is explained below.

Two different configurations it has been considered. The first one is a model of a board on which a meander delay line is printed: Fig. 27 shows the geometry for this model. The second one is the model of a board on which a straight line is printed whose length is equal to that of the meander line. This is referred as equivalent length straight line and its geometry is shown in Fig. 28. For both configurations, the source is a voltage pulse of trapezoidal shape as shown in Fig. 29. For both configurations it has been computed the transient voltage waveform across the load termination.

PCB Dimensions and Materials:

Meander Delay Line Model (see Fig. 27) - The PCB model has the following characteristics: the reference plane is in Perfect Electric Conductor (PEC) material whose dimensions are 23.25 mm \times 40.25 mm \times 0.2 mm (x,y,z axis). On the PEC plane there is a dielectric substrate of FR4 whose dimensions are 23.25 mm \times 40.25 mm \times 0.25 mm; its relative dielectric permittivity is $\epsilon_r = 4.5$ and no dielectric losses are considered. The meander trace, in PEC materials, is placed on the dielectric substrate and, like a serpentine, has a number of closely coupled legs. The trace has the following dimensions : 0.25mm wide; 0.2mm thick; 0.25mm legs separation. The trace is simulated as a PEC material. The exact characteristic impedance of the line is 56 Ω .

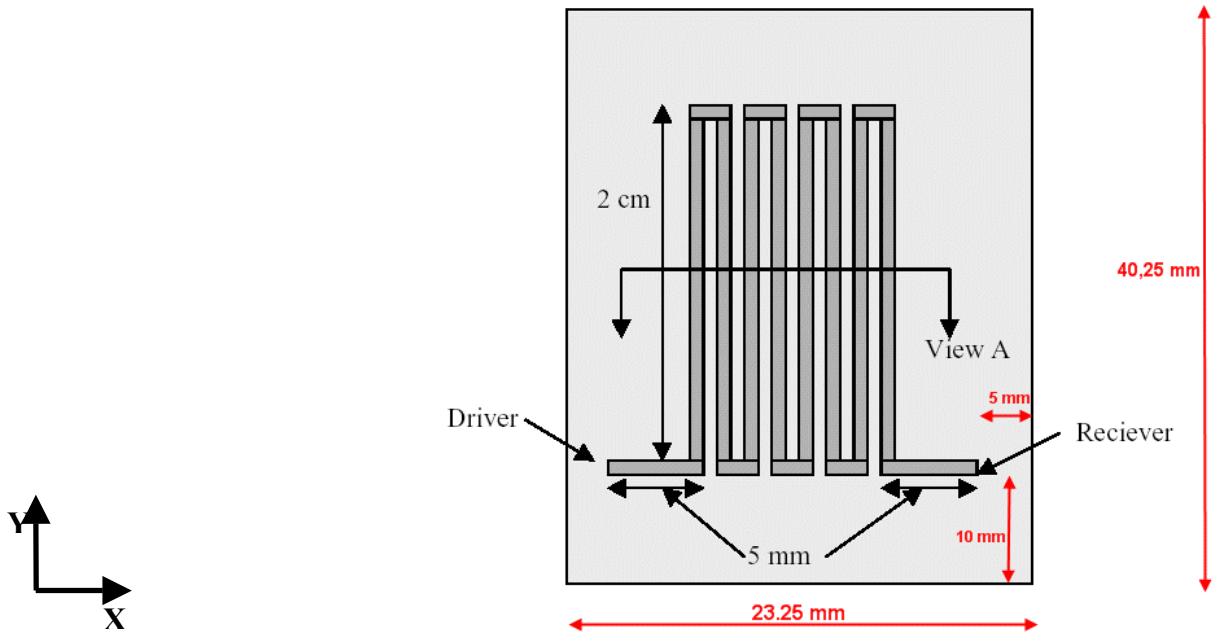


Fig. 27a - Meander delay line (Top View).

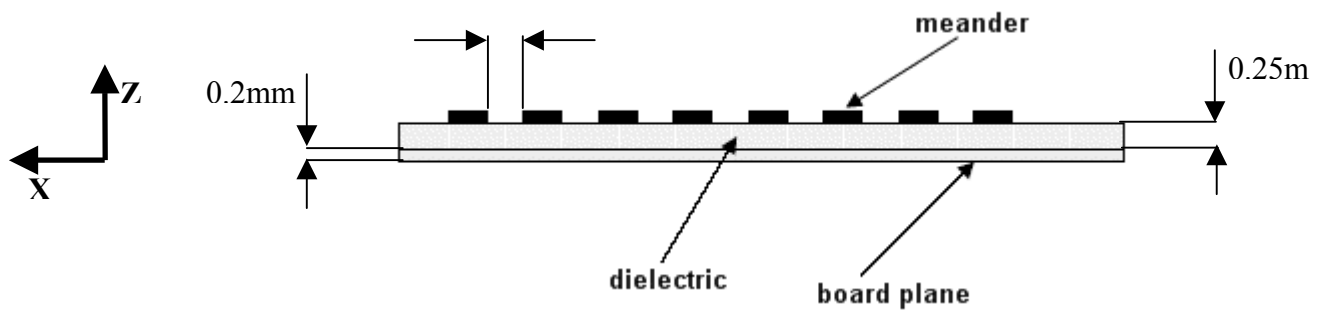


Fig. 27b - Meander delay line cross section (View A).

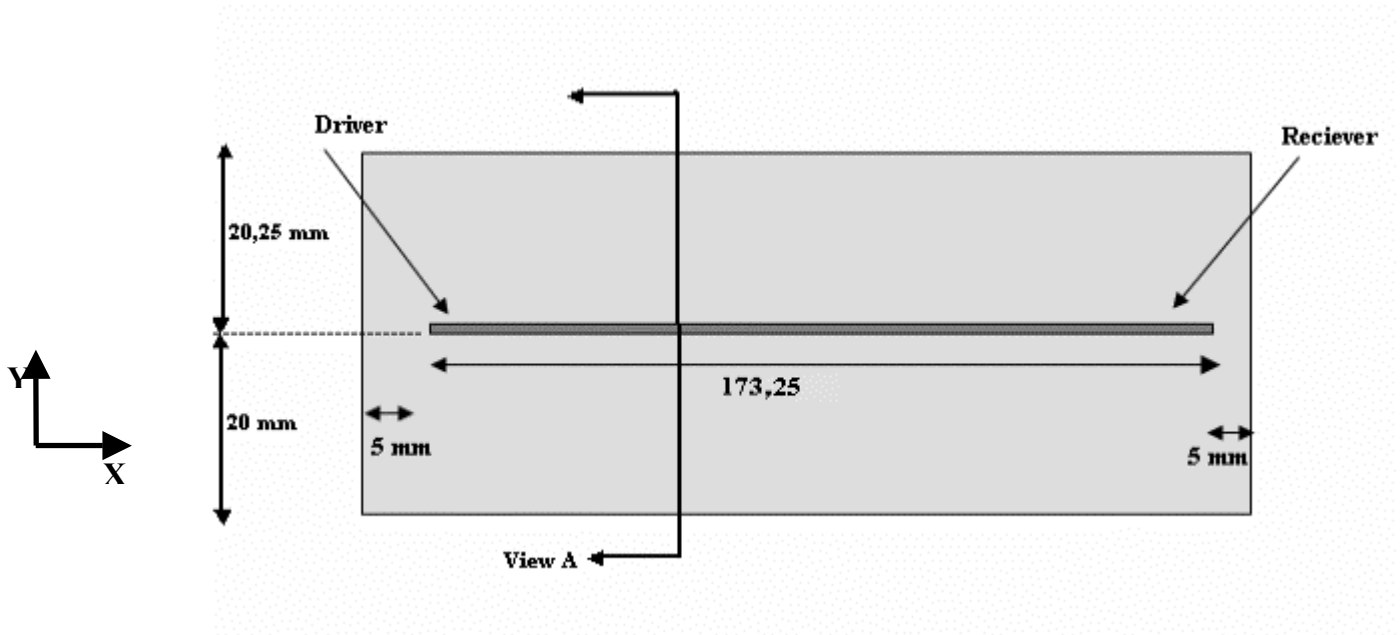


Fig. 28a – Equivalent length straight line.

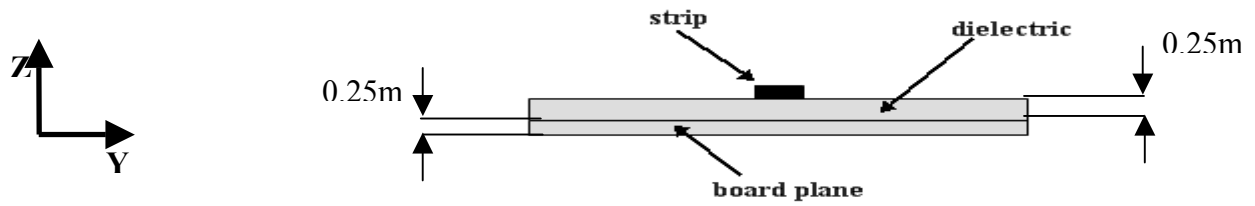


Fig. 28b – Equivalent length straight line cross section (View A).

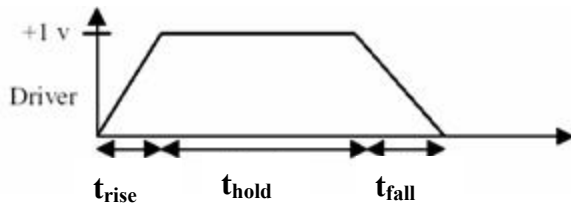


Fig. 29a – Excitation pulse;
 $t_{\text{rise}}=0.2\text{ns}$, $t_{\text{fall}}=0.2\text{ns}$, $t_{\text{hold}}=1\text{ns}$.



Fig. 29b – Excitation pulse,
 Microwave studio settings.

Equivalent Length Straight Line Model (see Fig. 28) - The PCB model has the following characteristics: the reference plane is in Perfect Electric Conductor (PEC) material whose dimensions are 183.25 mm x 40.25 mm x 0.2 mm (x,y,z axis). On the PEC plane there is a dielectric substrate of FR4 whose dimensions are 183.5 mm x 40.25 mm x 0.25 mm; its dielectric permittivity is $\epsilon_r = 4.5$ and no dielectric losses are considered. The straight trace in PEC materials is placed on the dielectric substrate. The trace is simulated as a PEC material. The characteristic impedance of the line is 50 Ω .

Source / Load Termination:

Meander Delay Line Model – The trace is driven against the reference plane by a trapezoidal voltage pulse of amplitude equal to 1V amplitude, $t_{\text{rise}}=0.2\text{ns}$, $t_{\text{fall}}=0.2\text{ns}$, and $t_{\text{hold}}=1\text{ns}$, as shown in Fig. 29. The length of the considered time window is 10ns. The load termination is a resistive impedance equal to the characteristic impedance of the line $Z_{\text{load}} = 56\Omega$; the internal impedance of the voltage source is set $Z_{\text{source}} = 0\Omega$. The structure it has been excited with a voltage discrete port [4].

Equivalent Length Straight Line Model - The trace is driven against the reference plane by a trapezoidal voltage pulse of amplitude equal to 1V amplitude, $t_{\text{rise}}=0.2\text{ns}$, $t_{\text{fall}}=0.2\text{ns}$, and $t_{\text{hold}}=1\text{ns}$, as shown in Fig. 29. The length of the considered time window is 10ns. The load termination is a resistive impedance equal to the characteristic impedance of the line $Z_{\text{load}}= 50\Omega$; the internal impedance of the voltage source set $Z_{\text{source}} = 0\Omega$. The structure it has been excited with a voltage discrete port [4].

5.1 Board with printed meander delay line

Considering the board with meander delay line it has been computed the transient voltage waveform across the load termination for two mesh settings of the empty space between meander legs: fine mesh and coarse mesh.

5.1.2 Fine mesh

The case with fine mesh is shown in Fig. 30. The free space between legs has been meshed with dense mesh lines.

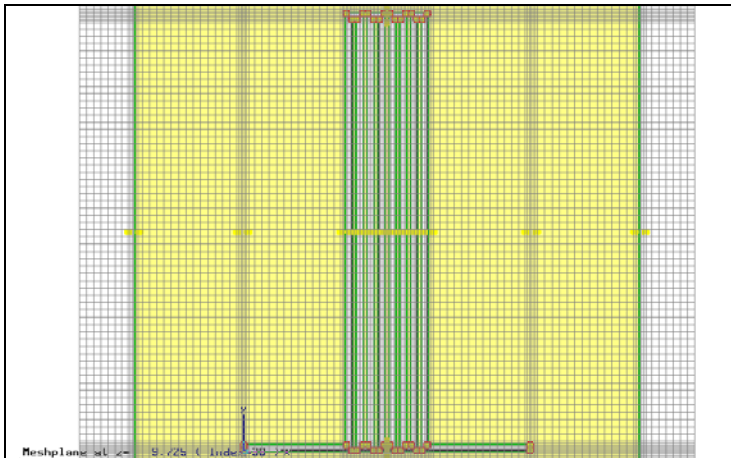


Fig. 30a – Fine meshing of the space between legs.

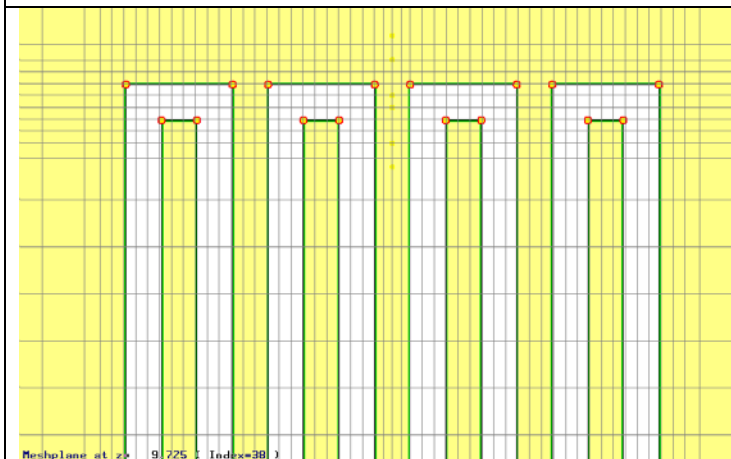


Fig. 30b – Zoom of the mesh between leg's space.

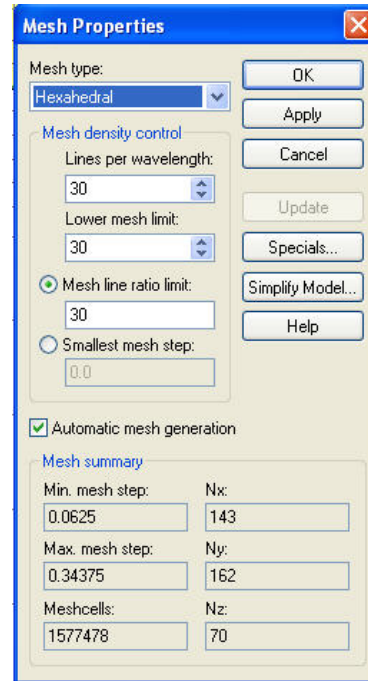


Fig. 30c – Mesh parameter settings.

5.1.3 Coarse mesh

The case with coarse mesh is shown in Fig 31. The mesh line is placed in order to contour the legs without vertical mesh lines between them.

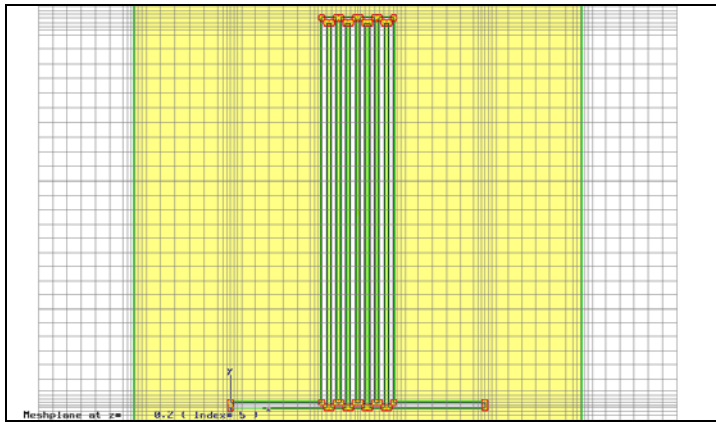


Fig. 31a – Coarse meshing of the space between legs.

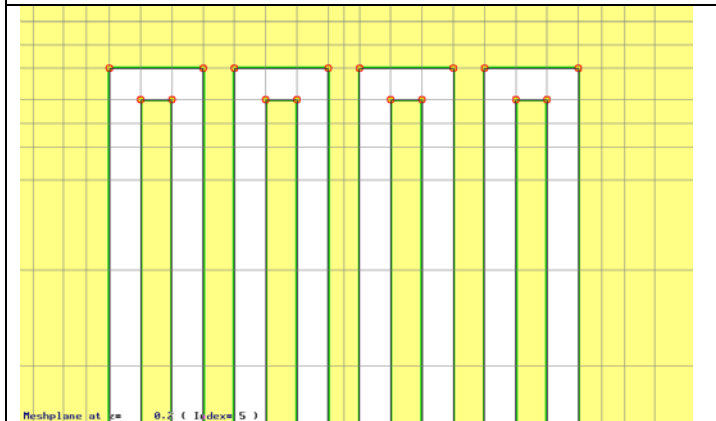


Fig. 31b – Zoom of the mesh between legs space.

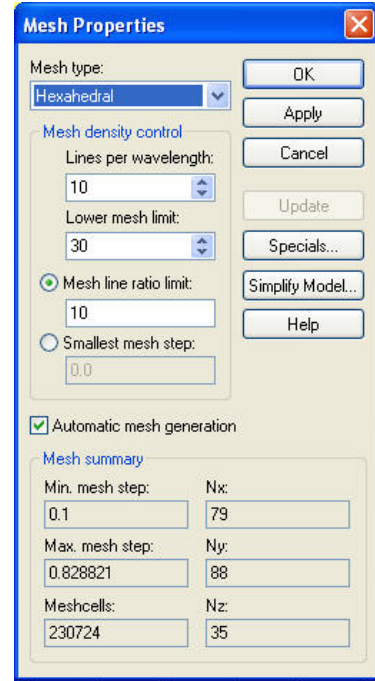


Fig. 31c – Mesh parameter settings.

Board with printed meander delay line: fine and coarse mesh results comparison

In Fig. 32 is shown the comparison, for fine and coarse mesh, of the transient voltage waveform across the load termination for the case board with printed meander delay line. Fig. 33 shown the FSV comparison.

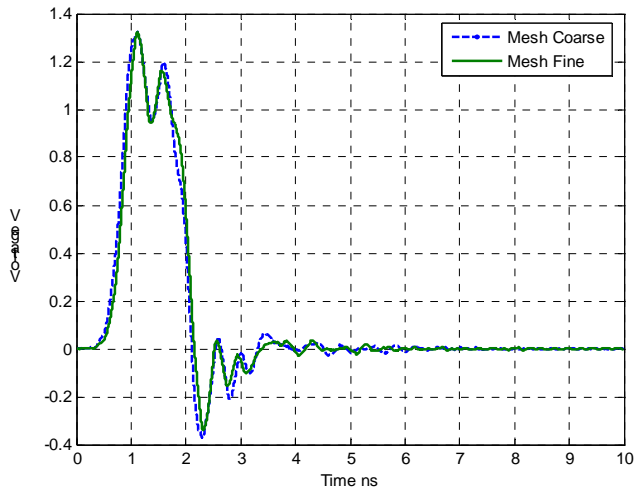


Fig. 32 – Comparison of the transient voltage waveform across the load termination: board with printed meander delay line.

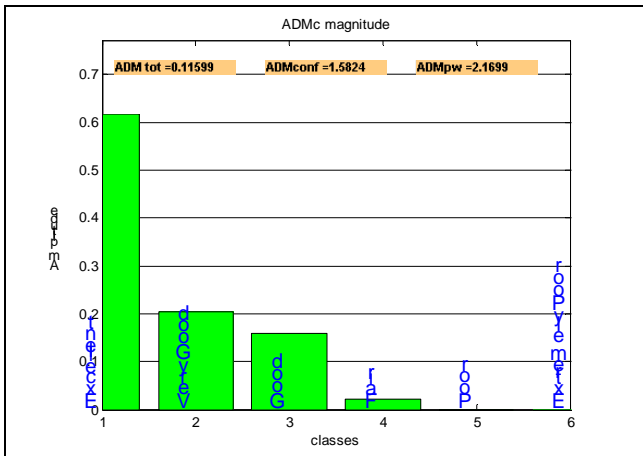


Fig. 33a - ADMc confidence diagram referred to Fig. 32.

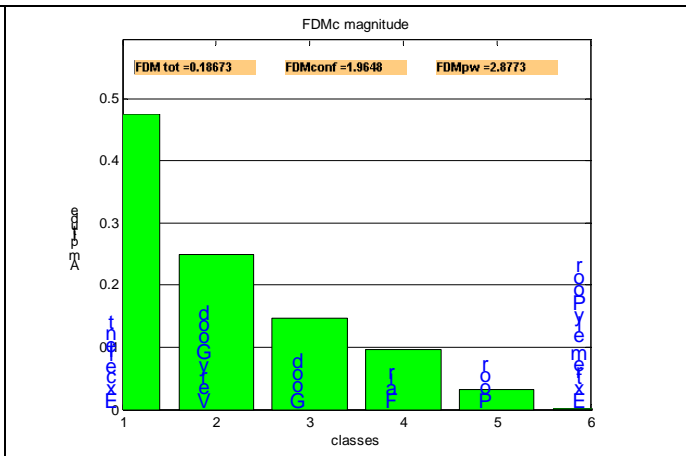


Fig. 33b - FDMc confidence diagram referred to Fig. 32.

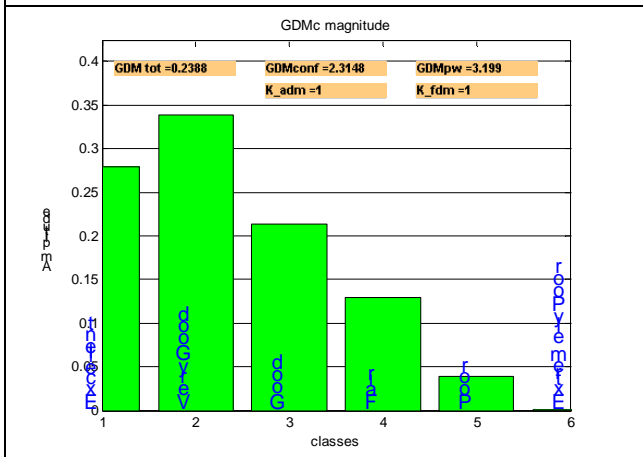


Fig. 33c - GDMc confidence diagram referred to Fig. 32.

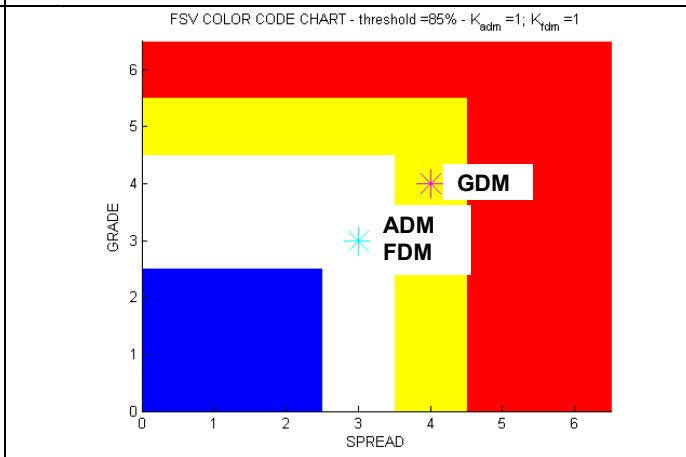


Fig. 33d – GRADE-SPREAD chart referred to Fig. 32.

5.2 Board with printed equivalent length straight line

Considering the board with the equivalent length straight line, the transient voltage waveform across the load termination for two different mesh settings of the substrate and the transient voltage waveform across the load termination considering two different extension of the GND plane has been computed.

Substrate meshing: Fine mesh

The case with fine mesh is shown in Fig. 34. The substrate has been meshed with dense mesh lines.

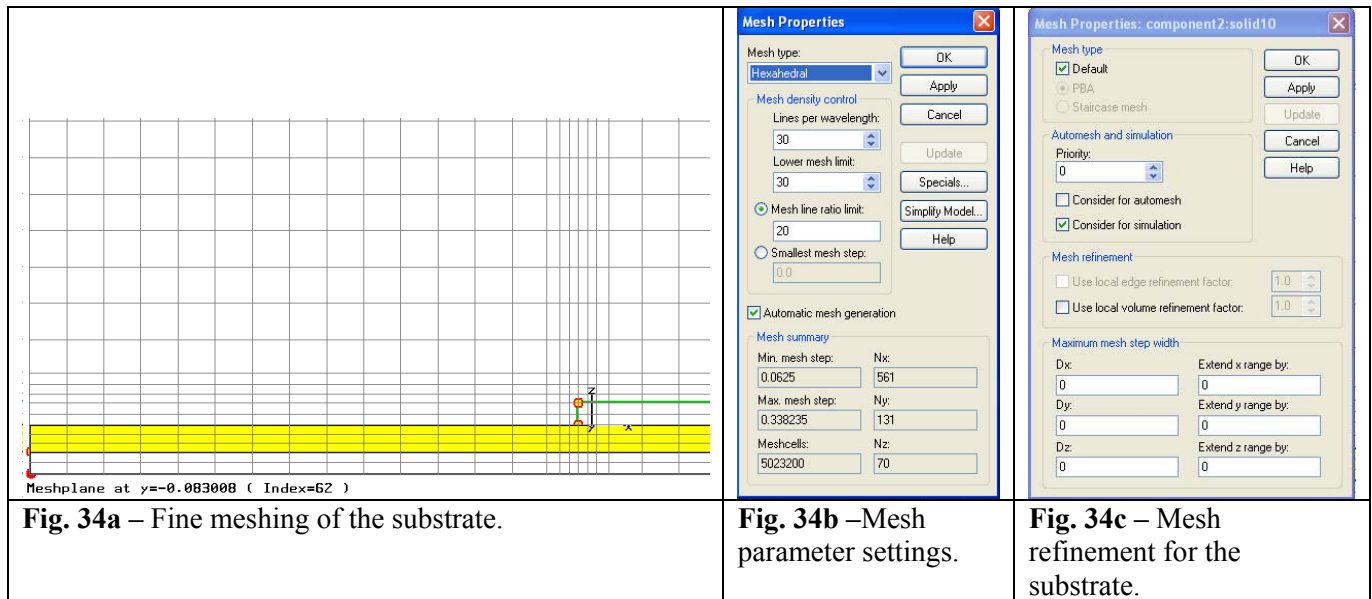


Fig. 34a – Fine meshing of the substrate.

Fig. 34b – Mesh parameter settings.

Fig. 34c – Mesh refinement for the substrate.

Substrate meshing: coarse mesh

The case with coarse mesh is shown in Fig 35. The substrate has been meshed with coarse mesh lines.

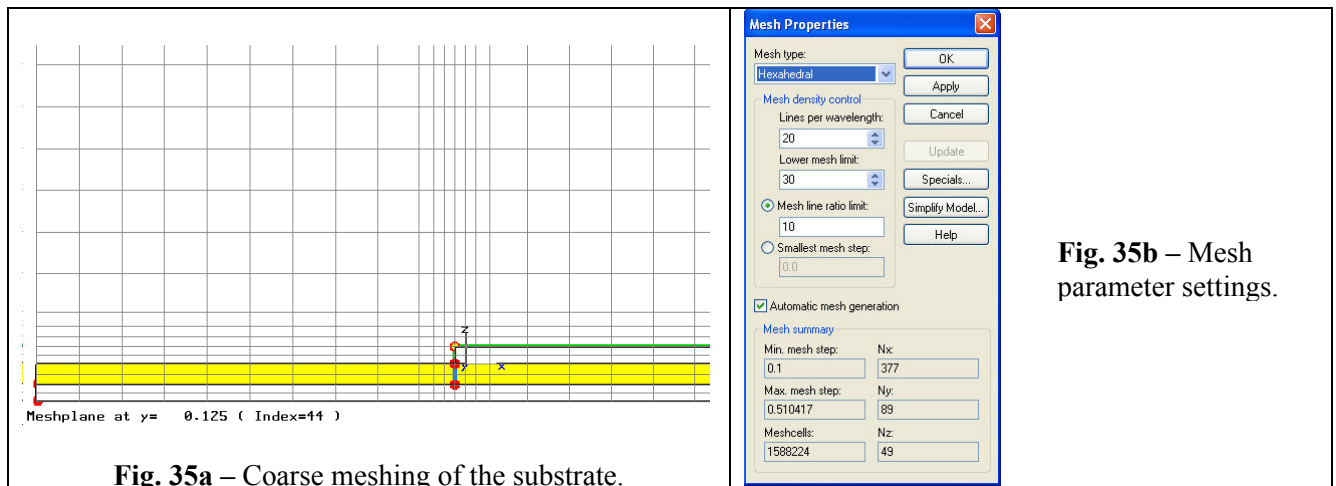


Fig. 35a – Coarse meshing of the substrate.

Fig. 35b – Mesh parameter settings.

Board with equivalent length straight line: substrate fine and coarse mesh results comparison

Fig. 36 shows the comparison, for fine and coarse mesh of the substrate, of the transient voltage waveform across the load termination for the case board with the equivalent length straight line. Fig. 37 shows the FSV comparison.

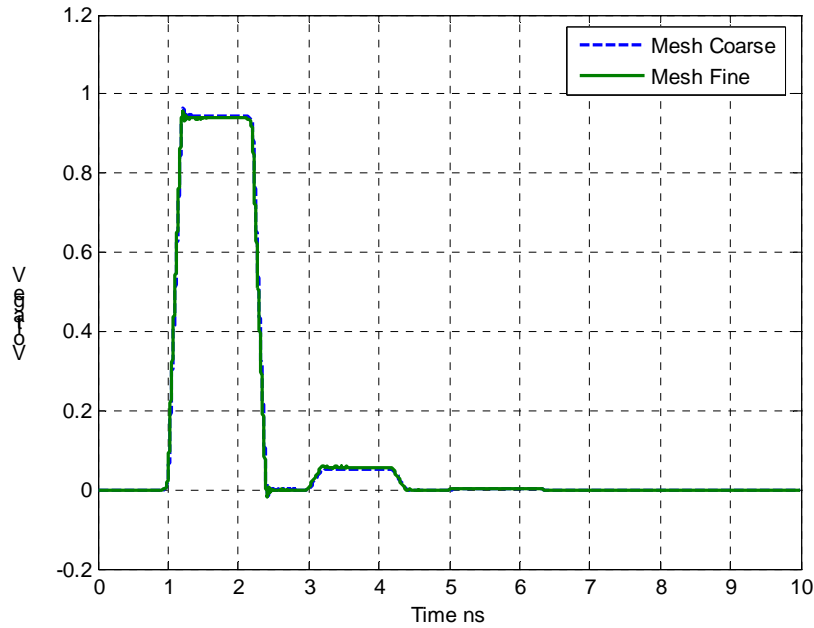
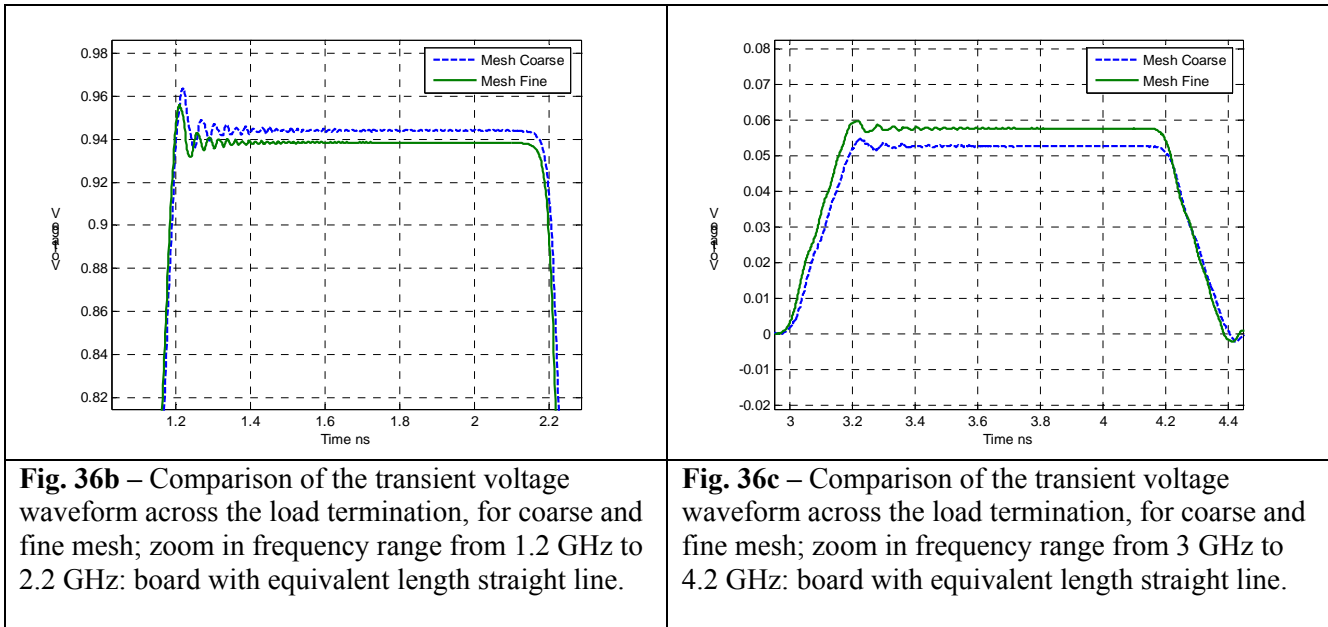


Fig. 36a – Comparison of the transient voltage waveform across the load termination: board with the equivalent length straight line.



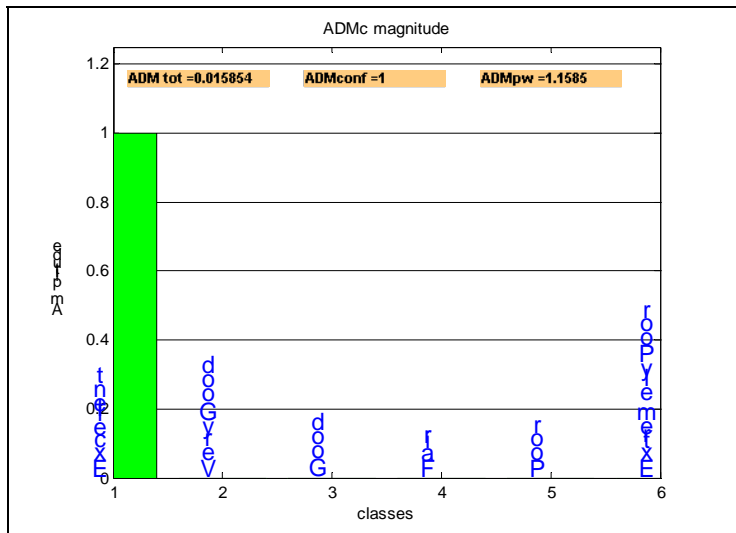


Fig. 37a – ADMc confidence diagram referred to Fig. 36.

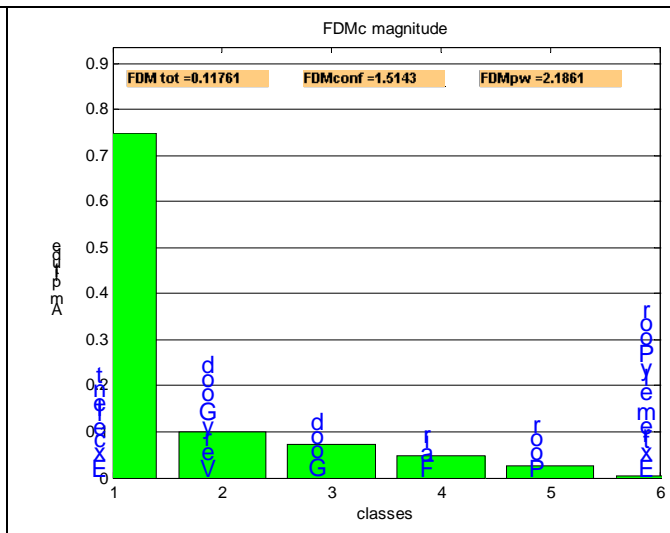


Fig. 37b – FDMc confidence diagram referred to Fig. 36.

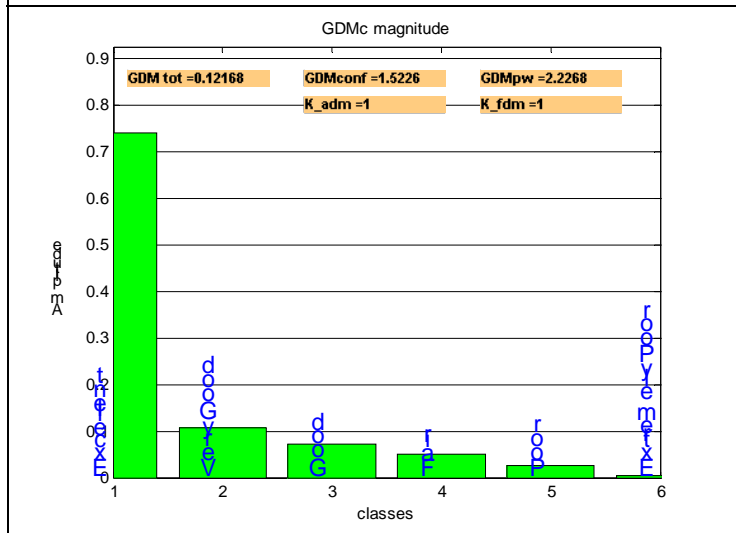


Fig. 37c – GDMc confidence diagram referred to Fig. 36.

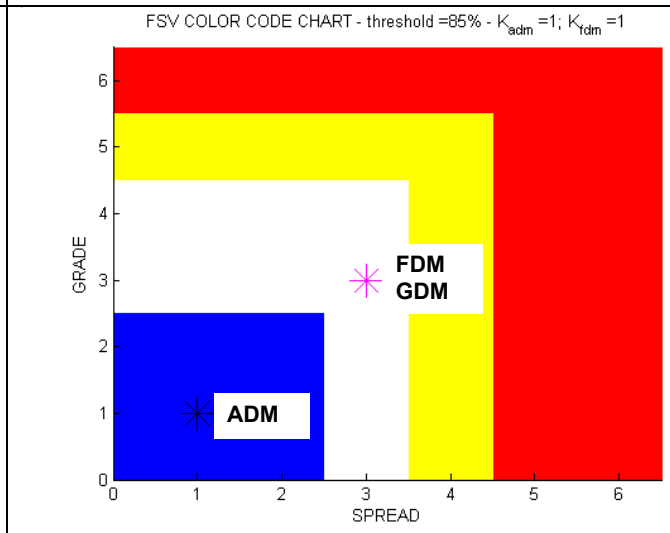


Fig. 37d – GRADE-SPREAD chart referred to Fig. 36.

5.3 Board with printed equivalent length straight line: wide GND plane

In order to investigate the effect on the result of the extension of the dimension of the reference plane and dielectric substrate, a new structure, as in Fig. 38, is considered.

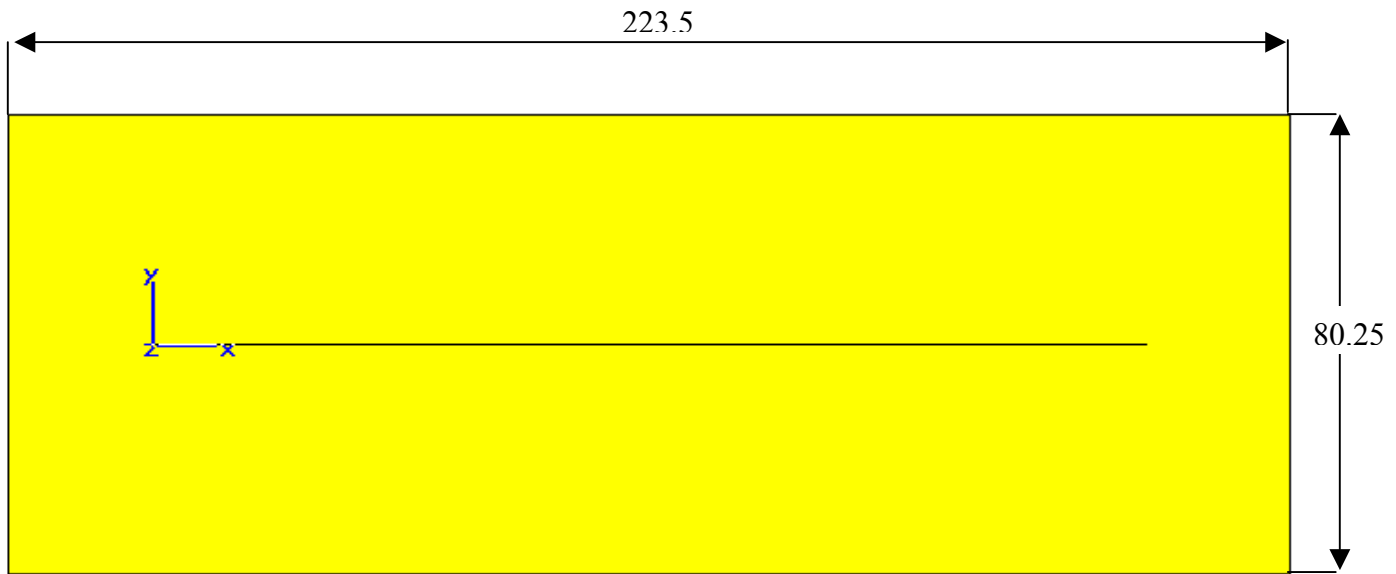


Fig. 38 – Top view: geometric dimensions of the board with printed equivalent length straight line and wide reference plane.

Equivalent Length Straight Line Model: wide reference plane (see Fig. 38) - The PCB model has the following characteristics: the reference plane is in Perfect Electric Conductor (PEC) material whose dimensions are 223.5 mm x 80.25 mm x 0.2 mm (x,y,z axis). On the PEC plane there is a dielectric substrate of FR4 whose dimensions are 223.5 mm x 80.25 mm x 0.25 mm; its dielectric permittivity is $\epsilon_r = 4.5$ and no dielectric losses are considered. The straight trace in PEC materials is placed on the dielectric substrate. The trace is simulated as a PEC material. The characteristic impedance of the line is 50 Ω .

Wide reference plane: comparison results

In Fig. 39 is shown the comparison of the transient voltage waveform across the load termination for the cases: board with equivalent length straight line and original reference plane size as shown in Fig. 28 and the case with wide reference plane as in Fig. 38. Fig. 40 show the corresponding FSV comparison.

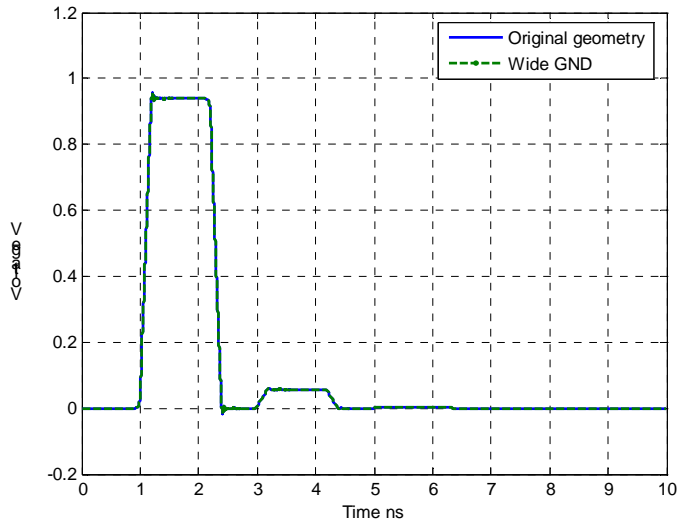


Fig. 39 – Comparison of the transient voltage waveform across the load termination: board with printed equivalent length straight line original dimensions and with wide GND plane.

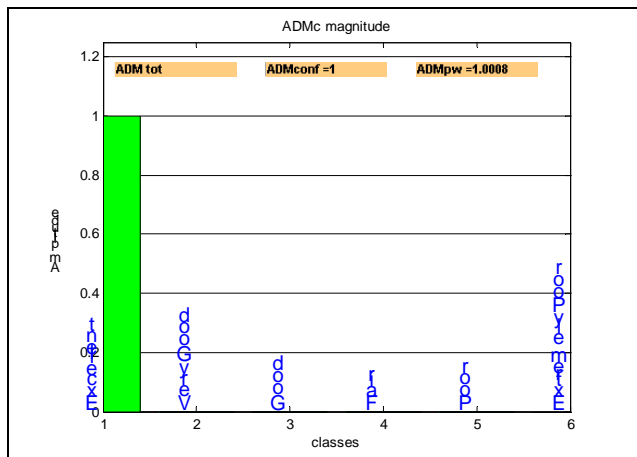


Fig. 40a - ADMc confidence diagram referred to Fig. 39.

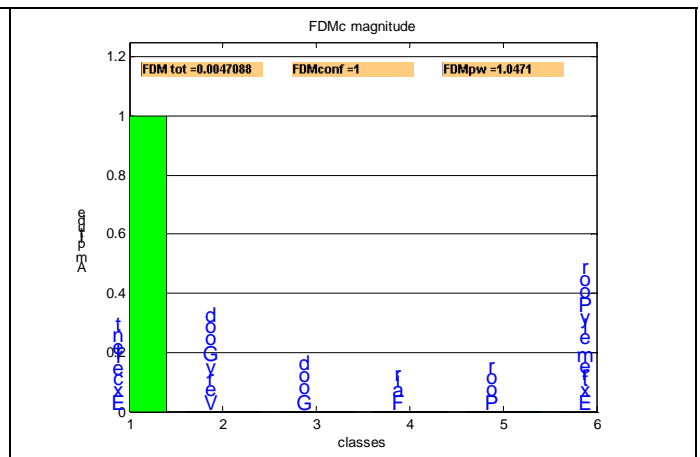


Fig. 40b - FDMc confidence diagram referred to Fig. 39.

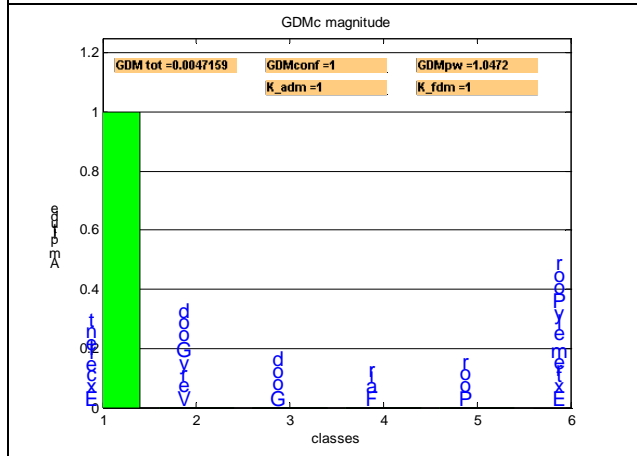


Fig. 40c - GDMc confidence diagram referred to Fig. 39.

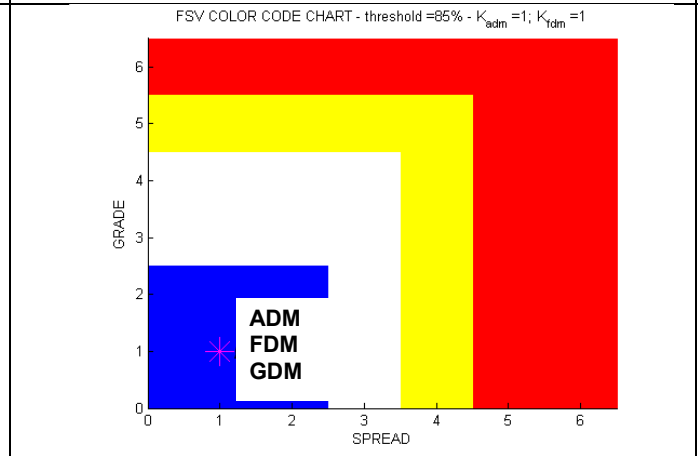


Fig. 40d – GRADE-SPREAD chart referred to Fig. 39.

5.4 Remarks

In the meander delay line model the variation of mesh parameters has a little impact on the computed results as well as in the equivalent length straight-line model in which different mesh for substrate is investigated. The extension of the GND plane has no impact on the computed transient voltage waveform at the end of the line.

6. CONCLUSION

With the proliferation of time domain electromagnetic solvers throughout microwave research and industry, their convergence properties become an issue of great practical importance. The FIT method is used in this paper to provide a general framework for the investigation of such convergence properties, along with the FSV technique, here operated to quantify the comparisons among different computational settings, so giving indications on the better choice of parameters according to the proposed aim. The sensitivity of the computed results has been investigated for different electromagnetic model varying the mesh parameter settings. The mesh is a critical feature in the numerical simulations that produce an impact on time simulations as well as an impact on the accuracy in the computed results. A proper trade-off should be always worked out.

REFERENCES

- [1] A.L.Drozdz, "Selected Methods for Validating Computational Electromagnetic Modeling Techniques", *IEEE EMC Society Newsletter*, n. 208, winter 2006.
- [2] A.L.Drozdz, "Progress on the development of standards and recommended practices for CEM computer modelling and code validation", in Proc. of 2003 IEEE Symposium on EMC, Boston, MA, August 2003.
- [3] IEEE Project 1597.1, "Standard for validation of computational electromagnetics (CEM) computer modelling and simulation", *IEEE P1597.1, Draft D1.2*, January 2005.
- [4] Computer Simulation Technology, *CST MicrowaveStudio Manual – ver. 5.1.2 -*, Vol I, II, www.cst.de.
- [5] T. Weiland, "A Discretization Method for the Solution of Maxwell's Equation for Six Component Fields", *Electronics and communication, (AEÜ)*, Vol.31 (1977), p. 116.
- [6] Martin AJM, "Quantitative data validation (automated visual evaluations)", PhD Thesis, De Montfort University, UK, 1999.
- [7] Woolfson MS, Benson TM, Christopoulos C and Duffy AP, 1995, "Quantitative Assessment of the Comparison of Electromagnetic Calculations with Experimental Data", *Applied Computational Electromagnetics Society Newsletter*, 1(1), pp 34-39.
- [8] A.P.Duffy, A.J.M.Martin, A.Orlandi, G.Antonini, T.M. Benson, M.S. Woolfson, "Feature Selective Validation (FSV) for Validation of Computational Electromagnetics (CEM) – Part I: The FSV Method", *IEEE Transactions on Electromagnetic Compatibility*, vol. 48, n.3, 2006.
- [9] A.P.Duffy, A.J.M.Martin, A.Orlandi, G.Antonini, T.M. Benson, M.S. Woolfson, "Feature Selective Validation (FSV) for Validation of Computational Electromagnetics (CEM) – Part II: Assessment of FSV Performances", *IEEE Transactions on Electromagnetic Compatibility*, vol. 48, n.3, 2006.

CEMPACK: A Benchmarking System for Hardware- and Software-Based Computational Electromagnetic Solvers

James P. Durbano, Fernando E. Ortiz, Ahmed S. Sharkawy, and Michael R. Bodnar
EM Photonics, Inc.
Newark, DE, USA
{durbano, ortiz, sharkawy, bodnar}@emphotonics.com

Abstract

Much like the computer industry of 20 years ago, the electromagnetics community is experiencing great difficulty in quantitatively analyzing the performance of different computational electromagnetic solvers. With the recent advent of hardware-based solvers, this issue has become even more important as these tools are focused almost entirely on speed. Without a clear mechanism to evaluate different solvers, tools will be unfairly compared to one another, misrepresentations will abound, and ultimately the users of these products will suffer. To eliminate such problems, in this paper we propose the development of a computational electromagnetics benchmarking suite. We discuss the three questions that must be addressed by such a benchmark suite and describe several representative problems that should be included in the package. Ultimately, this suite will allow different hardware and software researchers/companies to provide understandable performance results and enable the direct comparison of tools over a wide range of problems.

I. Introduction

Computational electromagnetic simulators are widely used in the early stages of research and development, in academic and industrial labs, in order to provide researchers with the

necessary tools to better understand various aspects of science and technology. Currently, these simulators are implemented on both software and hardware platforms. Hardware-based implementations of computational electromagnetic algorithms, specifically the Finite-Difference Time-Domain (FDTD) algorithm, have been researched for the past 15 years. In the early 1990s, the capabilities and performance of such implementations were severely limited because of the expense associated with developing custom silicon and the immaturity of programmable hardware solutions, such as field-programmable gate arrays (FPGAs). However, by the turn of the century, FPGAs were capable of supporting entire algorithm implementations, rather than simple proof-of-concept prototypes. Several groups have been involved in this “modern” era of hardware-based FDTD solvers and two companies have been formed to market successful implementations [1-6]. Moreover, an entire chapter is dedicated to hardware acceleration in the most recent edition of the authoritative FDTD text by Allen Taflove, one of the pioneers of the FDTD method [7]. Despite all of the advances in this research area, a standard method to directly compare hardware implementations has not been developed. In [8] we proposed a method for measuring the computational performance of hardware-based solvers. However, in [7] the authors suggest a slightly different metric. In addition, a third metric is mentioned in [4].

The basis of each of these metrics involves measuring the number of discretization points that can be “updated” per second. However, this measurement is not as straightforward as it sounds. For example, are they 2D or 3D nodes? 3D nodes have more field components, and thus require more computations, as compared with 2D nodes. Is a node considered processed after updating its electric or magnetic fields or both? What about the absorbing boundary condition chosen? Berenger’s perfectly-matched layer boundary conditions are more accurate, but more computationally intensive than others, such as second-order Mur boundaries [9, 10].

Without a consistent metric, misleading and confusing performance results will abound. For example, in Taflove's chapter, the metric cited is millions of cells per second (Mcels/s) [7]. However, the authors inaccurately compare the "cells" of one implementation to the "cells" of alternate implementations. If the developers of this technology cannot correctly distinguish among the metrics, one cannot expect end-users and other researchers to understand the relative performance.

The ability to quantitatively analyze the performance of different implementations is a problem that also plagued the computer industry. Specifically, hardware manufacturers wanted to compare their performance with those of competing companies. Comparisons included clock speed, floating-point operations per second (FLOPS), millions of instructions per second (MIPS), memory size/speed, cache size/speed, etc. Furthermore, because the requirements of different users varied, it was near impossible to make a statement such as "this is the best computer available." Rather, users needed to be able to evaluate machines under a variety of test problems and match up performance with the requirements of their application. Thus, benchmarking systems, such as SPEC and LINPACK were developed to help clarify system performance [11, 12].

Similarly, because discussing and quantifying the performance of both hardware and software solvers is more involved than simply quoting a single metric, such as cells per second or maximum problem size, we propose the development of a CEM-solver benchmarking suite, which we call CEMPACK. This will allow different hardware and software researchers/companies to provide understandable performance results and enable the direct comparison of tools over a wide range of problems. Section II discusses the shortcomings of related work in this area and how our proposed benchmark overcomes these weaknesses.

Section III discusses the requirements of the suite and proposes several simulations that should be included. Finally, in Section IV we draw concluding remarks and discuss future work in this area.

II. Related Work and Original Contribution

CEM methods have been extensively used for benchmarking computer systems, particularly parallel machines, because the algorithms stress many performance-critical components simultaneously, including the interconnection network and the memory subsystem [13-15]. For example, the temporal and spatial locality of the data dependencies tests the efficiency of the caching subsystem. Also, the depth and bandwidth of the main memory are challenged by substantial problem sizes and large, non-cacheable data sets. Rather than use CEM techniques to benchmark computers, as described above, we are proposing the development of a suite of electromagnetic simulation problems to test the performance of various CEM solver implementations. This will provide users with an unbiased assessment of the capabilities of various hardware and software solvers, in terms of functionality, speed, and accuracy.

CEM code and technique standardization has been a topic of great importance to the electromagnetics community, as evidenced through numerous papers and an IEEE standards group [16-25]. Although these works discuss topics ranging from the definition and need for standardization to the actual enumeration of specific benchmark problems, the recurring theme is validation. Specifically, much of this work has been focused on determining which method best suits the problem at hand, in order to provide the most accurate results. Of these papers, the work most similar to that contained in this paper is by Archambeault et al. [19]. In their 2001

paper, these researchers provided a set of problems that could be used to assist scientists concerned with electromagnetic compatibility. Unfortunately, the proposed set of problems was limited in scope, focusing primarily on printed circuit board analysis and device packaging. Although our paper presents benchmark problems in a similar fashion, they encompass a much broader spectrum of problem types in order to reach a more diverse audience, including engineers focused on radar design and nanophotonics. Previous work in this area is very limited and only consists of self-published benchmarks from software vendors, where they describe specific features and capabilities of their solvers [14, 26].

Similarly, the proposed IEEE Standards, 1597.1 and 1597.2, when fully realized, will cover the validation and standardization of computational electromagnetics models, methods, and numerical codes [27]. However, the standard does not include ‘performance’ as a key metric for evaluating CEM tools, which is certainly an important criterion for many simulation users. Additionally, the standard is neither finalized nor available in “pre-release” form for users to begin using. Our work aims to provide a suite of simple problems that test, not only accuracy, but also performance, and can be quickly realized on a variety of platforms.

As shown, previous work in this area is focused on CEM code validation or encompasses a narrow application band, while the proposed IEEE standards are not readily available nor consider CEM performance. Thus, there is a clear need to develop both a benchmarking system that is capable of fully characterizing a given CEM solver and also a clear method for comparing performance among different solvers. The CEMPACK benchmark suite, proposed in the next section, attempts to fill this void.

III. Benchmarking Suite

As outlined above, it is critical that the electromagnetics community develop a consistent metric to describe the performance of various CEM solvers. Moreover, only measuring processing throughputs, although important, does not provide enough information when comparing different implementations. For example, a user does not care how fast the solver is if it cannot solve their particular problem. Thus, the user wants to know the answer to three main questions: 1) Can it solve my problem? 2) How long will it take? 3) How accurate will the answer be? Therefore, the proposed metric must answer these three questions. In this section, we propose the Computational Electromagnetics Package (CEMPACK). CEMPACK (pronounced SEM-pack) consists of several synthetic benchmark problems that can be used to characterize CEM-solver implementations. The problems are “synthetic” in that they do not necessarily correspond to physically useful problems or scenarios. Rather, they attempt to stress various aspects of a solver implementation, including maximum problem size, absorbing boundary conditions, and various source types. We now address each of these questions.

Can It Solve My Problem?

The fastest computational platform available is of no use to researchers if it cannot solve the problem at hand. Thus, the benchmark suite must test a variety of problem types. For example, several source types, including uniform plane waves, point sources, and spatially and/or temporally modulated sources, should be exercised. In addition, the suite should test platform capabilities in various media, including inhomogeneous, dispersive, and non-linear materials. The suite should also examine performance with a range of problem sizes, because a very fast, accurate solver is not useful to many if it can only solve relatively small problems.

How Long Will It Take?

One of the most important requirements of this benchmarking suite is that actual runtimes be reported in terms of wall clock time, rather than metrics such as cells per second, nodes per second, or voxels per second [7, 8, 28]. These metrics, although useful, can be confusing as different vendors use these terms interchangeably, but measure the performance differently. Furthermore, if a particular solver implementation is capable of solving the same problem using fewer nodes, due to adaptive meshing or exploitation of symmetry, the metric may provide misleading information. For example, if two solvers are each capable of updating 10 million Yee cells per second [7], but Solver A utilizes adaptive meshing and Solver B does not, Solver A can solve the problem faster despite being “equivalent” to Solver B on paper. Because the end user is ultimately concerned with how much time the simulation requires, the benchmarking suite should simply measure wall clock time.

How Accurate Will The Answer Be?

Ultimately, a fast solver will not be used if it does not provide accurate results. Thus, it is important that the suite report the validity of benchmark results. However, because the needs of different users/applications vary, the necessary accuracy also varies. Whereas some applications may tolerate errors on the order of 10^{-2} , others may require accuracy to 10^{-5} or better. Because some solvers, such as those based on ADI-FDTD and fixed-point formats, may trade accuracy for speed, it is critical to evaluate how much accuracy is lost [1, 28-31]. If the numerical error is acceptable, these tools are highly desirable as they can potentially provide results faster than alternative platforms. Thus, the benchmark suite should test the accuracy of solvers against known analytic and experimental solutions whenever possible.

Now that we have discussed the three questions that must be addressed by a proposed benchmark suite, we present our initial problem suite. Each problem is briefly described and then several variations on the problem are presented in order to test numerous solver features.

A. Introduction to the Suite

Each of the test cases listed below is well defined, but not “over” defined. For example, it is not necessary (nor fair) to mandate the exact absorbing boundary condition used when different boundary conditions, with significantly different computational requirements, can prove equally effective for the same problem. Similarly, there are no pre-set accuracy requirements embedded with this suite. For example, CEMPACK does not require simulations to be performed within 1% accuracy of their analytic counterparts. Rather, our intention is that multiple simulations be run with varying criteria such that a performance vs. accuracy curve can be generated. Thus, tool providers could run the same problem many different times and describe their results. This will provide more information to the user who can examine the simulation results that are most applicable to his particular problem. Furthermore, temporally and spatially modulated waveforms are not mathematically described, as different vendors implement them differently. Once again, multiple simulations can be run with various source types in order to provide a wealth of information to the users and tool vendors can describe their particular source configurations.

Ultimately, the proposed suite is designed to be general. Certainly, this may not be desirable to every user and could allow tool vendors to perform simulations that show their tool in the best possible conditions. However, this will allow a variety of simulation tool developers to quickly report results and provide information that is of interest to researchers, rather than conform to a pre-set problem that does not reflect the needs of individual users.

B. Plane Wave Propagation in Homogeneous Media

Consider the propagation of uniform plane waves in unbounded free space. This problem is designed to stress the absorbing boundary conditions that surround the computational region. It also tests the plane-wave source. Accuracy can be verified by placing detectors at the beginning and end of the computational space, since the wave at the end is simply a time-delayed version of the initial wave. Note that “simulation time” is specified in the table in microseconds, rather than timesteps, to ensure that all platforms simulate wave propagation for the exact same length of time. Specifying timesteps is misleading, as a larger discretization grid will allow light to travel farther in the same number of timesteps.

Computational Space	250 mm x 250 mm x 500 mm
Source	On-axis (500 mm direction), uniform plane wave of 2.4 GHz
Materials	Free space
Geometry	N/A
Boundaries	Absorbing
Simulation time	10 μ s

Variation 1: Instead of directing the plane wave entirely along an axis, launch the wave at several oblique angles. This tests the ability of the software to launch oblique waves, as well as the boundaries to absorb off-axis waves.

Variation 2: Launch a spatially modulated plane wave, which tests support of this feature.

Variation 3: Launch a temporally modulated plane wave, which tests support of this feature.

Variation 4: Use a linear gallium arsenide (GaAs) as the background material, with the properties described in Section 9.7.2 of [7], which tests solver support for dispersive materials.

Variation 5: Use a non-linear Corning glass as the background material, with the properties described in Section 9.6.7 of [7], which tests solver support for non-linear materials.

C. Dielectric Sphere in Free Space

In this problem, a plane wave is launched at a dielectric sphere. Because this problem has an analytic solution (e.g., Mie Theory), it can be used to verify solver accuracy [32]. Furthermore, the problem size can be easily scaled by simply increasing the frequency of the incident wave (which necessitates a sampling rate change). Also, this problem allows solvers that support non-uniform meshing to sample the sphere and the surrounding free space at different rates to minimize computations.

Computational Space	250 mm x 250 mm x 500 mm
Source	On-axis (500 mm direction), uniform plane wave of 2.4 GHz
Materials	Free space, Glass
Geometry	Glass sphere (radius 62.5 mm)
Boundaries	Absorbing
Simulation time	10 μ s

Variation 1: Increase source frequency to 15 GHz, 20 GHz, and 30 GHz in order to test support for and performance of larger problem sizes.

Variation 2: Increase simulation time to 200 μ s to test algorithm stability.

D. Rectangular Waveguide

Here, a broadband pulse is launched into a single-mode, rectangular waveguide. The frequency of the guided mode can be calculated analytically and compared with the simulation results for accuracy computations. This problem also tests the performance of the solver when techniques such as non-uniform meshing cannot be employed and the ability of the solver to support Gaussian beams.

Computational Space	1.667 cm x 1.071 cm x 20 cm
Source	On-axis (20 cm direction), broadband pulse with center frequency = 12 GHz and a 4 GHz bandwidth
Materials	Free space, PEC
Geometry	Hollow metal parallelepiped
Boundaries	Absorbing
Simulation time	500 ps

Variation 1: Arbitrarily increase length of waveguide (and simulation time) in order to determine maximum supported problem size. This problem can also be used to generate Speed vs. Problem Size curves.

In this section, we presented the three questions that a CEM benchmark suite must address (Can it solve my problem? How long will it take? How accurate will the answer be?) and several benchmark problems that should be included in such a suite. Furthermore, we presented several variations associated with each test case that stress a variety of solver features and discussed the importance of each benchmark problem. However, this benchmark suite is not yet complete and, in the next section, we discuss the work that remains.

IV. Conclusion and Future Work

Much like the computer industry of 20 years ago, the electromagnetics community is experiencing great difficulty in quantitatively analyzing the performance of different CEM simulation tools. With the recent advent of hardware-based solvers, this issue has become even more important as these tools are focused almost entirely on speed. Without a clear mechanism to evaluate different solver platforms, tools will be unfairly compared to one another, misrepresentations will abound, and ultimately the users of these products will suffer.

Furthermore, only measuring processing throughputs, although important, does not provide enough information when comparing different implementations (a fast solver does not

help if it cannot solve the intended problem). Because discussing and quantifying the performance of both hardware and software solvers is more involved than simply quoting a single metric, such as cells per second or maximum problem size, in this paper we proposed the development of a computational electromagnetic benchmarking suite. This will allow different hardware and software researchers/developers to provide understandable performance results and enable the direct comparison of tools over a wide range of problems. This will greatly benefit users as they purchase commercial products and researchers as they compare their new methods/approaches against established implementations.

In order for such a suite to be beneficial, it is vital that those in the community embrace the benchmark. We encourage others to respond to this paper and suggest additional problems that should be included. Although we have attempted to cover an array of problem types that stress various solver features, other researchers and developers will undoubtedly suggest important test problems. For example, the authors are most familiar with the FDTD method and almost certainly overlooked test problems that stress various features of other methods, such as convergence for an eigenvalue solver. Further, we encourage all developers, hardware- and software-based, to solve as many of these problems as possible and post the results in a white paper on their websites. We also encourage independent researchers to verify these results by performing direct comparisons between the tools provided by various software and hardware vendors. Only when a clear, well defined suite of problems have been defined, will legitimate comparisons between tools exist. It is important that the electromagnetics community support such a suite so that users can effectively compare and contrast various solvers and new features without ambiguities and misrepresentations.

References

- [1] W. Chen, P. Kosmas, M. Leiser, and C. Rappaport, "An FPGA Implementation of the Two-Dimensional Finite-Difference Time-Domain (FDTD) Algorithm," presented at The Twelfth ACM International Symposium on Field-Programmable Gate Arrays (FPGA), 2004.
- [2] J. P. Durbano, F. E. Ortiz, J. R. Humphrey, and D. W. Prather, "FPGA-Based Acceleration of the 3D Finite-Difference Time-Domain Method," presented at 12th Annual IEEE Symposium on Field-Programmable Custom Computing Machines (FCCM), 2004.
- [3] R. N. Schneider, L. E. Turner, and M. M. Okoniewski, "Application of FPGA technology to accelerate the Finite-Difference Time-Domain (FDTD) method," presented at The Tenth ACM International Symposium on Field-Programmable Gate Arrays, Monterey, CA, 2002.
- [4] H. Kawaguchi, K. Takahara, and D. Yamauchi, "Design Study of Ultrahigh-Speed Microwave Simulator Engine," *IEEE Transactions on Magnetics*, vol. 38, pp. 689-692, 2002.
- [5] "EM Photonics, Inc.," www.emphotonics.com.
- [6] "Acceleware," www.acceleware.com.
- [7] A. Taflove and S. C. Hagness, *Computational Electrodynamics: The Finite-Difference Time-Domain Method*, 3rd ed. Norwood: Artech House, 2005.
- [8] J. P. Durbano, F. E. Ortiz, J. R. Humphrey, D. W. Prather, and M. S. Mirotznik, "Hardware implementation of a three-dimensional Finite-Difference Time-Domain algorithm," *IEEE Antennas and Wireless Propagation Letters*, vol. 2, pp. 54-57, 2003.
- [9] G. Mur, "Absorbing Boundary Conditions for the Finite-Difference Approximation of the Time-Domain Electromagnetic-Field Equations," *IEEE Transactions on Electromagnetic Compatibility*, vol. 23, pp. 377-382, 1981.
- [10] J.-P. Berenger, "Three-Dimensional Perfectly Matched Layer for the Absorption of Electromagnetic Waves," *Journal of Computational Physics*, vol. 127, pp. 363-379, 1996.
- [11] "Standard Performance Evaluation Corporation (SPEC)," www.spec.org.
- [12] "Top 500 Supercomputer Sites," <http://www.top500.org/lists/linpack.php>.
- [13] "FDTD Cube Grid Benchmark," <http://lc.cray.com/fdtd/>, 1999.

- [14] M. Martínez-Vázquez and D. Sánchez-Hernández, "Benchmarking of Commercial Electromagnetic Simulators for the Design of Printed Antennas," <http://www.rc.fer.hr/cost260/davos/p0063.pdf>.
- [15] U. Anderson, P. Ekman, and P. Oster, "Performance and performance counters on the Itanium 2 - A benchmarking case study," <https://rparco.urz.tu-dresden.de/Parco2003/up/1page-abstract/1p-abstract-103.pdf>.
- [16] B. Archambeault and C. Brench, "Proposed standard EMI modeling problems," presented at IEEE International Symposium on EMC, 1994.
- [17] B. Archambeault, "Evaluating tools which predict the shielding effectiveness of metal enclosures using a set of proposed standard EMI modeling problems," presented at IEEE International Symposium on EMC, 1998.
- [18] B. Archambeault, "Modeling and simulation validation for EMC applications," presented at IEEE International Symposium on EMC, 1999.
- [19] B. Archambeault, S. Pratapneni, L. Zhang, D. C. Wittwer, and J. Chen, "A Proposed Set of Specific Standard EMC Problems To Help Engineers Evaluate EMC Modeling Tools," presented at IEEE International Symposium on EMC, 2001.
- [20] B. Archambeault, "Concerns and approaches for accurate EMC simulation validation," presented at IEEE International Symposium on EMC, 2003.
- [21] B. Archambeault and S. Connor, "Various approaches to validating full wave simulations," presented at IEEE International Symposium on EMC, 2004.
- [22] A. L. Drozd, "Progress on the Development of Standards and Recommended Practices for CEM Computer Modeling and Code Validation," presented at IEEE International Symposium on EMC, 2003.
- [23] A. L. Drozd and B. Archambeault, "Recent Developments in the Formation of Standards and Recommended Practices for Validating Computational Electromagnetics Models and Numerical Codes," presented at IEEE International Symposium on EMC, 2004.
- [24] A. Duffy, A. Drozd, B. Archambeault, and D. Coleby, "Measuring Similarity For Validation of Computational Electromagnetic Modelling (sic)," presented at IEEE International Symposium on EMC, 2004.
- [25] H. Jordan, S. Bokhari, S. Staker, J. Sauer, M. ElHelbawy, and M. Piket-May, "Experience with ADI-FDTD techniques on the Cray MTA supercomputer," *Proc. of the SPIE - Commercial Applications for High-Performance Computing*, vol. 4528, pp. 68-76, 2001.
- [26] "IE3D Benchmark Simulation Examples," http://www.bay-technology.com/IE3D_Benchmark.pdf.

- [27] "P1597.1 - IEEE Standard for Validation of Computational Electromagnetics (CEM) Computer Modeling and Simulation & P1597.2 - IEEE Recommended Practice for Computational Electromagnetics (CEM) Computer Modeling and Simulation Applications," IEEE EMC Society Standards Development Committee.
- [28] H. Songoro, "On the Real-World Performance of ADI-FDTD," http://www.semcad.com/publications/hs_poster_05.pdf, 2005.
- [29] S. G. García, T.-W. Lee, and S. C. Hagness, "On the Accuracy of the ADI-FDTD Method," *IEEE Antennas and Wireless Propagation Letters*, vol. 1, pp. 31-34, 2002.
- [30] T. Namiki, "A new FDTD algorithm based on alternating-direction implicit method," *IEEE Transactions on Microwave Theory and Techniques*, vol. 47, pp. 2003-2007, 1999.
- [31] F. Zheng, Z. Chen, and J. Zhang, "A finite-difference time-domain method without the Courant stability conditions," *IEEE Microwave and Guided Wave Letters*, vol. 9, pp. 441-443, 1999.
- [32] G. Mie, "Beiträge zur Optik trüber Medien, speziell kolloidaler Metallösungen (Contributions on optical properties of turbid solutions, with special reference to colloid metallic solutions)." *Ann. Physik*, vol. 25, pp. 377-445, 1908.

Reduced Order Models for Metamaterial Transmission Lines

Giulio Antonini, *Senior Member, IEEE*

UAq EMC Laboratory

Dipartimento di Ingegneria Elettrica e dell'Informazione

Università degli Studi di L'Aquila

Montelucio di Roio, 67040 AQ, Italy

Abstract - This paper presents a reduced order model of metamaterial transmission lines. The metamaterial transmission line can be regarded as a ladder network characterized by propagating and evanescent modes generated by negative permeability and permittivity. Quasi-closed form of poles and residues are computed, taking advantage of the periodic structure of such type of structure, thus leading to an efficient time domain macromodel. Furthermore, the same methodology can be also efficiently used when the metamaterial is characterized in terms of equivalent dispersive and lossy permeability and permittivity over a frequency range. A model order reduction (MOR) technique is proposed allowing to reduce the computational effort in carrying out time domain simulations and allowing fast parametric models generation. In addition, the capability of the proposed method to properly reproduce the physics of metamaterials and to reduce the computational complexity due to the dispersive behavior of such artificial materials is demonstrated by the numerical results.

Index terms-Metamaterials, transient analysis, dispersive and lossy materials, model-order reduction techniques, parametric models.

I. INTRODUCTION

In the late 1960s, Veselago proposed that materials with simultaneously negative permittivity and permeability are physically permissible and have a negative index of refraction [1], [2]. He called these left-handed (LH) materials because the vectors \mathbf{E} , \mathbf{H} and \mathbf{k} form a left-handed triplet instead of right-handed triplet, as in the case of conventional right-handed (RH) media. Although it has been known for some time that arrays of thin metallic wires can produce an effectively negative dielectric permittivity, it was not clear as to how produce a negative permeability until the recent development of the split-ring resonator (SRR) by Pendry *et al.* was successful in this effort [3]. Experimental evidence of LH materials properties has been given by Smith *et al.* [4], [5] who demonstrated an LH structure made of negative- ϵ thin-wires and negative- μ split-ring resonators exhibiting anomalous refraction at the boundary. More than 30 years passed before such media, referred to as *metamaterials* (MTMs), were first realized by several research groups [4]-[7], based on resonant periodic structures with series capacitors and shunt inductors.

Such artificial media are characterized by negative values of permeability and permittivity over a wide frequency band and exhibit an evident and necessary dispersive behavior [2] which requires a special care when implementing a time domain algorithm. So far metamaterials have been extensively studied in the frequency domain and only recently time domain schemes have been proposed to capture the dispersive nature of the metamaterial itself. In [8] a one-dimensional (1-D) Finite Difference Time Domain (FDTD) method is presented to investigate the super-luminal properties of a particular type of metamaterial, the two time derivative Lorentz material (2TDLM), in propagating signals through the medium. Although the obtained results allow to gain deeper insight into the physics of such materials, the developed FDTD code is complex to be implemented and simulations are quite time-memory consuming. Also in [9] the behavior of an evanescent wave interacting with a slab of a backward material with Lorentz-type frequency dependence is studied via FDTD simulations based on a pseudo-spectral time domain (PSTD) method [10]. As in the previous work, a dedicated algorithm

Corresponding Author: G. Antonini, *UAq EMC Laboratory*, Dipartimento di Ingegneria Elettrica, Università degli Studi di L'Aquila, Montelucio di Roio, 67040, L'Aquila, Italy. Tel.:+39-0862-434462, fax: +39-0862-434403, e-mail: antonini@ing.univaq.it

must be implemented to perform time domain computations and a special care is required to ensure the necessary stability.

One of the most successful approaches to model left-handed (LH) materials has been presented in [7] where an equivalent circuit for a left-handed transmission line (LH-TL) is proposed. Such equivalent circuit has been then extended to composite right/left handed (CRLH) metamaterials in [11]. A more complex unit cell of the equivalent line circuit of a metamaterial constituted by a split-ring resonator/wire medium is presented in [6]. The same authors have presented in [12] a two-dimensional (2-D) L, C loaded transmission line acting as an isotropic left handed or negative refracting index (NRI) material. In [13] a 2-D Composite right/left handed transmission line (CRLH-TL) model is presented and the dispersion diagram of the two-dimensional CRLH-TL is obtained analytically based on the Bloch-Floquet theory. The main advantage of a circuit description is that the same equivalent circuit can be used in both the frequency and time domain computations; the main drawback is that the proposed circuits assume particular dispersive laws of the material and cannot be used to model different type of metamaterials (e.g. 2TDLM).

One of the most challenging task in using metamaterials in practical applications is their miniaturization in order to make them well suited for mobile communication systems. Much progress has been recently done as shown in [14] where a super-compact diplexer is presented and characterized as a multilayered composite left/right transmission line (ML-CRLH-TL).

Metamaterials surely will keep drawing interest in the microwave community and new artificial materials belonging to their family will be designed and new devices will be constructed. This increasing interest in MTMs calls for new numerical techniques which are able to reproduce their intrinsic dispersive nature at a reduced cost. Nowadays, as pointed out above, time domain methods require a special care, when dealing with dispersive media, which causes them to be extremely more time consuming when compared with their non-dispersive counterpart.

More recently time domain modeling of MTMs has received an increasing interest and led to the publication of several papers on it [15]-[17] where 2D and 3D numerical models are presented. As several practical implementations of MTMs are based on circuit and transmission lines, one of the most used techniques for modeling such kind of materials is the Transmission Line Matrix (TLM) method [18], [19].

Aim of this work is to present a novel methodology for the transient analysis of metamaterial transmission lines (MMTLs) exhibiting a general dispersive behavior, based on the analytical characterization of the half-T ladder network approximating the metamaterial transmission line. The most important features of the proposed approach are: 1) it allows straightforward computation of the poles of the two-port representation of the MMTL with machine-accuracy; 2) the knowledge of the MMTL poles allows to generate a macromodel which can be used in both time and frequency domain; 3) the knowledge of the poles allows developing a reduced order model, by retaining only the poles which significantly impact the physical behavior of the MMTL in the frequency range of interest; 4) the proposed method can be used for any type of metamaterial as it doesn't assume any particular kind of dispersive behavior nor law for negative equivalent parameters μ and ε ; 5) the proposed methodology can be used as building block for modeling metamaterials and, in general, dispersive media, in the framework of the TLM method [19]-[16]; 6) a quasi analytical correspondence between per-unit length parameters of the MMTL and the poles of the system is extremely useful at the design stage as it allows to select the stop and pass-bands and, thus, to design the frequency response of the system; 7) parameterized reduced order models can be easily generated.

The paper is organized as follows. Section II presents the formulation for modeling MMTLs with general constitutive parameters of equivalent materials. In Section III the two port representation of the MMTL in both the cases of CRLH and 2DTLM metamaterials is presented; in Section IV relevant formulas for computing poles and residues of CRLH materials are derived. The knowledge of poles allows to select only the dominant ones, within a fixed frequency band, that really impact the physical

behavior of the MMTL; the pole pruning is described in Section V pointing out that a special care is needed in order to ensure high accuracy as the interaction of longitudinal and transversal resonators cause the poles to be located mostly in well separated frequency bands. The possibility to adopt the proposed method to generate parameterized macromodels of MMTL is reported in Section VI. Numerical results for CRLH and 2DTLM MMTLs are presented in Section VII where the accuracy of the proposed method in reproducing the physical behavior of MMTLs is demonstrated along with the reduction of the computational complexity. Section VIII draws the conclusions.

II. GENERAL FORMULATION FOR PROPAGATING AND EVANESCENT MODES

Several previous studies of metamaterials have been carried out considering the propagation of electromagnetic signals through a slab characterized by negative ε and μ over a frequency range [8]; more recently a composite right/left handed transmission line has been presented [7], [11] and studied by using standard techniques in the frequency domain. Both these two problems can be studied by means of the transmission line theory (TLT). Thus, we will start by considering the first kind of problem keeping in mind that the second one can be analyzed by using the same formalism. Fig. 1 shows an uniform plane wave normally impinging on a slab of a metamaterial.

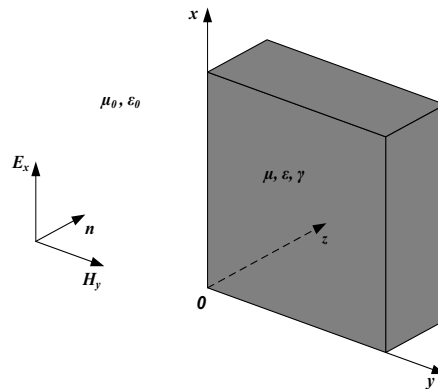


Fig. 1. An uniform TEM plane wave impinging on a slab of metamaterial.

Although the methodology illustrated in the following holds also for non orthogonal incidence [22], for the sake of clarity, only the orthogonal incidence will be here presented. For a $\mathbf{E}_x - \mathbf{H}_y$ TEM uniform plane wave Maxwell's equations in Laplace's domain read:

$$\frac{\partial}{\partial z} \mathbf{E}_x(z, s) = -s\mu(s) \mathbf{H}_y(z, s) \quad (1a)$$

$$\frac{\partial}{\partial z} \mathbf{H}_y(z, s) = -(s\varepsilon(s) + \gamma) \mathbf{E}_x(z, s) \quad (1b)$$

where $\mu(s)$ and $\varepsilon(s)$ are the frequency dependent permeability and permittivity of the metamaterial and γ its electric conductivity. The difficulty in finding the transient solution of such kind of equations is related to the dispersive behavior of the $\mu(s)$ and $\varepsilon(s)$ parameters which requires a special treatment. The physics of metamaterials is strictly related to the fact that they exhibit simultaneously negative permeability and permittivity. As pointed out before, TEM propagation through a slab can be studied by using transmission line theory (TLT). In the case of metamaterials the per unit length parameters of the equivalent transmission line may be frequency dependent making their transient analysis an even more difficult task.

The development of transient analysis algorithms for lossy and dispersive transmission lines with frequency dependent parameters has recently received much attention and efficient techniques have

been proposed [23]-[27]. In these papers MOR techniques, based on Padé approximations, together with the state-space formulation of the solution of the transmission line system, are used to develop reduced-order macromodels of the transmission line (TL). More recently a new method has been presented [28] based on half-T ladder network (HTLN) theory and special polynomials known as DFF and DDFz [29]-[31], allows the extraction of poles and residues of the half-T ladder network approximating the MTL which pawns the way to an efficient model order reduction technique; the method has been more recently extended to frequency dependent per unit length parameters (FDPUL) [32] and will be rapidly reviewed in Section III. Although the methodology illustrated in [32] can be adopted *tout-court* to capture the physics of CRLH metamaterials which exhibit a dispersive behavior along with their typical properties such as backward waves [33], a different approach is used in this work. An HTLN is considered to model both the metamaterial slab or transmission line. Thus, in the following, we will refer indifferently to the slab and the transmission line.

A classification of metamaterials can be done according to the kind of dispersion from which they are characterized. We will consider two classes of metamaterials which are widely studied in the literature and used for practical applications: CRLH and 2TDLM metamaterials.

A. CRLH metamaterials

Such kind of artificial materials have a simple equivalent circuit synthesis. In [34] the authors show that both propagating and evanescent TM modes exist in double negative media (DNG) and equivalent TL models have been proposed which are characterized by longitudinal capacitances and transversal inductances. The same typology of elementary half-T cell is adopted in [11]. For this reason in the following it will be assumed the equivalent circuit shown in Fig. 2 which represents a possible model for an electrically short section of a composite right/left handed transmission line (CRLH-TL), although more complex models can be considered; sub-indexes R and L refer to right and left handed properties.

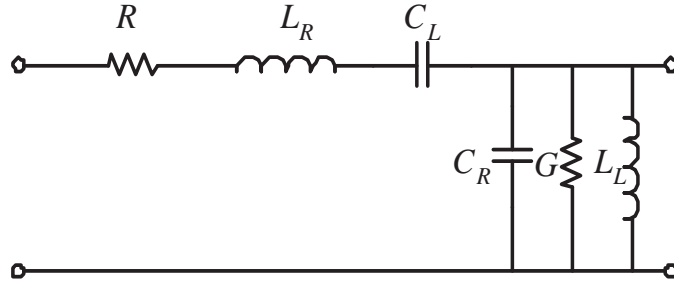


Fig. 2. Elementary half-T cell for a CRLH-TL.

Transient analysis of TLs, under the assumption that only the TEM mode propagates, is based on the set of partial differential equations known as Telegrapher's equations which, in Laplace domain, are given by:

$$\frac{\partial}{\partial z} V(z, s) = - \left(R' + sL'_R + \frac{1}{s}C'_L{}^{-1} \right) I(z, s) \quad (2a)$$

$$\frac{\partial}{\partial z} I(z, s) = - \left(G' + sC'_R + \frac{1}{s}L'_L{}^{-1} \right) V(z, s) \quad (2b)$$

where $R' \in \Re$, $L'_R \in \Re$, $C'_R \in \Re$, $G' \in \Re$, $L'_L \in \Re$ and $C'_L \in \Re$ are frequency-independent per-unit-length (FIPUL) parameters [35], [36]. The exponential form of Telegrapher's equations [35], in the

case of FIPUL parameters, reads:

$$\begin{bmatrix} V(\ell, s) \\ -I(\ell, s) \end{bmatrix} = e^{\Psi} \begin{bmatrix} V(0, s) \\ I(0, s) \end{bmatrix} \quad (3)$$

where

$$\Psi(s) = \left(\alpha + s\beta + \frac{1}{s}\gamma \right) \ell \quad \alpha = \begin{bmatrix} 0 & -R' \\ -G' & 0 \end{bmatrix} \quad \beta = \begin{bmatrix} 0 & -L'_R \\ -C'_R & 0 \end{bmatrix} \quad \gamma = \begin{bmatrix} 0 & -C'_L{}^{-1} \\ -L'_L{}^{-1} & 0 \end{bmatrix} \quad (4)$$

It is easy to verify that the equivalent circuit described in Fig. 2 is adequate to model the basic property of CRLH media which is the simultaneous negativity, at least within a certain frequency range, of permittivity and permeability. This is essential to correctly model such as backward waves and evanescent modes. For a lossless material the propagation constant is $\beta = \omega\sqrt{\mu\varepsilon}$; thus, as the propagation constant of a TL is $j\beta = \sqrt{Z'Y'}$, the following relation can be set up [11]:

$$-\omega^2\mu\varepsilon = Z'Y' \quad (5)$$

Furthermore, the TL's characteristic impedance $Z_c = \sqrt{Z'/Y'}$ and the material's intrinsic impedance $\eta = \sqrt{\mu/\varepsilon}$ can be related such that

$$Z_c = \eta \rightarrow \frac{Z'}{Y'} = \frac{\mu}{\varepsilon} \quad (6)$$

Finally, equivalent magnetic permeability and electric permittivity can be written as

$$\mu(\omega) = \frac{Z'}{j\omega} = L'_R - \frac{1}{\omega^2 C'_L} \quad (7)$$

$$\varepsilon(\omega) = \frac{Y'}{j\omega} = C'_R - \frac{1}{\omega^2 L'_L} \quad (8)$$

which can be negative up to a given frequency determined by the values of per unit length right and left parameters. The corresponding parameters in the Laplace domain read:

$$\mu(s) = \frac{Z'}{s} = L'_R + \frac{1}{s^2 C'_L} \quad (9)$$

$$\varepsilon(s) = \frac{Y'}{s} = C'_R + \frac{1}{s^2 L'_L} \quad (10)$$

B. 2DTLM medium

In [8] it has been presented a different metamaterial model, the two time derivative Lorentz material (2TDLM), which can be designed so that it allows communication signals to propagate in the medium at speeds exceeding the speed of light in vacuum without violating causality. Such a medium is characterized by frequency dependent parameters μ and ε :

$$\mu(s) = \mu_0 [1 + \chi_{2TDLM}^m(s)] \quad (11)$$

$$\varepsilon(s) = \varepsilon_0 [1 + \chi_{2TDLM}^e(s)] \quad (12)$$

where the Laplace domain electric and magnetic susceptibilities $\chi_{2TDLM}(s)$ are:

$$\chi_{2TDLM}^m(s) = \chi_{2TDLM}^e(s) = \chi_{2TDLM}(s) = \frac{\omega_p^2 \chi_\alpha + s\omega_p \chi_\beta + s^2 \chi_\gamma}{s^2 + s\Gamma + \omega_0^2} \quad (13)$$

This choice of the parameters guarantees that the wave impedance in this matched 2DTLM medium equals that from the free space thus leading to a zero reflection coefficient. Properly setting the parameters in (13) leads to values of μ and ε smaller than their values in free space over a large range of frequencies.

The previous model for μ and ε can be easily synthesized into equivalent circuits which look like with those in Fig. 2. In the case of more complex dispersive behaviors (e.g. when higher order rational representations are used for $\chi_{2TDLM}(s)$) it is always possible to use the HTLN model; in fact, an equivalent HTLN can be built to model such a medium which is characterized by frequency dependent per unit length parameters. In this case Telegrapher's equations, in Laplace domain, are given by:

$$\frac{\partial}{\partial z} V(z, s) = -(R'(s) + sL'(s)) I(z, s) \quad (14a)$$

$$\frac{\partial}{\partial z} I(z, s) = -(G'(s) + sC'(s)) V(z, s) \quad (14b)$$

where $R'(s) \in \mathfrak{R}$, $L'(s) \in \mathfrak{R}$, $C'(s) \in \mathfrak{R}$, $G'(s) \in \mathfrak{R}$ are frequency-dependent per-unit-length (FD-PUL) parameters. Equations (14a-14b) can be re-written in the Laplace domain by using the same exponential matrix function as in (3) where, in this case, Ψ reads

$$\Psi(s) = (\alpha(s) + s\beta(s))l \quad \alpha = \begin{bmatrix} 0 & -R'(s) \\ -G'(s) & 0 \end{bmatrix} \quad \beta(s) = \begin{bmatrix} 0 & -L'(s) \\ -C'(s) & 0 \end{bmatrix} \quad (15)$$

III. TWO PORT REPRESENTATION

A. FIPUL parameters

Let's assume that an order n half-T ladder network (HTLN) is used for approximating the TEM modes in the metamaterial slab or MMTL; the parameters for a single cell are:

$$R = R' \frac{\ell}{n} \quad L_R = L'_R \frac{\ell}{n} \quad C_L = C'_L \frac{n}{\ell} \quad (16a)$$

$$G = G' \frac{\ell}{n} \quad C_R = C'_R \frac{\ell}{n} \quad L_L = L'_L \frac{n}{\ell} \quad (16b)$$

where ℓ is the thickness of the slab or the length of the transmission line. The unit cell quantities can be defined as:

$$Z_1(s) = \left(R' + sL'_R + \frac{1}{sC'_L} \right) \frac{\ell}{n} = Z'(s) \frac{\ell}{n} = R + sL_R + \frac{1}{sC_L} \quad (17a)$$

$$Y_2(s) = \left(G' + sC'_R + \frac{1}{sL'_L} \right) \frac{\ell}{n} = Y'(s) \frac{\ell}{n} = G + sC_R + \frac{1}{sL_L} \quad (17b)$$

The standard case of RH propagation presented in [28],[32] is obtained when $L_L = C_L = \infty$.

B. FDPUL parameters

In the case of FDPUL parameters it is assumed that a suitable rational approximation of $Z_1(s)$ and $Y_2(s)$ matrices is obtained by using standard fitting techniques [37], leading to the following rational representations:

$$Z_1(s) \cong Z_{fit,1}(s) = R_0 + sL_0 + \sum_{m=1}^{P_1} \frac{R_1}{s - p_{m,1}} \quad (18a)$$

$$Y_2(s) \cong Y_{fit,2}(s) = G_0 + sC_0 + \sum_{m=1}^{P_2} \frac{R_2}{s - p_{m,2}} \quad (18b)$$

where P_1 and P_2 represent the number of poles used in the rational approximation. The zero-pole form is better suited for algebraic manipulations and polynomials convolutions [38]; for matrices Z_1 and Y_2 it reads:

$$Z_1(s) \cong \frac{b_1 s^{P_1+1} + b_2 s^{P_1} s + \dots + b_{P_1} s + b_{P_1+1}}{a_1 s^{P_1} + a_2 s^{P_1-1} + \dots + a_{P_1} s + a_{P_1+1}} = \frac{B_p(s)}{A_p(s)} \quad (19a)$$

$$Y_2(s) \cong \frac{d_1 s^{P_2+1} + d_2 s^{P_2} s + \dots + d_{P_2} s + d_{P_2+1}}{c_1 s^{P_2} + c_2 s^{P_2-1} + \dots + c_{P_2} s + c_{P_2+1}} = \frac{D_p(s)}{C_p(s)} \quad (19b)$$

where $B_p(s)$ and $D_p(s)$ are positive real polynomial and $A_p(s)$ and $C_p(s)$ are strictly Hurwitz polynomials. A strict Hurwitz polynomial has its roots only in the left half-plane. Hence, the poles of the rational approximations (19) are strictly in the left half-plane.

C. Y matrix representation

In [30] it has been shown that a half-T ladder network can be analytically characterized in terms of Chebyshev polynomials. The polynomial based approach presented in [30] and then extended to transmission lines in [28],[32],[39] is here briefly summarized for the sake of clarity. To this aim let's define the half-T cell factor $K(s)$ as:

$$K(s) = Z_1(s) Y_2(s) \quad (20)$$

In [30] it was shown that all the electrical characteristics of a HTLN can be expressed in terms of two polynomials (namely DFF and DFFz) depending on the cell matrix factor $K(s)$:

$$P_b^n(K(s)) = \sum_{j=0}^n b_{j,n} K^j(s) \quad \text{DFF polynomial of order } n \quad (21)$$

$$P_c^n(K(s)) = \sum_{j=0}^n c_{j,n} K^{j+1}(s) \quad \text{DFFz polynomial of order } n \quad (22)$$

where coefficients $b_{j,n}$ and $c_{j,n}$ can be computed analytically as:

$$b_{i,j} = \binom{i+j}{j-i} \quad (23a)$$

$$c_{i,j} = \binom{i+j+1}{j-i} \quad (23b)$$

Two port A, B, C and D parameters can be expressed in terms of DFF and DFFz polynomials as:

$$A(s) = \sum_{j=0}^n b_{j,n} K^j(s) = P_b^n(K(s)) \quad (24a)$$

$$B(s) = \left(\sum_{j=0}^n c_{j,n} K^{j+1}(s) \right) \cdot Y_2^{-1}(s) = P_c^n(K(s)) \cdot Y_2^{-1}(s) \quad (24b)$$

$$C(s) = Z_1^{-1}(s) \cdot \left(\sum_{j=0}^n c_{j,n} K^{j+1}(s) \right) = Z_1^{-1}(s) \cdot P_c^n(K(s)) \quad (24c)$$

$$D(s) = \sum_{j=0}^{n-1} b_{j,n-1} K^j(s)^T = P_b^{n-1}(K(s))^T \quad (24d)$$

The knowledge of the ABCD representation allows to obtain any two port matrix representation. In the case of linear and isotropic media the symmetry and reciprocity properties hold thus ensuring that $D = A^T$, $B = B^T$, $C = C^T$ and that $\det(AD - BC) = 1$.

The Y matrix entries can be evaluated by computing Y_{11} and Y_{21} in terms of ABCD parameters and then by enforcing the reciprocity and symmetry of the transmission line.

$$Y_{11} = DB^{-1} = P_b^{n-1}(K(s)) \cdot (P_c^n(K(s)) \cdot Y_2^{-1}(s))^{-1} \quad (25a)$$

$$Y_{21} = -B^{-1} = -(P_c^n(K(s)) \cdot Y_2^{-1}(s))^{-1} \quad (25b)$$

Reciprocity and symmetry properties of the transmission line are guaranteed by the conditions:

$$Y_{12} = Y_{21} \quad (26a)$$

$$Y_{22} = Y_{11} \quad (26b)$$

Polynomials $P_b^{n-1}(K(s))$ and $P_c^n(K(s))$ can be factored by using the roots presented in [28]:

$$P_b^{n-1}(K(s)) = \prod_{j=1}^{n-1} (K(s) - u_{j,n-1}U) \quad (27a)$$

$$P_c^n(K(s)) = \prod_{j=1}^{n-1} (K(s) - v_{j,n-1}U) \cdot K \quad (27b)$$

where U is the unitary matrix. Considering that $K(s) \cdot Y_2^{-1}(s) = Z_1(s)$, the previous expressions (25a) and (25b) can be factored as:

$$Y_{11} = Y_{22} = \prod_{j=1}^{n-1} (K(s) - u_{j,n-1}U) \cdot \left[\prod_{j=1}^{n-1} (K(s) - v_{j,n-1}U) \cdot Z_1(s) \right]^{-1} \quad (28a)$$

$$Y_{21} = Y_{12} = - \left[\prod_{j=1}^{n-1} (K(s) - v_{j,n-1}U) \cdot Z_1(s) \right]^{-1} \quad (28b)$$

where roots $u_{j,n-1}$ and $v_{j,n-1}$ are given by [29]:

$$u_{j,n-1} = -4\sin^2 \left(\frac{(2j-1)\pi}{(2n-1)2} \right) \quad j = 1 \cdots n-1 \quad (29a)$$

$$v_{j,n-1} = -4\sin^2 \left(\frac{j\pi}{2n} \right) \quad j = 1 \cdots n-1 \quad (29b)$$

It is to be pointed out that the frequency dependence of per unit length parameters is completely described by $K(s)$ function and that the roots $u_{j,n-1}$ and $v_{j,n-1}$ of P_b^{n-1} and P_c^n polynomials are frequency independent [30].

IV. COMPUTATION OF POLES AND RESIDUES OF MMTLS

The computation of poles and corresponding residues of transmission lines with frequency dependent per-unit length parameters requires solving the following equation:

$$\left[\prod_{j=1}^{n-1} (K(s) - v_{j,n-1}) \cdot Z_1(s) \right] = 0 \quad (30)$$

In the following we will focus on CRLH-TLs which are characterized by frequency independent parameters although their nature is complicated by the presence of left-handed parameters (C'_L and L'_L) which causes many poles to be located close to zero. The derivation leads to low order algebraic equations and allows exploiting important properties of CRLH-TLs.

A. Approximate poles of CRLH MMTLs

Poles of Y matrix functions are obtained as the zeros of the following equation:

$$\left[\prod_{j=1}^{n-1} (K(s) - v_{j,n-1}) \cdot Z_1(s) \right] = 0 \quad (31)$$

thus allowing to solve n equations separately.

The poles of the HTLN can be identified as:

1. zeros of polynomial $Z_1(s)$
2. zeros of polynomial $Z_1(s)Y_2(s) - v_{j,n-1}$, for $j = 1 \cdots n-1$

A.1 Poles 1

Poles of the first type satisfy the equation:

$$s^2 L_R C_L + s C_L R + 1 = 0 \quad (32)$$

A.2 Poles 2

Poles of the second type are obtained as the solutions of the equation:

$$Z_1(s)Y_2(s) - v_{j,n-1} = 0, \quad \text{for } j = 1 \cdots n-1 \quad (33)$$

It can be re-written in terms of parameters of the elementary CRLH cell as:

$$\left(RG + \frac{L_R}{L_L} + \frac{C_R}{C_L} \right) + s(RC_R + GL_R) + s^2 L_R C_R + \frac{1}{s} \left(\frac{R}{C_L} + \frac{G}{C_L} \right) + \frac{1}{s^2} \frac{1}{L_L C_L} - v_{j,n-1} = 0, \quad \text{for } j = 1 \cdots n-1 \quad (34)$$

In the general case, for each root $v_{j,n-1}$, the following equation is to be solved:

$$a + bs + cs^2 + \frac{d}{s} + \frac{e}{s^2} = 0 \quad (35)$$

where

$$a = RG + \frac{L_R}{L_L} + \frac{C_R}{C_L} - v_{j,n-1} \quad (36a)$$

$$b = RC_R + GL_R \quad (36b)$$

$$c = L_R C_R \quad (36c)$$

$$d = \frac{R}{C_L} + \frac{G}{C_L} \quad (36d)$$

$$e = \frac{1}{L_L C_L} \quad (36e)$$

The roots finally satisfy the equation

$$as^2 + bs^3 + cs^4 + ds + e = 0 \quad (37)$$

Thus, for each root $v_{j,n-1}$, $j = 1 \cdots n-1$, four different poles are generated in the CRLH case, while in the RH case only two poles corresponds to each root $v_{j,n-1}$ [39]. It is also worth considering the lossless case $R = G = 0$. Coefficients b and d in (36) are zero and the equation to be solved reduces to

$$as^2 + cs^4 + e = 0 \quad (38)$$

whose roots come in pair. As the poles of the HTLN can be computed by solving low order algebraic equations, they are continuously depending on the physical parameters (circuit parameters, length of the MMTL). This allows to claim that parameterized reduced order models corresponding to a variation of such parameters with respect to a fixed point of the parameter space can be generated just by perturbing the model for that point.

B. Computation of residues of Y matrix

Residues of pole p_i can be obtained as:

$$R_{11,i} = R_{22,i} = \left[\left(\prod_{j=1}^{n-1} (K(s) - v_{j,n-1}U) \right) \cdot Z_1(s) \right] / \left[\det \left[\left(\prod_{j=1}^{n-1} (K(s) - v_{j,n-1}U) \right) \cdot Z_1(s) \right] \cdot \prod_{j=1}^{n-1} (K(s) - u_{j,n-1}U) (s - p_i) \right]_{s=p_i} \quad (39)$$

$$R_{12,i} = R_{21,i} = - \left[\left(\prod_{j=1}^{n-1} (K(s) - v_{j,n-1}U) \right) \cdot Z_1(s) \right] / \left[\det \left[\left(\prod_{j=1}^{n-1} (K(s) - v_{j,n-1}U) \right) \cdot Z_1(s) \right] \cdot (s - p_i) \right]_{s=p_i} \quad (40)$$

for $i = 1 \dots P_Y$, being P_Y the total number of poles of the \mathbf{Y} matrix entries.

V. MODEL ORDER REDUCTION

In Section III it has been shown that the proposed approach allows to provide a rational approximation of Y matrix entries (25) in terms of residues and poles whose computation is straightforward. The development of a MOR technique requires the determination of the dominant poles of the system, which significantly influence the time as well as the frequency characteristics of the system under analysis [23]. In the recent past moment-matching techniques have been widely adopted to extract the dominant poles of a given system [40]-[43]. It is known that such techniques are extremely time consuming as they require computing and matching moments; on the contrary the proposed method is extremely fast in extracting the poles among which the dominant ones have to be selected.

In [32] it has been presented a model order reduction approach which is based on a two step process: 1) poles within a given bandwidth $k\omega_{max}$ (where $k > 1$ and ω_{max} corresponds to the required bandwidth (e.g. the angular frequency beyond which the power of the excitation is negligible) are selected; 2) as the corresponding residues are known, only those that significantly impact the frequency and time responses are retained.

When dealing with metamaterials the co-existence of both longitudinal and transversal resonators (see Fig. 2) cause many poles to be located near zero; the magnitude of the corresponding residues is ordinarily small if compared to those of other poles; nevertheless they are important to correctly model the physical behavior in the low frequency range. Furthermore, it has been observed that poles are not spread over the entire frequency axis but tend to be concentrated in bandwidths which may be also far away one from each other. This fact causes the typical pass-band and stop band behavior of metamaterials frequency response. This suggests to adopt a frequency hopping poles selection within each bandwidth.

The procedure can be formalized by the following algorithm:

- the maximum angular frequency $\omega_{MOR} = k\omega_{max}$ is selected;
- the bandwidth $[-\omega_{MOR}, \omega_{MOR}]$ is subdivided in sub-bands according to a suitable algorithm;
- dominant poles selection is performed within each band.

Once the dominant poles have been selected and the corresponding residues computed, a macromodel can be generated [28] by using standard techniques.

A. Macromodel synthesis

Once the reduced order poles-residues representation of functions Y_{11} , Y_{12} , Y_{21} and Y_{22} is obtained a macromodel can be easily derived by generating the $ABCD$ state-space domain representation leading to a set of first order differential equations which reads:

$$\begin{aligned}\frac{d}{dt}\mathbf{x}(\mathbf{t}) &= \mathcal{A}\mathbf{x}(\mathbf{t}) + \mathcal{B}\mathbf{u}(\mathbf{t}) \\ \mathbf{y}(\mathbf{t}) &= \mathcal{C}\mathbf{x}(\mathbf{t}) + \mathcal{D}\mathbf{u}(\mathbf{t})\end{aligned}\quad (41)$$

where $\mathcal{A} \in \mathbb{R}^{p \times p}$, $\mathcal{B} \in \mathbb{R}^{p \times n}$, $\mathcal{C} \in \mathbb{R}^{n \times p}$, $\mathcal{D} \in \mathbb{R}^{n \times n}$, p is the number of states and n the order of the proposed model. Obviously, as the admittance matrix representation is used, the input vector $\mathbf{u}(\mathbf{t})$ and output vector $\mathbf{y}(\mathbf{t})$ correspond to port voltages $\mathbf{v}(t)$ or electric fields $\mathbf{E}_x(t)$ and currents $\mathbf{i}(t)$ or magnetic fields $\mathbf{H}_y(t)$, respectively. Since a model reduction has already been applied, a standard minimal-order realization can be efficiently used [44]-[47]. The set of first order differential equations (41) are completed with the terminal conditions and solved numerically.

VI. PARAMETERIZED MACROMODELS FOR MMTLS

The design of systems and devices based on MMTLs usually requires optimization procedures which call for a fast evaluation of MMTLs performances for varying physical and geometrical parameters. The proposed method is well suited to this aim. In fact it allows an easy computation of poles and residues of the MMTLs by solving low order algebraic equations.

Let's assume that the MMTL depends on a set of physical and/or geometrical parameters $\lambda_1, \lambda_2, \dots, \lambda_n$. Telegrapher's equations, in the case of CRLH MMTL, can be expressed as

$$\frac{\partial}{\partial z}V(z, s; \lambda) = -\left(R'(s; \lambda) + sL'_R(s; \lambda) + \frac{1}{s}C'_L(s; \lambda)^{-1}\right)I(z, s; \lambda) \quad (42a)$$

$$\frac{\partial}{\partial z}I(z, s; \lambda) = -\left(G'(s; \lambda) + sC'_R(s; \lambda) + \frac{1}{s}L'_L(s; \lambda)^{-1}\right)V(z, s; \lambda) \quad (42b)$$

The possibility to compute poles and residues of the \mathbf{Y} matrix by solving low order algebraic equations and to select only the dominant ones is exploited for the automatic generation of reduced order parameterized models. The half-T cell factor becomes:

$$K(s; \lambda) = Z_1(s; \lambda)Y_2(s; \lambda) \quad (43)$$

The poles of the parameterized \mathbf{Y} matrix functions are obtained as the zeros of the following equation:

$$\left[\prod_{j=1}^{n-1} (K(s; \lambda) - v_{j,n-1}) \cdot Z_1(s; \lambda)\right] = 0 \quad (44)$$

which implies that, as pointed before, separate algebraic equations have to be solved. As described in Section V only the dominant poles are retained to generate the reduced order model. Usually, per unit length parameters are smooth functions of geometrical parameters. As a consequence, also the solutions of (43) changes continuously with respect to the parameters. Location of dominant poles in the complex plane can be monitored at the design stage such that special performances of the MMTL can be obtained. It is worth mentioning that the ease computation of poles by solving low order algebraic equations makes this procedure to be preferred to any interpolation scheme to recover poles from unit-cell parameters. The generation of the macromodel corresponding to a generic set of unit-cell parameters in the parameter space requires the efficient computation of residues; it can be done by means of (39) or, as an alternative, by multidimensional linear interpolation.

VII. NUMERICAL RESULTS

A. Unbalanced CRLH-TL

As a first example it has been considered the lossless CRLH-TL described in [11], with global parameters $R = 10^{-3} \Omega$, $L_R = 2.45$ nH, $C_L = 0.68$ pF, $G = 10^{-3}$ S, $C_R = 0.5$ pF and $L_L = 3.38$ nH and a length $l = 6.1$ mm. Fig. 3 shows the dispersion diagram for such material along with the linear dispersive curve and that of the balanced case ($L_R C_L = L_L C_R$).

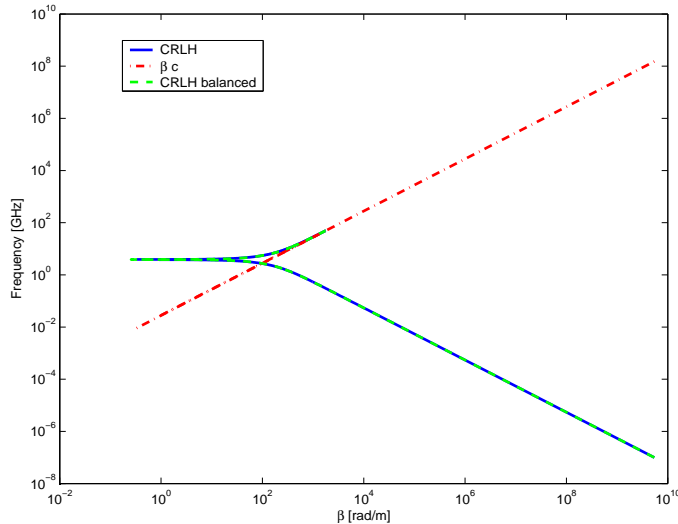


Fig. 3. Dispersion diagram for the CRLH-TL of example VII-A.

The effective permeability and permittivity (7) have been computed exhibiting simultaneous negative values up to about 4 GHz; their magnitude is shown in Fig. 4.

The ABCD parameters have been computed in the frequency range 0-50 GHz by using the transmission line theory (TLT), the half-T ladder network (HTLN) and the polynomial representation (DFP). Fig. 5 shows the comparison of coefficients A, B, C and D as evaluated by the three techniques. As clearly seen the results are in a good agreement over the entire frequency range. As pointed out in Section V, the higher complexity of the unit cell of CRLH-TLs, with respect to the one of standard RH-TLs, causes the low frequency behavior to be much more complex, thus requiring great attention in applying the model order reduction.

Fig. 6 shows the poles of the \mathbf{Y} matrix entries in the complex plane. As seen, all the poles lie in the left-half complex plane thus strictly ensuring the stability of the model.

The co-existence of two resonators in the unit cell makes the low frequency and high frequency behaviors not well separated in the sense that there are low frequencies resonances (below 200 MHz) due to the presence of the longitudinal resonator and the interaction between the same resonator and the transversal one. This fact has the consequence that a large number of poles is located near zero, as shown in Fig. 7.

The accuracy of transient broadband models of metamaterials is significantly dependent on such kind of poles as they determines the behavior in the low frequency range. The proposed MOR technique allows to select the most important low frequency poles thus preserving accuracy also below 200 MHz. Fig. 8 shows the selected poles providing excellent accuracy up to 50 GHz. Magnitude and phase of Y_{12} are shown in Fig. 9. The number of poles of the original model is 238 and that of the reduced one is 136. If only the criterion based on the magnitude of residues is used to select dominant poles, the number of poles decreases to 12 but the accuracy is lost below 100 MHz, as shown in Fig. 10

The importance of low frequency poles is then investigated looking at the magnitude of the corresponding residues for the same example VII-A. Fig. 11 shows the magnitude and phase spectra of

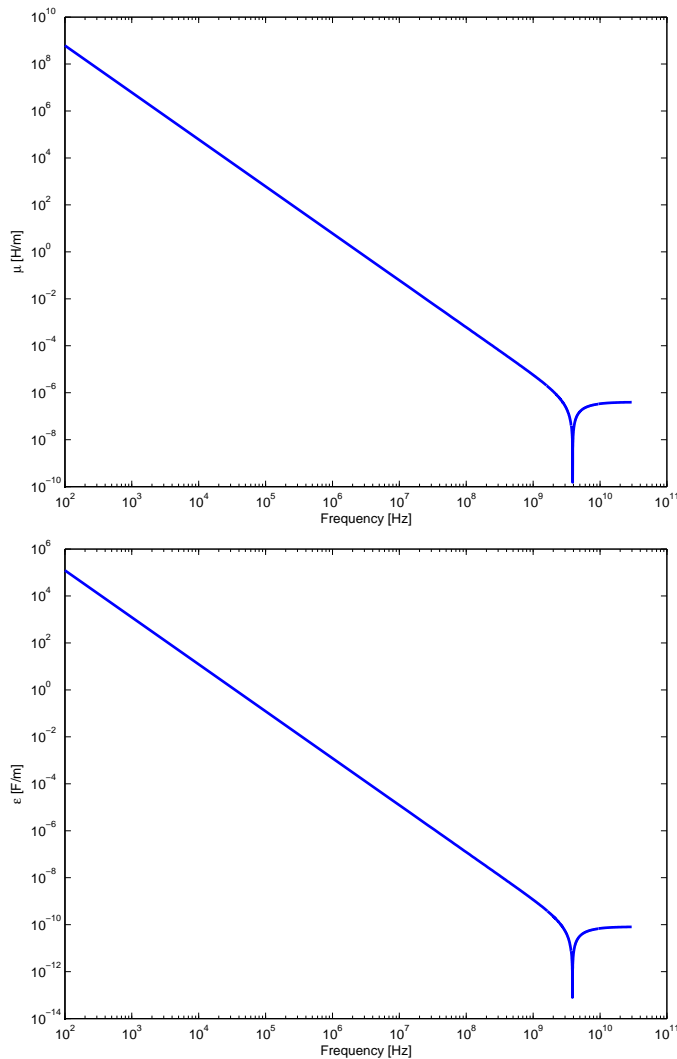


Fig. 4. Effective permeability (top) and permittivity (bottom) for example VII-A.

the Y_{12} function as obtained by considering the HTLN network (HTLN) and the reduced order model (MOR); if only the residue magnitude criterion is used in selecting poles, all the low frequency poles are excluded thus leading to loss of accuracy, as seen in Fig. 10. In this case a threshold $thresh = 1/100$ has been used. It is clearly recognized that neglecting poles with small residues in the low frequency range results into a significant error in modeling Y_{12} in the same frequency band.

The MMTL has been excited by a voltage source $v_s(t)$ whose time behavior is the second time derivative of a gaussian pulse; Fig. 12 shows the waveform along with the corresponding magnitude spectrum.

The output voltage is plotted in Fig. 13 as obtained by the HTLN model via IFFT by using all the poles (Reference) and by generating the reduced order macromodel and integrating the differential equation by means of the Gear-Shichman scheme (MOR-GE-SH) [48]. The two curves are practically overlapped. It is also worth to notice that causality is strictly preserved.

B. 2TDLM metamaterial

In the second test the 2TDLM metamaterial described in II-B has been considered. Such a medium is characterized by negative values of permeability and permittivity over a wide frequency range. Fig. 1 shows the real and imaginary part of the 2TDLM susceptibility with $\chi_\alpha = 1.0$, $\chi_\beta = 1.0 \times 10^{-5}$,

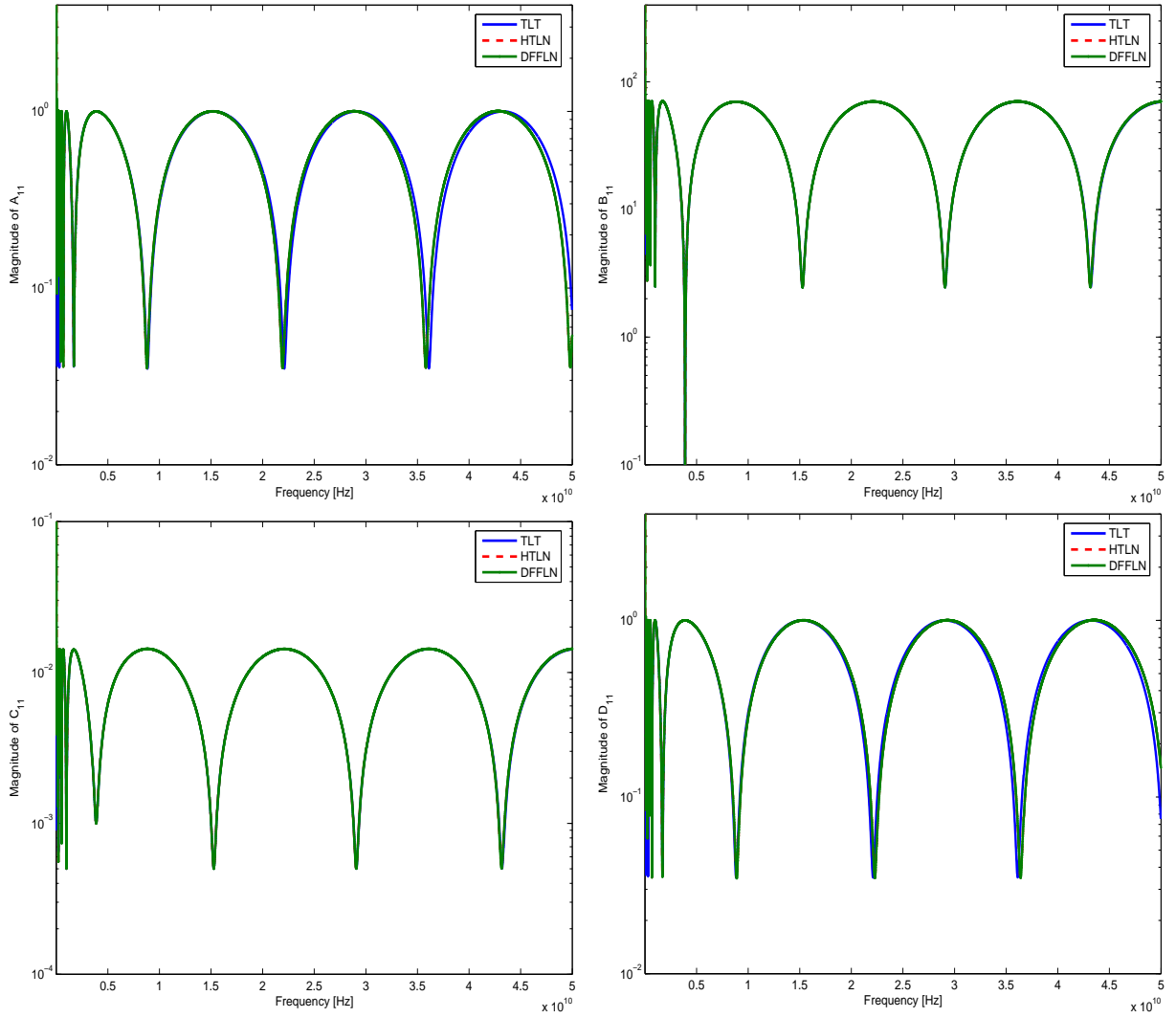


Fig. 5. Transmission coefficients ABCD for example VII-A. Upper left: A; upper right: B; lower right: C; lower right: D.

$\chi_\gamma = -0.5$, $\Gamma = 1.0 \times 10^{-1}\omega_0$ and $\omega_p = \omega_0 = 2\pi f_0$ for $f_0 = 1$ GHz. In [8] the propagation through a slab of such a metamaterial is computed by using a specialized 1-D FDTD code involving, besides electric and magnetic fields, polarization and magnetization fields as well to take into account the frequency dependence of equivalent $\mu(s)$ and $\varepsilon(s)$. The difficulty in carrying out a FDTD simulation involving dispersive media relies into the existence of many wave speeds in the system and, thus, Courant-Friedrichs-Levy (CFL) condition must be set carefully to achieve a stable algorithm. In the HTLN model proposed in this work stability is automatically guaranteed provided that a stable and passive model for the unit cell longitudinal impedance $Z_1(s)$ and transversal admittance $Y_2(s)$ are used. 2TDLM elementary cell is surely stable as it can be synthesized as a CRLH cell; as a consequence, the overall equivalent circuit is stable as well.

In order to reduce the effect of absorption near resonance, the parameters of the 2TDLM medium have been assumed as [8]: $\chi_\alpha = 1.0$, $\chi_\beta = 1.0 \times 10^{-5}$, $\chi_\gamma = -0.5$, $\Gamma = 1.0 \times 10^{-5}\omega_0$ and $\omega_p = \omega_0 = 2\pi f_0$ for $f_0 = 0.01$ GHz. As pointed out in [8], such parameter setting allows to preserve the shape of the single-cycle pulse having a peak frequency $f_{00} = 1$ GHz which should travel without distortion at the speed $2c_0$ through the slab.

A 20 cm long MMTL has been considered. The MOR technique has been applied leading to a reduced set of poles well describing the behavior of the MMTL in the frequency range 0-30 GHz. The

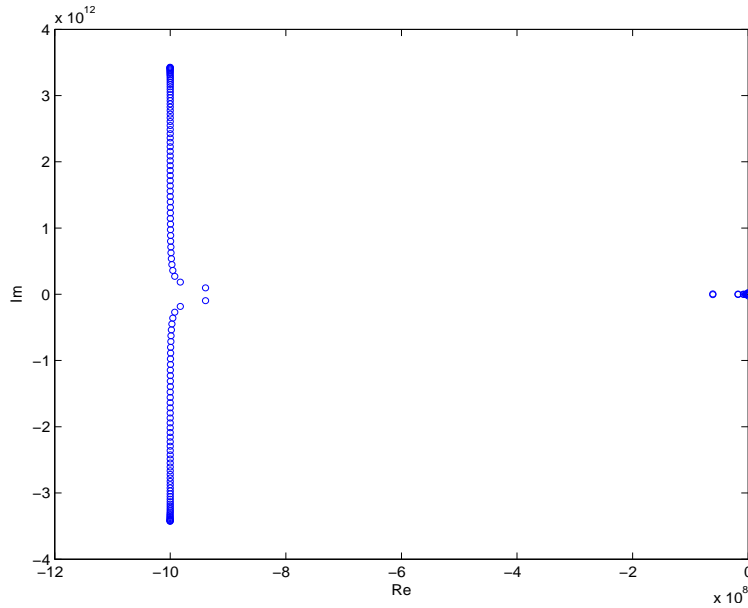


Fig. 6. Location of poles in the complex plane for example VII-A.

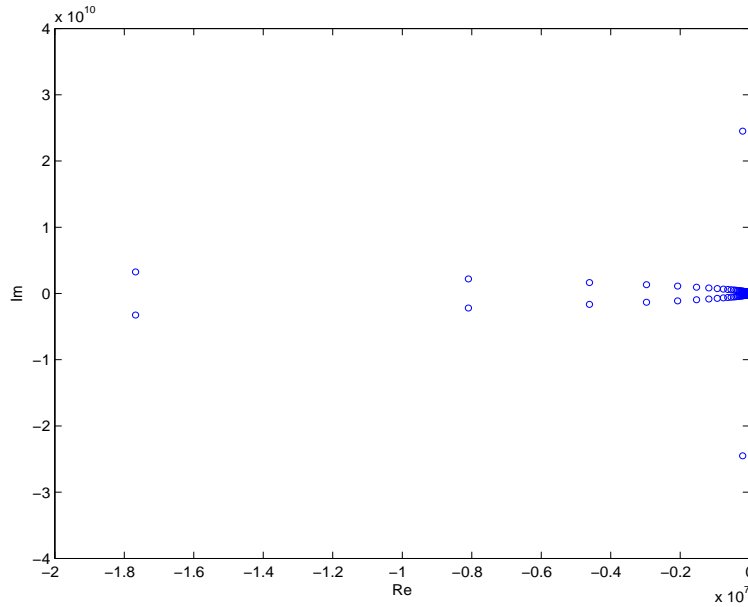


Fig. 7. Zoom of poles around zero for example VII-A.

initial set of 357 poles has been reduced to only 53. Fig. 15 shows the magnitude spectra of Y_{11} and Y_{21} as evaluated by the transmission line theory (TLT) and the proposed reduced order model (MOR); as seen, a very good accuracy is achieved over the entire frequency range. In order to check the accuracy of the reduced order model the Feature Selective Validation procedure has been applied. The Feature Selective Validation (FSV) techniques aims to perform the comparison of different datasets by mimic the behavior of a group of experienced engineers when they perform such a comparison by means of a visual approach [49]-[51]. The FSV method is based on the decomposition of the original data into two parts: amplitude (trend/envelope) data and feature data. The former component accounts for the slowly varying data across the data set and the latter accounts for the sharp peaks and troughs often found in CEM data. The numerical figures of merit obtained as output from the FSV procedure

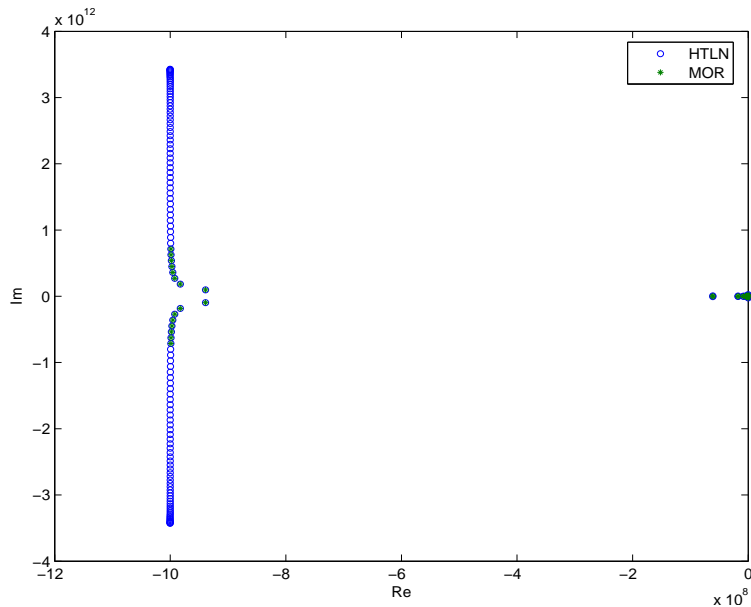


Fig. 8. Model order reduction for example VII-A: selected poles in the half left complex plane.

can be converted in a natural language descriptor (excellent, very good, good, fair, poor, very poor comparison). The essential meaning of the FSV figures of merit are: ADM (Amplitude Difference Measure), FDM (Feature Difference Measure) and GDM (Global Difference Measure). ADM and FDM can be combined by using a Grade-Spread chart which gives a numerical value to the Grade by counting how many categories are required (starting from Excellent) for the cumulative total of the histogram to exceed a given value. A numerical value is given to the Spread by counting how many adjacent categories (starting from the largest) are required to cumulatively exceed a given value.

The models obtained considering all the poles and only the dominant ones have been compared over the frequency range 0-30 GHz. Fig. 16 shows the FSV comparison of the magnitude of Y_{12} matrix entry. As seen, all the figures of merit confirm that the reduced order model perfectly captures the physics of the system and provides a very good approximation over the entire frequency band 0-30 GHz.

A single-cycle pulse for the source of unit amplitude is used to excite the material:

$$f(t) = \begin{cases} \sqrt{7} (7/6)^3 \left(\frac{t-T_p/2}{T_p/2} \right) \left[1 - \left(\frac{t-T_p/2}{T_p/2} \right)^2 \right]^3 & \text{for } 0 \leq t \leq T_p \\ 0 & \text{for } t > T_p \end{cases} \quad (45)$$

where T_p is the length of time the pulse has a non-zero value; in the simulation it has been assumed $T_p = 1$ ns.

Fig. 17 shows the single cycle pulse used as source of the MMTL in example VII-B along with its frequency magnitude spectrum.

Fig. 18 shows the voltages of the 2DTLM transmission line as obtained by using both the transmission line theory via inverse Fourier Transform (TLT-IFFT) and the proposed macromodel after the pole pruning has been performed (MOR-Macromodel).

It is worth of notice that, as expected, the input pulse propagates through the MMTL, at speed $2c_0$, with almost no attenuation. Also, it is to be observed that the proposed model strictly preserves causality.

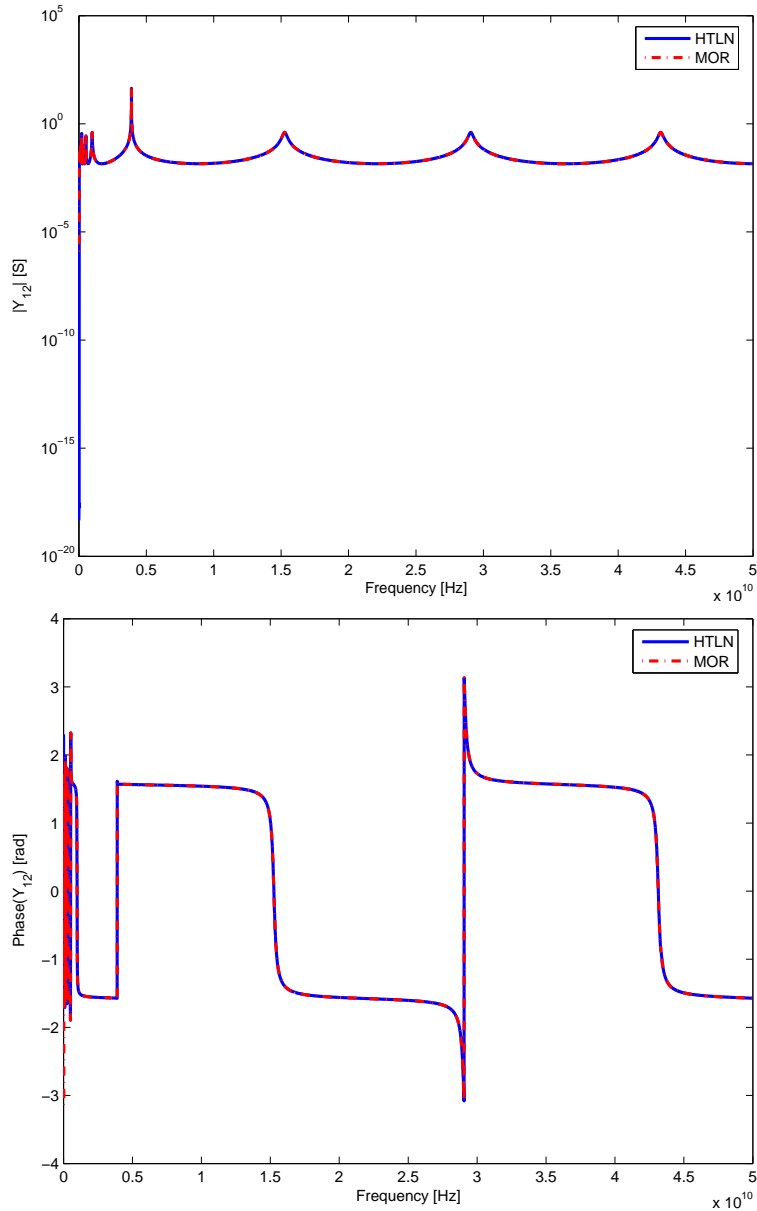


Fig. 9. Model order reduction for example VII-A. Top: magnitude of Y_{12} , bottom: phase of Y_{12} .

C. Parameterized CRLH-TL

As last example a macromodel has been generated for a MMTL for several different values of L_L . Fig. 19 shows the location of poles in the left half complex plane for increasing values of L_L and $L_R = 4.7$ nH, $C_R = 0.1$ pF, $C_L = 9.6$ pF, $R = 1$ m Ω , $G = 1$ mS, $l = 120$ mils.

It is clearly seen that all the poles have a strict negative real part, thus ensuring the stability of the macromodel, and that, increasing the value of L_L , results into a reduction of the imaginary part of complex poles.

The transmission line has been modeled as a 20-th order half-T ladder network, with 78 poles; the reduced order model has been generated to be accurate within the 0-30 GHz range; only four poles have been selected as dominant ones. Thus, extremely simplified state-space models are generated, at a reduced cost, for different values of L_L . Fig. 20 shows the output voltage of the CRLH-TL excited by a normalized second order derivative of a gaussian pulse.

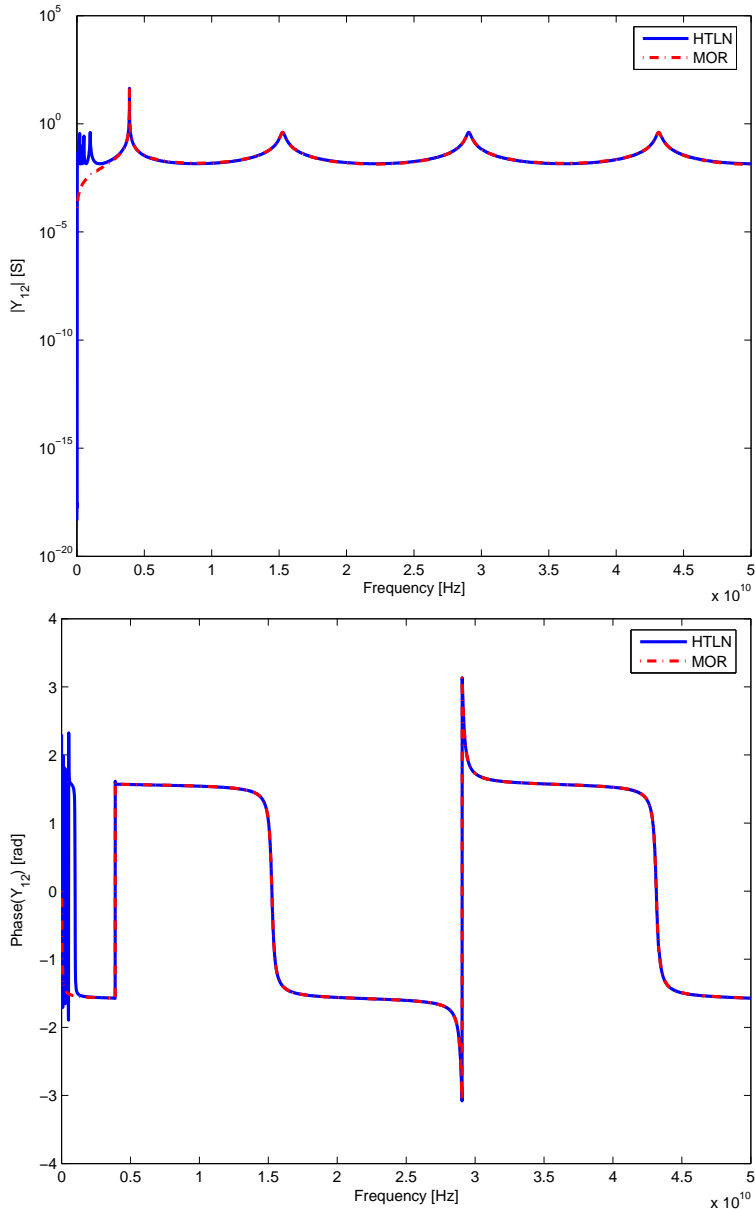


Fig. 10. Not accurate model order reduction in the low frequency range for example VII-A. Top: magnitude of Y_{12} , bottom: phase of Y_{12} .

VIII. CONCLUSIONS

A general methodology for the transient analysis of MMTLs has been presented. A rational approximation of the metamaterial transmission line is obtained by extracting the poles of the Y matrix representation of the half-T ladder network describing the MMTL; pole pruning allows the generation of a reduced order macromodel which has been used for carrying out accurate transient analysis of MMTLs. The proposed methodology can be applied to any type of metamaterial and/or lossy and dispersive medium being based on a polynomial closed-form representation of half-T ladder network which is totally independent on the nature of materials; moreover it can be used as a building block for modeling dispersive materials in the framework of TLM method. The robustness and accuracy of the method has been confirmed by the numerical results; in particular typical metamaterial phenomena such as superluminal speeds of propagation over a large band of frequencies and well separated stop/pass bands have been successfully modeled.

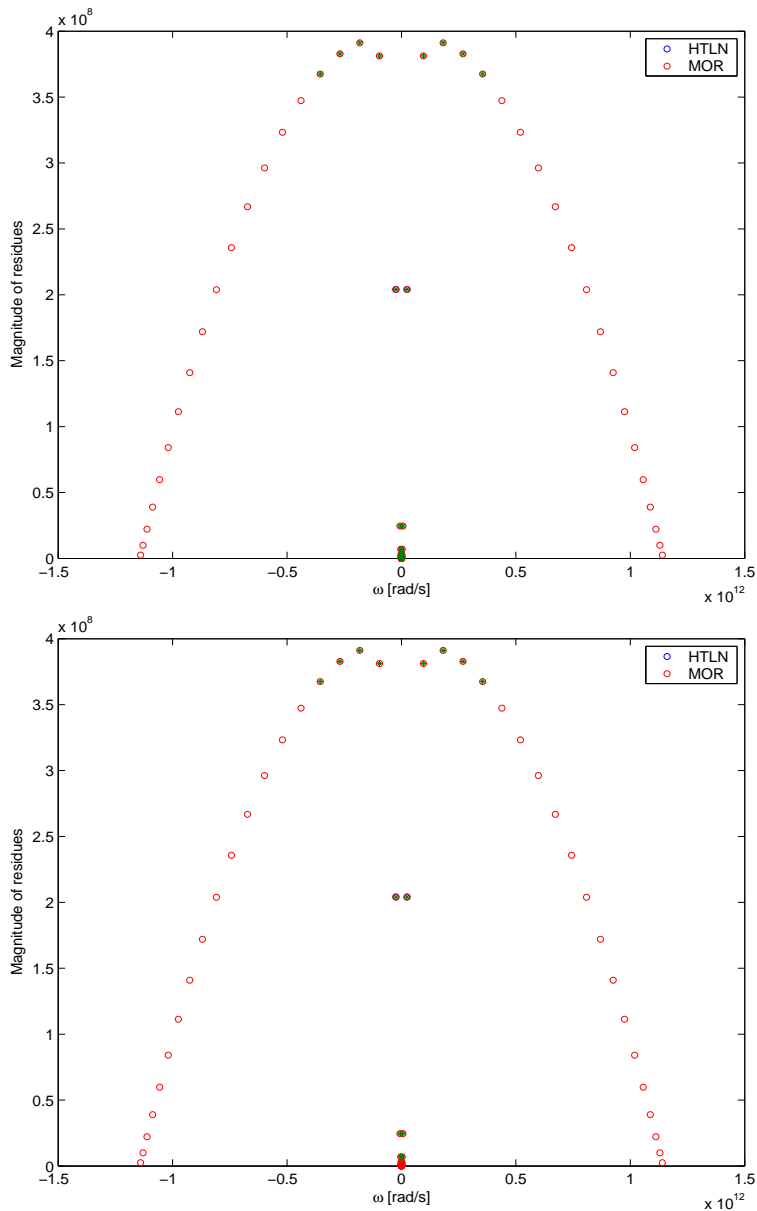


Fig. 11. Magnitude of residues for example VII-A. Top: including all the low frequency poles; bottom: excluding low frequency poles with residues below the fixed threshold.

REFERENCES

- [1] V. G. Veselago. The electrodynamics of substances with simultaneously negative values of ϵ and μ (in Russian). *Usp. Fiz. Nauk.*, 92:517–526, 1967.
- [2] V. G. Veselago. The electrodynamics of substances with simultaneously negative values of ϵ and μ . *Sov. Phys. Usp.*, 47:509–514, Jan.-Feb., 1968.
- [3] J. B. Pendry, A. J. Holden, D. J. Robins and W. J. Stewart. Magnetism from conductors and enhanced nonlinear phenomena. *IEEE Transactions on Microwave Theory and Techniques*, 47(11):2075–2084, November 1999.
- [4] D. R. Smith, D. C. Vier, W. J. Padilla, S. C. Nemat-Nasser and S. Schultz. Loop-wire for investigating plasmons at microwave frequencies. *Appl. Phys. Lett.*, 75(10):1425–1427, September 1999.
- [5] D. R. Smith, W. J. Padilla, D. C. Vier, S. C. Nemat-Nasser and S. Schultz. Composite medium with simultaneously negative permittivity and permeability. *Phys. Rev. Lett.*, 84:4184–4187, May 2000.
- [6] G. V. Eleftheriades, O. Siddiqui and A. K. Iyer. Transmission Line Models for negative Refractive Index Media and Associated Implementations Without Excess Resonators. *IEEE Microwave and Wireless Components Letters*, 13(2):51–53, February 2003.
- [7] C. Caloz and T. Itoh. Transmission Line Approach of Left-Handed (LH) Materials and Microstrip Implementation of an Artificial LH Transmission Line. *IEEE Transactions on Antennas and Propagation*, 52(5):1159–1166, May 2004.

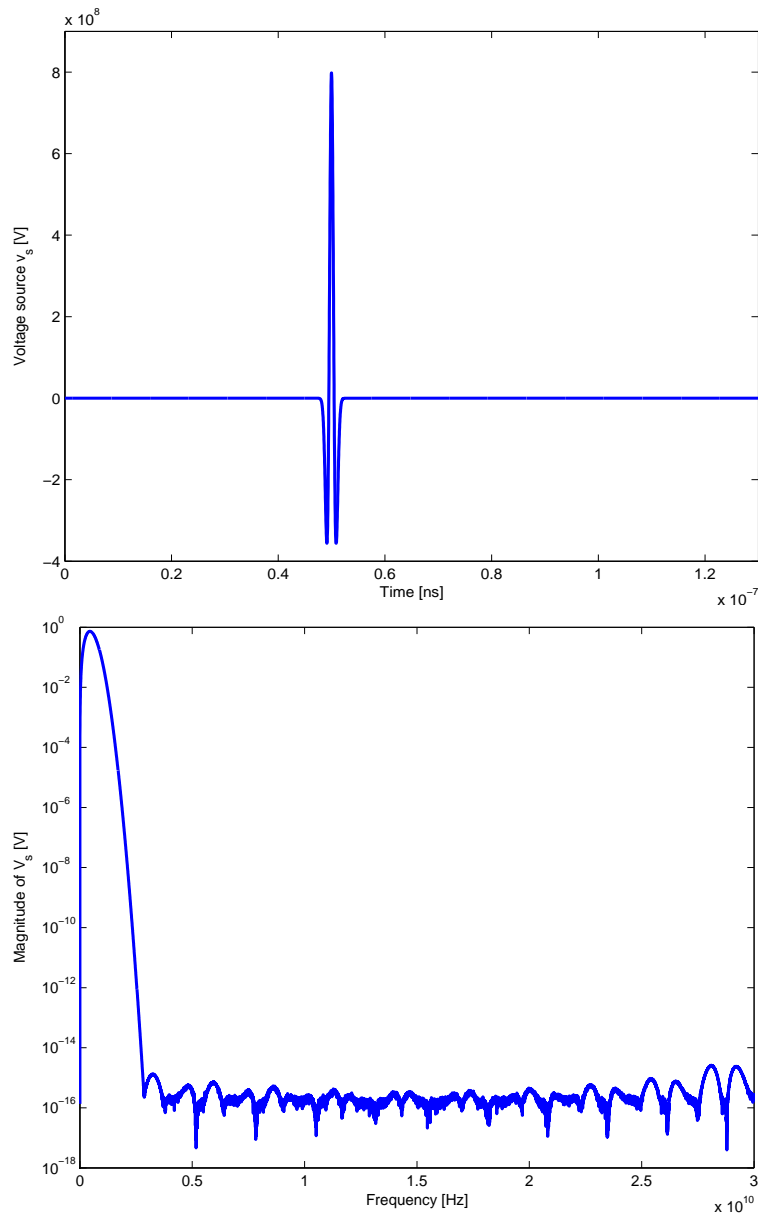


Fig. 12. CRLH-TL excitation (example VII-A). Top: time domain waveform v_s ; bottom: magnitude spectrum of V_s .

- [8] R. W. Ziolkowski. Superluminal transmission of information through an electromagnetic metamaterial. *Phys. Rev. E*, 63, 2001.
- [9] M. W. Feise, J. B. Schneider and P. J. Bevelacqua. Finite-Difference and Pseudospectral Time-Domain Methods Applied to Backward-Wave Metamaterials. *IEEE Transactions on Antennas and Propagation*, 52(11):2955–2962, November 2004.
- [10] Q. H. Liu. The PSTD algorithm: a time-domain method requiring only two cells per wavelength. *Microwave and Optical Technology Letters*, 15(3):158–165, June 1997.
- [11] A. Lai, C. Caloz and T. Itoh. Composite Right/Left-Handed Transmission Line Metamaterials. *IEEE Antenna and Propagation Magazine*, pages 34–50, September 2004.
- [12] A. Grbic and G. V. Eleftheriades. Negative Refraction, Growing Evanescent Waves and Sub-Diffraction Imaging in Loaded Transmission-Line Metamaterials. *IEEE Transactions on Antennas and Propagation*, 51(12):2297–2305, December 2003.
- [13] A. Sanada, C. Caloz and T. Itoh. Characteristics of the Composite Right/Left-Handed Transmission Lines. *IEEE Microwave and Wireless Components Letters*, 14(2):68–70, November 2004.
- [14] Y. Horii, C. Caloz, T. Itoh. Super-compact Multilayered Left-Handed Transmission Line and Diplexer Application. *IEEE Transactions on Microwave Theory and Techniques*, 53(4):1527–1534, April 2005.
- [15] P. P. So and W. J. R. Hofer. Time Domain TLM Modeling of Metamaterials with Negative Refractive Index. In *2004 IEEE MTT-S Int. Microwave Symp. Dig.*, pages 1779–1782, Jun 2004.
- [16] P. P. So, H. Du and W. J. R. Hofer. Modeling of metamaterials with negative Refractive Index using 2-D shunt and 3-D SCN TLM networks. *IEEE Transactions on Microwave Theory and Techniques*, 53(4):1496–1505, April 2005.

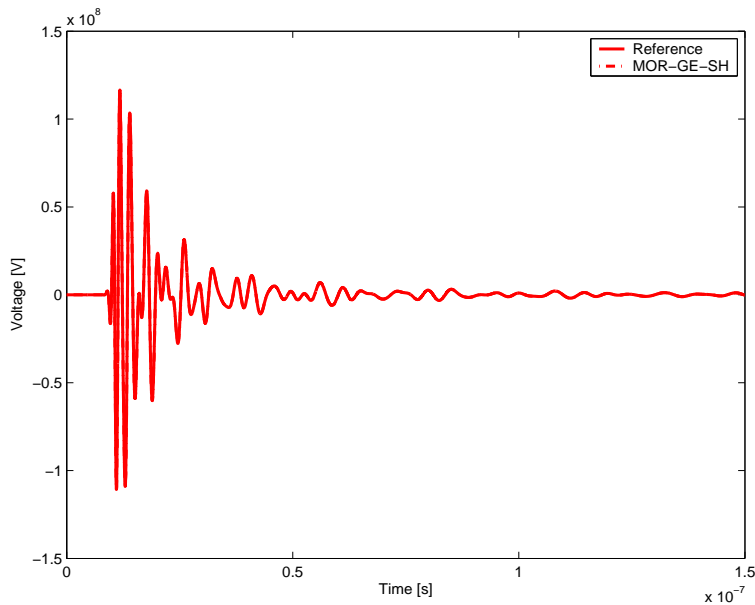


Fig. 13. Output voltage (example VII-A).

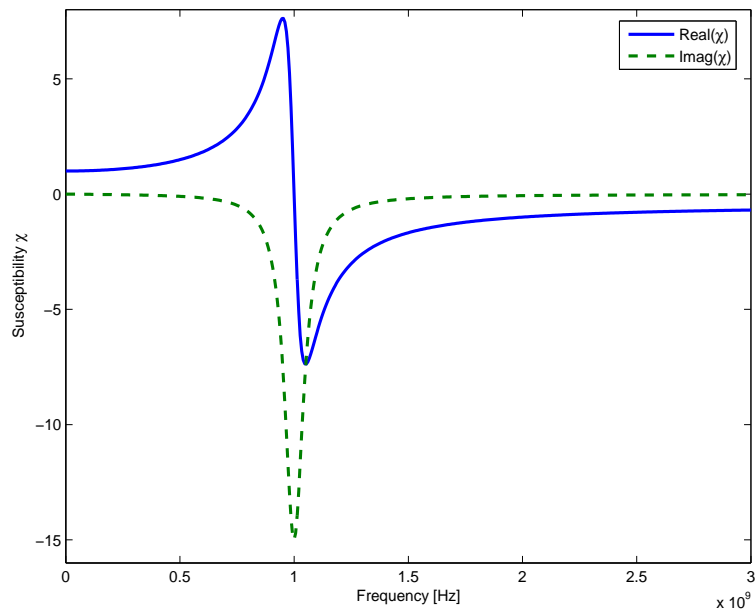


Fig. 14. Real and imaginary part of the 2TDLM susceptibility of example VII-B with $\chi_\alpha = 1.0$, $\chi_\beta = 1.0 \times 10^{-5}$, $\chi_\gamma = -0.5$, $\Gamma = 1.0 \times 10^{-5}\omega_0$ and $\omega_p = \omega_0 = 2\pi f_0$ for $f_0 = 1$ GHz.

- [17] A. Rennings, S. Otto, C. Caloz, A. Lauer, W. Bilgic and P. Waldow. Composite right/left-handed extended equivalent circuit (CRLH-EEC)FDTD: Stability and dispersion analysis with examples. *International Journal Numerical Modeling*, 19:141–172, 2006.
- [18] W. J. R. Hofer. *The transmission line matrix (TLM) method*. in Numerical Techniques for Microwave and Millimeter Wave Passive Structures, (T. Itoh, ed), Wiley, N.Y., 1989.
- [19] W. J. R. Hofer. Transmission line matrix (TLM) models of electromagnetic fields in space and time. In *Proceedings International Zurich Symposium on EMC*, volume 11, Zürich, Switzerland, February 1997.
- [20] C. Christopoulos. *An introduction to the Transmission-Line Modelling (TLM method)*. IEEE Press, New York, 1992.
- [21] J. Paul, C. Christopoulos and D. W. P. Thomas. Generalized Material Models in TLM - Part I: Materials with Frequency-Dependent Properties. *IEEE Transactions on Antennas and Propagation*, 47(10):1528–1534, October 1999.
- [22] G. Antonini, A. Orlandi. Ultra Wide Band Plane Waves Propagation Through Lossy and Dispersive Media. In *EMC Europe Workshop 2005: EMC of Wireless Systems*, Roma, Italy, September 2005.
- [23] R. Achar, M. Nakhla. Simulation of High-Speed Interconnects. *Proceedings of the IEEE*, 89(5):693–728, May 2001.

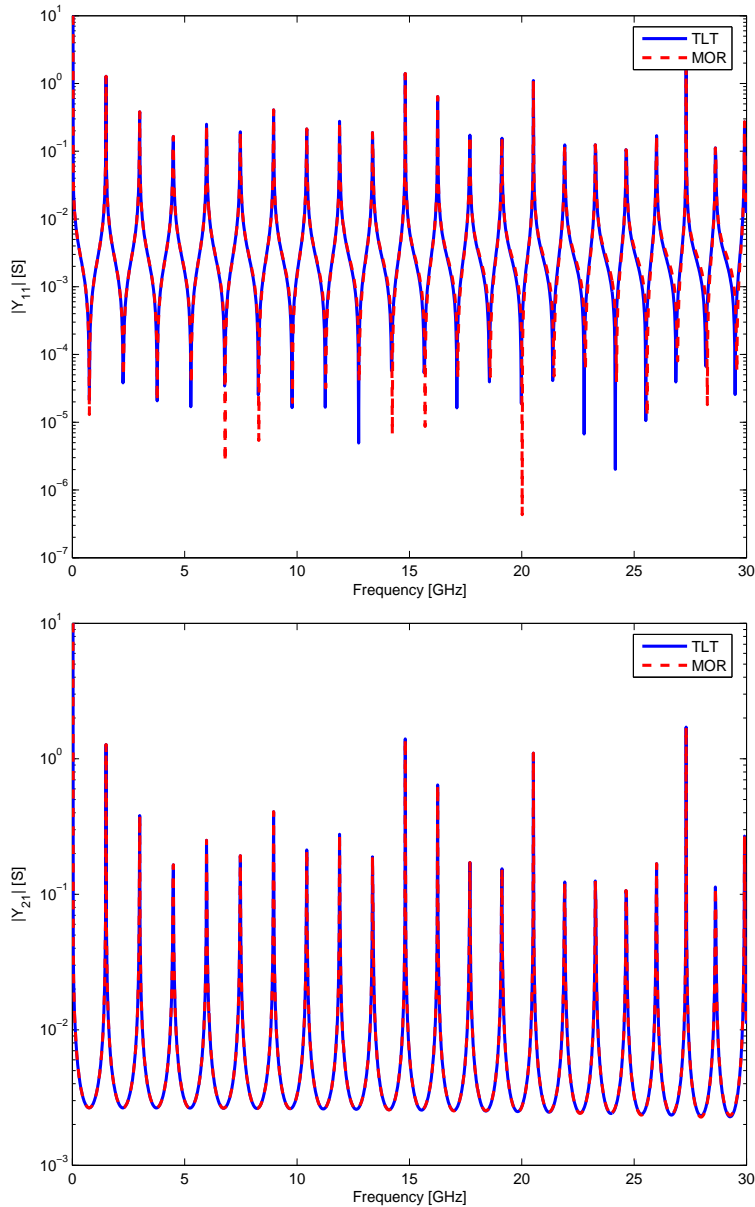


Fig. 15. Comparison of \mathbf{Y} matrix entries for example VII-B. Top: Y_{11} magnitude spectrum; bottom: Y_{21} magnitude spectrum.

- [24] M. S. Nakhla, R. Achar, A. Dounavis, X. Li. Passive Closed-Form Transmission-Line Model for General-Purpose Circuit Simulators. *IEEE Transactions on Microwave Theory and Techniques*, 47(12):2450–2459, December 1999.
- [25] A. Dounavis, R. Achar, M. Nakhla. Efficient Passive Circuit Models for Distributed Networks with Frequency-Dependent Parameters. *IEEE Transactions on Advanced Packaging*, 23(3):382–392, August 2000.
- [26] A. Dounavis, R. Achar, M. Nakhla. A General Class of Passive Macromodels for Lossy Multiconductor Transmission Lines. *IEEE Transactions on Microwave Theory and Techniques*, 49(10):1686–1696, October 2001.
- [27] I. M. Elfadel, H-M. Huang, A. E. Ruehli, A. Dounavis, M. S. Nakhla. A Comparative Study of Two Transient Analysis Algorithms for Lossy Transmission Lines With Frequency-Dependent Data. *IEEE Transactions on Advanced Packaging*, 25(2), May 2002.
- [28] G. Antonini, G. Ferri. A New Approach for Closed-Form Transient Analysis of Multiconductor Transmission Lines. *IEEE Transactions on Electromagnetic Compatibility*, 46(4):529–543, November 2004.
- [29] M. Faccio, G. Ferri, A. D’Amico. The DFF and DFFz Triangles and Their Mathematical Properties. *Applications of Fibonacci Numbers*, G. E. Bergum et al.,(eds), 5:199–206, 1990.
- [30] M. Faccio, G. Ferri, A. D’Amico. A New Fast Method for Ladder Networks Characterization. *IEEE Transactions on Circuits and Systems, I*, 38(11):1377–1382, September 1991.
- [31] G. Ferri, M. Faccio, A. D’Amico. Fibonacci Numbers and Ladder Network Impedance. *Fibonacci Quarterly*, 30:62–67, February 1992.

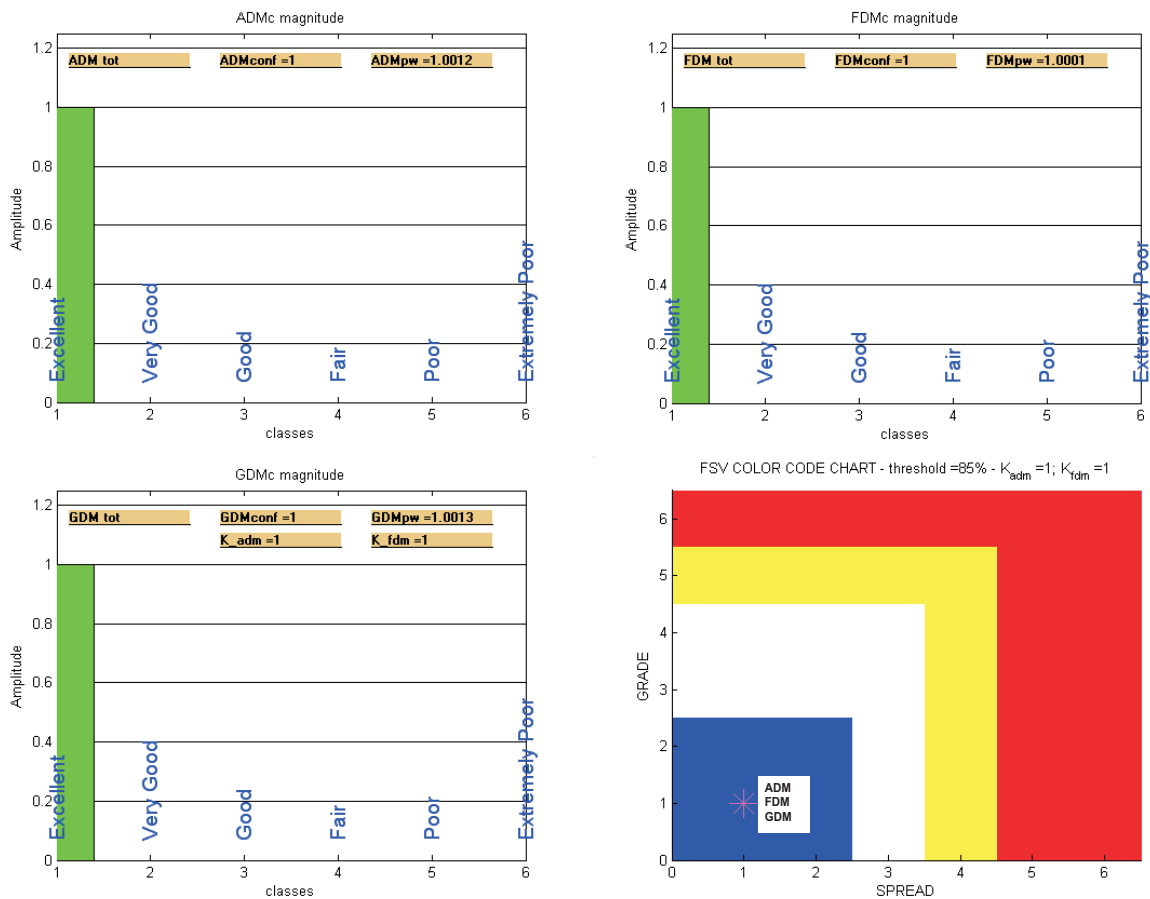


Fig. 16. ADMc, FDMc GDMc confidence histograms and Grade-Spread chart.

- [32] G. Antonini. A New Methodology for the Transient Analysis of Lossy and Dispersive Multiconductor Transmission Lines. *IEEE Transactions on Microwave Theory and Techniques*, 52(9):2227–2239, September 2004.
- [33] S. Ramo, J. R. Whinnery and T. Van Duzer. *Fields and Waves in Communication Electronics*. John Wiley and Sons, New York, 1994.
- [34] A. Alù, N. Engheta. Pairing an epsilon-negative slab with a mu-negative slab: resonance, tunneling and transparency. *IEEE Transactions on Antennas and Propagation*, 51(10):2558–2571, October 2003.
- [35] C. R. Paul. *Analysis of Multiconductor Transmission Lines*. John Wiley & Sons, New York, NY, 1992.
- [36] J. Brandão Faria. *Multiconductor Transmission-Line Structures: Modal Analysis Technique*. John Wiley & Sons, New York, NY, 1993.
- [37] B. Gustavsen and A. Semlyen. Rational Approximation of Frequency Domain Responses by Vector Fitting. *IEEE Transactions on Power Apparatus and Systems*, 14(3):1052–1061, July 1999.
- [38] G. Strang, T. Nguyen. *Wavelets and Filter Banks*. Wellesley, Cambridge Press, MA, 1997.
- [39] G. Antonini, G. Ferri. Compact Transmission Lines Representation. *IEE Proceedings-Science, Measurement and Technology*, 151(3):211–217, May 2004.
- [40] L. T. Pillage and R. A. Rohrer. Asymptotic Waveform Evaluation for Timing Analysis. *IEEE Transactions on Computer-Aided Design*, 9(4):352–366, 1990.
- [41] E. Chiprout, M.S. Nakhla. *Asymptotic Waveform Evaluation*. KLUWER, 1994.
- [42] K. Gallivan, E. Grimme, P. Van Dooren. Asymptotic Waveform Evaluation Via a Lanczos Method. *Applied Math.*, 7(5):75–80, September 1994.
- [43] L. Pileggi, R. Rohrer, C. Visweswariah. *Electronic Circuits and System Simulation Methods*. McGraw-Hill Book Company, 1995.
- [44] T. Kailath. *Linear Systems*. Prentice Hall, Englewood Cliffs, NJ, 1980.
- [45] C. T. Chen. *Linear System Theory and Design*. Holt, Rinehart, Winston, New York, 1984.
- [46] A. Ruberti, S. Monaco. *Teoria dei Sistemi*. Pitagora Editrice Bologna, 1998.
- [47] R. Neumayer, A. Steltzer, F. Haslinger, R. Weigel. On the Synthesis of Equivalent-Circuit Models for Multiports Characterized by Frequency-Dependent Parameters. *IEEE Transactions on Microwave Theory and Techniques*, 50(12):2789–2796, December 2002.
- [48] H. Shichman. Integration system of a nonlinear network analysis program. *IEEE Transactions on Circuits and Systems*, 17:378–386, August 1970.

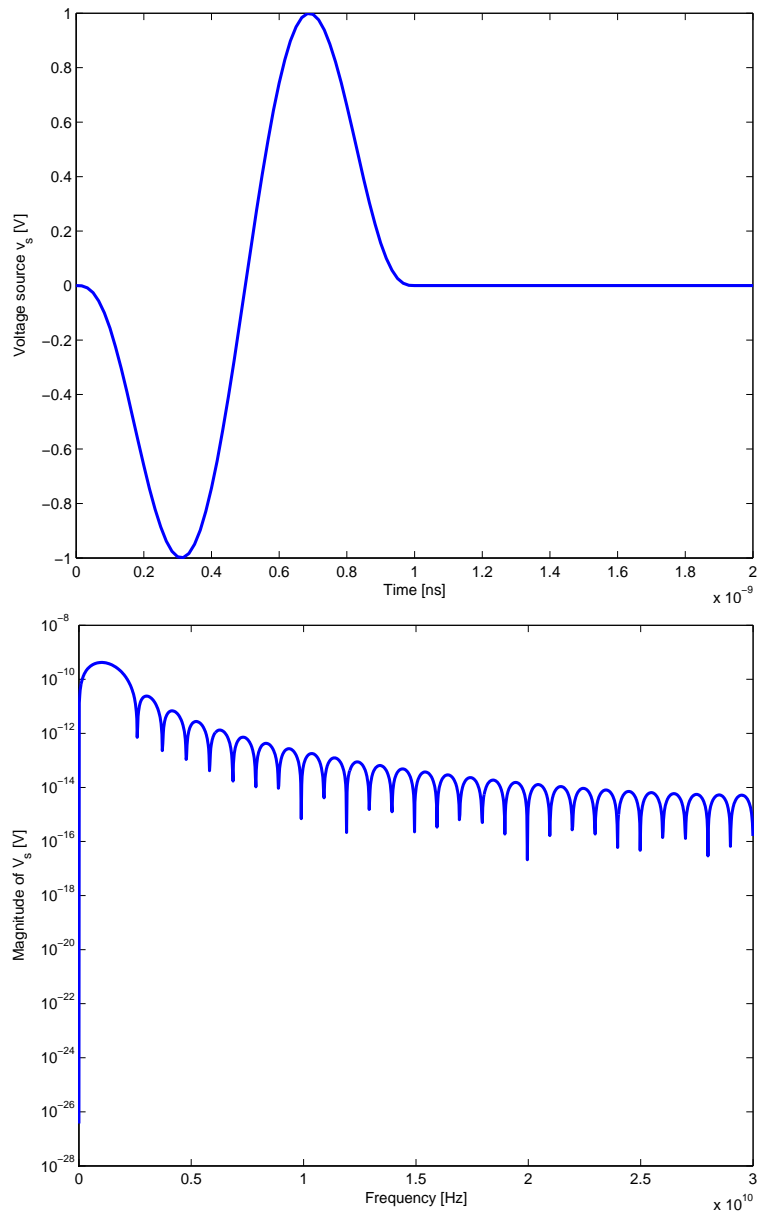


Fig. 17. Single cycle pulse excitation for example VII-B. Top: time domain waveform; bottom: frequency magnitude spectrum.

- [49] A. Duffy, A. Martin, G. Antonini, A. Orlandi, C. Ritota. The Feature Selective Validation (FSV) Method. In *Proc. of the IEEE Int. Symp. on Electromagnetic Compatibility*, Chicago, IL, USA, August 2005.
- [50] A. Duffy, A. Martin, A. Orlandi, G. Antonini, T. M. Benson, M. Woolfson. Feature Selective Validation (FSV) for validation of Computational Electromagnetics (CEM). Part I - The FSV Method. *IEEE Transactions on Electromagnetic Compatibility*, 48(2), August 2006.
- [51] A. Duffy, A. Martin, A. Orlandi, G. Antonini, T. M. Benson, M. Woolfson. Feature Selective Validation (FSV) for validation of Computational Electromagnetics (CEM). Part II - Numerical Verification. *IEEE Transactions on Electromagnetic Compatibility*, 48(2), August 2006.

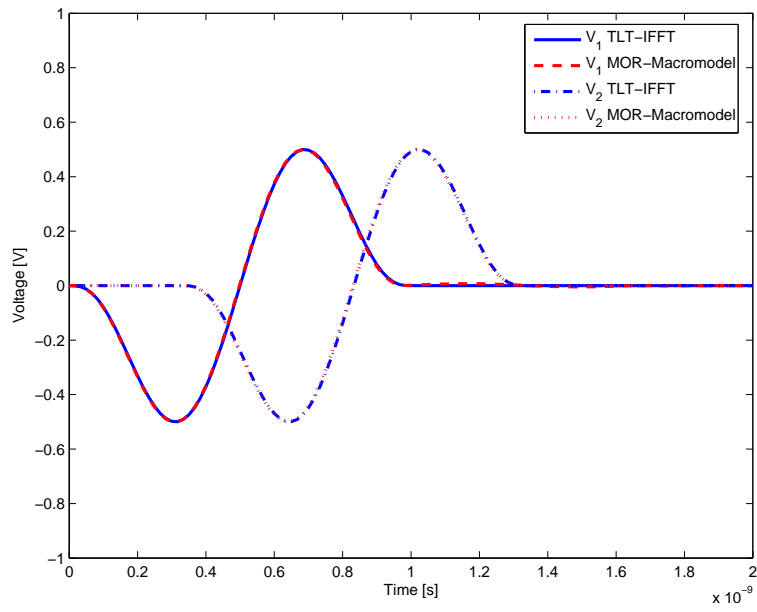


Fig. 18. Comparison of voltages at the input and output ports of a 2TDLM transmission line for example VII-B.

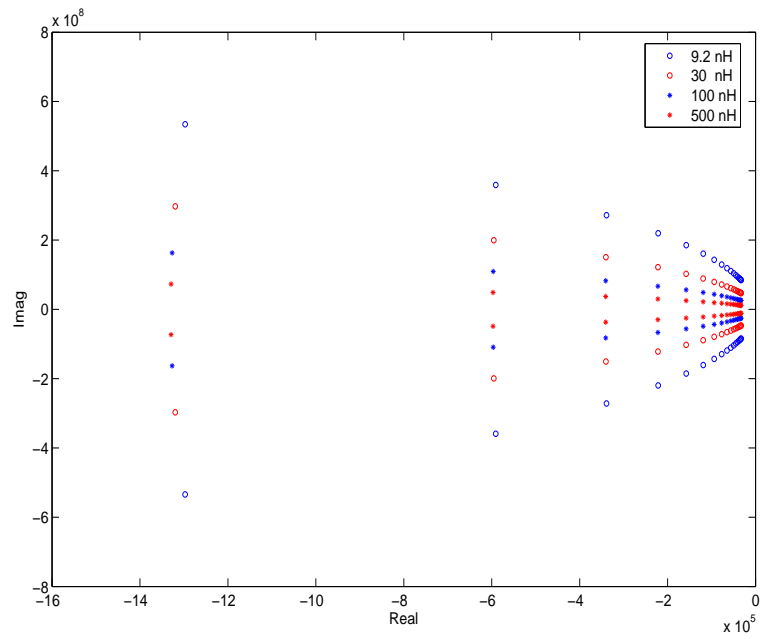


Fig. 19. Poles location in the complex plane for increasing values of L_L (example VII-C).

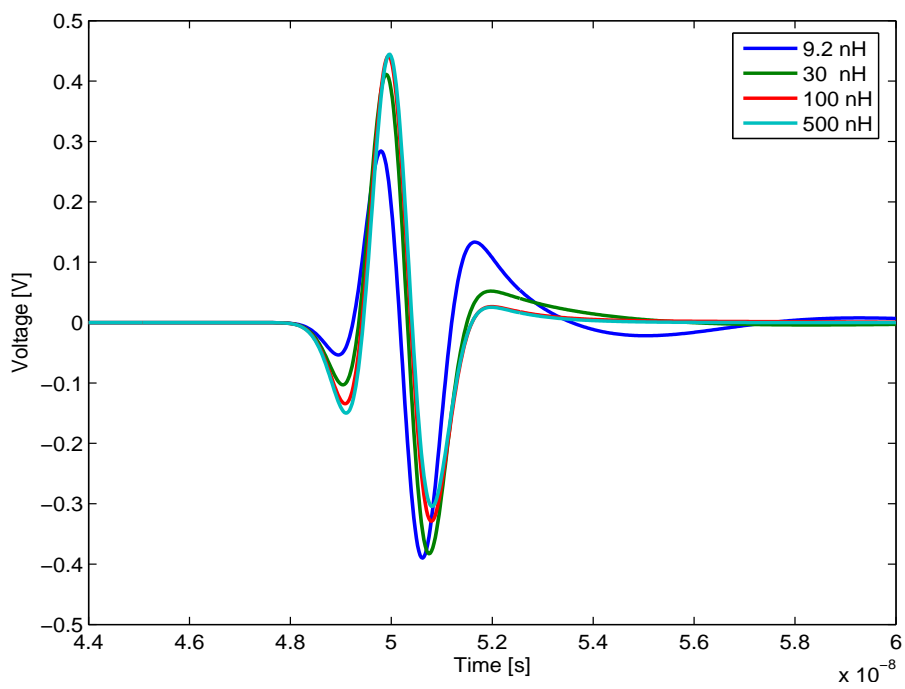


Fig. 20. Output voltage of the CRLH-TL for different values of L_L (example VII-C).

ADVERTISING RATES		
	FEE	PRINTED SIZE
Full page	\$200	7.5" × 10.0"
1/2 page	\$100	7.5" × 4.7" or 3.5" × 10.0"
1/4 page	\$50	3.5" × 4.7"
<p>All ads must be camera ready copy.</p> <p>Ad deadlines are same as Newsletter copy deadlines.</p> <p>Place ads with Ray Perez, Newsletter Editor, Martin Marietta Astronautics, MS 58700, PO Box 179, Denver, CO 80201, USA. The editor reserves the right to reject ads.</p>		

DEADLINE FOR THE SUBMISSION OF ARTICLES	
Issue	Copy Deadline
March	February 1
July	June 1
November	October 1

For the **ACES NEWSLETTER**, send copy to Bruce Archambeault in the following formats:

1. A PDF copy.
2. A MS Word (ver. 97 or higher) copy. If any software other than WORD has been used, contact the Managing Editor, Richard W. Adler **before** submitting a diskette, CD-R or electronic file.

Last Word

"A little knowledge is a dangerous thing. So is a lot"
Albert Einstein